

# NOVEL INSIGHTS INTO PROTOPORPHYRIN IX-INDUCED LIVER INJURY

by

**Madhav Sachar**

B.Tech. (Biotechnology), Guru Gobind Singh Indraprastha University, 2009

Submitted to the Graduate Faculty of  
The School of Pharmacy in partial fulfillment  
of the requirements for the degree of  
Doctor of Philosophy

University of Pittsburgh

2016

UNIVERSITY OF PITTSBURGH

School of Pharmacy

This thesis was presented

by

**Madhav Sachar**

It was defended on

November 9<sup>th</sup>, 2016

and approved by

Wen Xie, MD, PhD, Professor, Department of Pharmaceutical Sciences

Song Li, MD, PhD, Professor, Department of Pharmaceutical Sciences

Thomas W. Kensler, Professor, Department of Pharmacology and Chemical Biology

Philip E. Empey, PharmD, Ph.D, Assistant Professor, Department of Pharmaceutical Sciences

Dissertation Advisor: Xiaochao Ma, PhD, Associate Professor, Department of Pharmaceutical Sciences

**NOVEL INSIGHTS INTO PROTOPORPHYRIN IX-INDUCED LIVER INJURY**

Madhav Sachar

University of Pittsburgh, 2016

Copyright © by Madhav Sachar

2016

# NOVEL INSIGHTS INTO PROTOPORPHYRIN IX-INDUCED LIVER INJURY

Madhav Sachar, PhD

University of Pittsburgh, 2016

Protoporphyrin IX (PPIX) is an endogenous hepatotoxin produced by all the cells as an intermediate in the heme biosynthesis pathway. In normal conditions, PPIX is efficiently converted into heme. However, genetic disease or xenobiotics can disrupt homeostasis in the heme biosynthesis pathway to cause PPIX accumulation.

The first part of my thesis research revealed the mechanism by which isoniazid dysregulates the heme biosynthesis pathway. Isoniazid is an anti-tuberculosis drug known to cause liver injury when used with rifampicin. Here, I showed that isoniazid treatment independently induced the accumulation of PPIX in the liver of wild-type mice. Isoniazid dysregulates the heme biosynthesis pathway in the liver in part through the induction of delta-aminolevulinate synthase 1 protein as well as by the downregulation of ferrochelatase protein. Results from this study established the porphyrinogenic properties of isoniazid and explained how isoniazid can potentiate toxicity when administered with rifampicin.

In the second part of this thesis, I showed that the ATP-binding cassette sub family G member 2 (ABCG2) is a key facilitator in the PPIX-mediated liver injury. ABCG2 is an ATP dependent transporter present in the liver which excretes PPIX from hepatocytes into the bile. Using genetic and chemical PPIX-mediated liver injury mouse models, I showed that *Abcg2* deficiency

abolished liver injury. In the genetic mouse model, I showed that the deficiency of Abcg2 in bone marrow cells redistributed PPIX produced by bone marrow into the spleen and decreased PPIX available in the serum to be collected by the liver. Also, Abcg2-deficiency in hepatocytes reduced the excretion of PPIX into the bile duct thus preventing PPIX-induced bile-duct blockage and consequently averting colestatic liver injury. I further showed that accumulated PPIX in the hepatocytes with Abcg2 deficiency was metabolized into detoxified metabolite which was excreted easily into the bile for fecal elimination. This study is important as it provides a novel therapeutic approach for the management of PPIX-mediated liver injury.

Collectively, this work has provided greater insights into drug-induced PPIX accumulation and mechanism of PPIX-mediated liver injury. In addition, it is hoped that this work can help to develop strategies for preventing PPIX-mediated liver injury.

## TABLE OF CONTENT

<b>LIST OF TABLES .....</b>	<b>xi</b>
<b>LIST OF FIGURES .....</b>	<b>xii</b>
<b>PREFACE.....</b>	<b>xiv</b>
<b>ABBREVIATIONS .....</b>	<b>xvi</b>
<b>1. Introduction.....</b>	<b>1</b>
<b>1.1 Background.....</b>	<b>1</b>
<b>1.2 PPIX biosynthesis.....</b>	<b>3</b>
<b>1.3 Regulation of PPIX biosynthesis through ALAS .....</b>	<b>4</b>
<b>1.4 Dysregulation of PPIX homeostasis.....</b>	<b>7</b>
<b>1.4.1 ALA loading to bypass ALAS1. ....</b>	<b>7</b>
<b>1.4.2 Gain of function of ALAS2.....</b>	<b>8</b>
<b>1.4.3 Decreased ALAD activity. ....</b>	<b>8</b>
<b>1.4.4 Decreased PPOX activity.....</b>	<b>9</b>
<b>1.4.5 Decreased FECH activity. ....</b>	<b>9</b>
<b>1.4.6 Decreased iron availability .....</b>	<b>10</b>
<b>1.4.7 PPIX accumulation with normal PPOX and FECH activity and iron supply. 11</b>	
<b>1.4.8 PPIX transporters in PPIX accumulation. ....</b>	<b>12</b>

<b>1.5.</b>	<b>Clinical manifestations and management of PPIX toxicity .....</b>	<b>13</b>
<b>1.5.1.</b>	<b>PPIX-mediated skin damage. ....</b>	<b>13</b>
<b>1.5.2.</b>	<b>PPIX-mediated hepatobiliary disease.....</b>	<b>14</b>
<b>1.6.</b>	<b>PPIX-based strategies for diagnosis and the rapy .....</b>	<b>18</b>
<b>1.7.</b>	<b>Conclusions .....</b>	<b>20</b>
<b>2.</b>	<b>Chronic treatment with isoniazid causes protoporphyrin IX accumulation in mouse liver.....</b>	<b>21</b>
<b>2.1.</b>	<b>Introduction.....</b>	<b>21</b>
<b>2.1.1.</b>	<b>An overvie w of tuberculosis and isoniazid.....</b>	<b>21</b>
<b>2.1.2.</b>	<b>Porphyrogenic effect of isoniazid. ....</b>	<b>22</b>
<b>2.1.3.</b>	<b>Experimental design. ....</b>	<b>22</b>
<b>2.2.</b>	<b>Material and Methods.....</b>	<b>23</b>
<b>2.2.1.</b>	<b>Chemicals and reagents.....</b>	<b>23</b>
<b>2.2.2.</b>	<b>Animals and treatment. ....</b>	<b>23</b>
<b>2.2.1.</b>	<b>Bioche mical and pathological analysis.....</b>	<b>24</b>
<b>2.2.2.</b>	<b>Metabolomic analysis.....</b>	<b>25</b>
<b>2.2.3.</b>	<b>Data analysis.....</b>	<b>25</b>
<b>2.2.4.</b>	<b>PPIX quantification. ....</b>	<b>26</b>
<b>2.2.5.</b>	<b>FECH activity assay.....</b>	<b>27</b>
<b>2.2.6.</b>	<b>ALAS activity assay.....</b>	<b>28</b>

2.2.7.	Western blotting.....	29
2.2.8.	Real-time PCR.....	30
2.2.9.	Statistical analysis.....	30
2.3.	Results .....	30
2.3.1.	Effect of INH on liver injury.....	30
2.3.2.	Effect of INH on PPIX homeostasis in the liver.....	31
2.3.1.	Effect of INH on PPIX levels in BMCs, serum and RBCs.....	35
2.3.2.	Effect of INH on FECH expression and function in the liver.....	35
2.3.3.	Effect of INH on ALAS1 expression and function in the liver.....	35
2.4.	Discussion.....	40
3.	Deficiency of ATP-binding cassette sub-family G member 2 attenuates protoporphyrin IX-mediated liver injury.....	42
3.1.	Introduction .....	42
3.1.1.	ATP-binding cassette sub-family G member 2 (ABCG2).....	42
3.1.2.	Role of ABCG2 in PPIX homeostasis.....	43
3.1.3.	Animal models used to study PPIX-mediated liver injury.....	44
3.1.4.	Experimental Design.....	45
3.2.	Material and Methods.....	46
3.2.1.	Chemicals.....	46
3.2.2.	Animal treatment.....	46

3.2.3.	Development and treatment of hPXR/Abcg2-null mice. ....	46
3.2.4.	Development of Fech-mut (Fech <sup>m1pas</sup> /Fech <sup>m1pas</sup> )/Abcg2-null mice. ....	47
3.2.5.	Biochemical and histological analysis. ....	47
3.2.6.	Metabolite analysis.....	48
3.2.7.	PPIX and protoporphyrin-1-O-acyl-glucouronide quantification. ....	49
3.2.8.	Synthesis of protoporphyrin-1-O-acyl-glucouronide (PPIX-glu). ....	50
3.2.9.	Statistical analysis. ....	50
3.3.	Results .....	51
3.3.1.	Abcg2 deficiency prevents RIF and INH-induced hepatotoxicity. ....	51
3.3.2.	Abcg2 deficiency prevents DDC-induced liver injury. ....	53
3.3.3.	Abcg2 deficiency prevents GSF-induced liver injury. ....	55
3.3.4.	Abcg2 deficiency in a genetic EPP mouse model abolishes PPIX-mediated liver injury. ....	57
3.3.5.	Abcg2 deficiency in erythroid progenitor cells of Fech-mut/Abcg2-null mice redistributes PPIX from bone marrow. ....	58
3.3.6.	ABCG2 deficiency in the liver causes PPIX accumulation in hepatocytes.....	60
3.3.7.	ABCG2 deficiency in the liver induces PPIX metabolism to PPIX metabolites. ....	61
3.3.8.	PPIX-glu conjugate is excreted into bile for fecal elimination .....	64
3.4.	Discussion.....	66

<b>4. Summary and perspectives .....</b>	<b>70</b>
<b>4.1. Major Findings and Implications .....</b>	<b>70</b>
<b>4.2. Limitations and future directions .....</b>	<b>74</b>
<b>APPENDIX A .....</b>	<b>77</b>
<b>BIBLIOGRAPHY .....</b>	<b>78</b>

## LIST OF TABLES

<b>Table 1. Pharmacological approaches for management of photosensitivity in EPP patients.</b> .....	<b>15</b>
<b>Table 2. Water consumption of mice treated with isoniazid (INH). .....</b>	<b>24</b>

**LIST OF FIGURES**

**Figure 1. PPIX/heme biosynthesis and disposition in mammalian cells.....2**

**Figure 2. Regulation of PPIX homeostasis.....6**

**Figure 3. Mechanisms of PPIX-mediated liver injury and strategies to manage this injury.....16**

**Figure 4. Evaluation of liver damage in mice treated with INH.....32**

**Figure 5. Effect of INH on mouse liver metabolome.....33**

**Figure 6. Identification and quantification of PPIX.....34**

**Figure 7. Effect of INH on PPIX levels in bone marrow cells (BMCs), serum and red blood cells (RBCs).....36**

**Figure 8. Hemoglobin in the liver of mice treated with INH.....37**

**Figure 9. Effect of INH and its metabolites on FECH activity.....37**

**Figure 10. Effect of INH on FECH mRNA expression in mouse liver.....38**

**Figure 11. Effect of INH on FECH expression in the liver.....38**

**Figure 12. Effect of INH on ALAS1 expression and activity in the liver.....39**

**Figure 13. Generation of hPXR/Abcg2-null mice.....51**

**Figure 14. hPXR/Abcg2-null mice are resistant to RIF and INH induced liver injury.....52**

**Figure 15. Abcg2-null mice are resistant to DDC-mediated liver injury.....54**

**Figure 16. Abcg2-null mice are resistant to GSF-mediated liver injury.....56**

**Figure 17. Fech-mut/Abcg2-null mice are resistant to PPIX-induced liver injury.....58**

**Figure 18. Redistribution of PPIX produced by bone marrow in Fech-mut/Abcg2-null mice.....59**

**Figure 19. Formation of D16-PPIX in the liver of Fech-mut and Fech-mut/Abcg2-null mice.....60**

**Figure 20. Identification and synthesis of PPIX metabolite protoporphyrin-1-O-acyl-glucouronide. ....62**

**Figure 21. D16-protoporphyrin-1-O-acyl-glucouronide in WT and Abcg2-null mice.....63**

**Figure 22. Protoporphyrin-1-O-acyl-glucouronide in the liver of drug-induced porphyria models.....64**

**Figure 23. D16-Protoporphyrin-1-O-acyl-glucouronide in the gall bladder and feces of genetic porphyria models.....65**

**Figure 24. A scheme showing mechanism of INH-induced PPIX accumulation.....71**

**Figure 25. A scheme showing mechanism by which Abcg2-deficiency prevents PPIX-mediated liver injury.....73**

## PREFACE

I am dedicating my dissertation to the most valuable people in my life, my mother (Rashmi Sachar) and father (Verinder Kumar Sachar) for instilling the strength and providing vision to complete this incredible journey of life.

This project is an outcome of the invaluable guidance from my advisor Dr. Xiaochao Ma. I was fortunate to work under his supervision and in his lab. Thank you for your encouragement and faith in me and providing me with the opportunity to grow both personally and professionally. I will always remember what I have learned from you and am grateful to you for these life-long lessons. I am also indebted to my committee members, Dr. Wen Xie, Dr. Song Li, Dr. Thomas W. Kensler, and Dr. Philip Empey for their generous support and valuable feedback. I would like to extend my sincere gratitude to Jie Lu (Lucy) for helping me; this work would not be possible without her constant assistance. I am thankful to Dr. Pengchang Wang for sharing his valuable experience in the progress of this project. A big thank you to Dr. Ke Liu (Michael) for teaching me metabolomics and UPLC-QTOF. My sincere thanks to all the past and present members of Dr. Ma's lab: Dr. Feng Li, Dr. Hye Joung Choi, Dr. Junjie Zhu, Amina Shehu, Danfeng Shen, Shinlan Lu and Komal Pradhan for their strong support and friendship during the course of my PhD.

I am very grateful to all the members at the Center for Pharmacogenetics. I feel very fortunate as a part of this group as this experience enriched me with a wide range of expertise. I am also

thankful to all the faculty, staff and students in the Department of Pharmaceutical Sciences, especially Dr. Maggie Folan and Lori Schmotzer for their help and provision.

Special thanks to my wife, Upasana Shokal and my brother, Devesh Sachar for all the encouragement and inspiration that pushed me to work hard and strive for success. Lastly, I would like to thank my family for their blessings and moral support.

## ABBREVIATIONS

ABCB10	ATP-binding cassette sub family B member 10
ABCB6	ATP-binding cassette sub family B member 6
ABCG2	ATP-binding cassette sub family G member 2
Abcg2-null	Abcg2- knock out
AcHz	acetyl hydrazine
AcINH	acetyl isoniazid
ALA	5-aminolevulinic acid
ALAD	aminolevulinic acid dehydratase
ALAS1	aminolevulinic acid synthase 1
ALAS2	aminolevulinic acid synthase 2
ALP	alkaline phosphatase
ALT	alanine transaminase
AST	aspartate amino transferase
BMCs	bone marrow cells
CAR	constitutive androstane receptor
CPOX	coproporphyrinogen oxidase
D <sub>16</sub> -PPIX	protoporphyrin-d <sub>16</sub> IX
D <sub>16</sub> -PPIX-glu	D <sub>16</sub> -protoporphyrin-1-O-acyl-glucouronide
D <sub>2</sub> -ALA	5-Aminolevulinic-2,2-d <sub>2</sub> acid
DDC	3,5-diethoxycarbonyl-1,4-dihydrocollidine
EPP	erythropoietic protoporphyria
FECH	ferrochelatase
Fech-mut	Fech-mutant (Fech <sup>m1pas</sup> /Fech <sup>m1pas</sup> )
FLVCR1	feline leukemia virus subgroup c receptor 1
GSF	griseofulvin
HIV	human immunodeficiency virus
HMBS	hydroxymethylbilane synthase
hPXR	Humanized pregnane X receptor
HZ	hydrazine
INH	isoniazid
LTBI	latent tuberculosis
MFRN1	mitoferrin 1
OPLS-DA	orthogonal partial least-squares discriminant analysis
P450	cytochrome P450 enzymes
PBzR	peripheral benzodiazepine receptor
PCA	principal component analysis
PGC-1 $\alpha$	proliferator-activated receptor- $\gamma$ coactivator 1 $\alpha$

PLP	pyridoxal phosphate
PPIX	protoporphyrin IX
PPIX-glu	protoporphyrin-1-O-acyl-glucouronide
PPOX	protoporphyrinogen oxidase
PXR	pregnane X receptor
QTOFMS	quadrupole time-of-flight mass spectrometry
RBCs	red blood cells
RIF	rifampicin
ROS	reactive oxygen species
SLC25A38	solute carrier family 25 member 38
TB	tuberculosis
UPLC	ultra-performance liquid chromatography
UROD	uroporphyrinogen decarboxylase
UROS	uroporphyrinogen III synthase
VP	variegate porphyria
WT	wild type
XLP	X-linked protoporphyria

## **1. Introduction**

### **1.1 Background**

Protoporphyrin IX (PPIX) is a heterocyclic organic compound, which consists of four pyrrole rings, and is the final intermediate in the heme biosynthetic pathway. Its tetrapyrrole structure enables it to chelate transition metals to form metalloporphyrins, which perform a variety of biologic functions. Chelation of PPIX with iron forms heme (iron PPIX), which is a constituent of hemoproteins that play critical roles in oxygen transport, cellular oxidations and reductions, electron transport, and drug metabolism [1-3]. Amounts of PPIX in cells actively synthesizing heme remain low under physiologic conditions, because the amount supplied does not exceed what is needed for heme synthesis. Thus, PPIX is efficiently converted to heme by the mitochondrial enzyme ferrochelatase (FECH), the final enzyme in the heme biosynthetic pathway. Inherited and acquired diseases and some xenobiotics can disturb heme synthesis and PPIX homeostasis, causing accumulation of PPIX in amounts that are sufficient to produce photosensitivity and liver damage [4-8]. Clinically useful aspects of PPIX include its use for cancer diagnosis and therapy [9, 10]. In this chapter, the broad aspects of PPIX are discussed including its biosynthesis and regulation, its toxicity and clinical manifestations when present in excess, and its therapeutic applications.

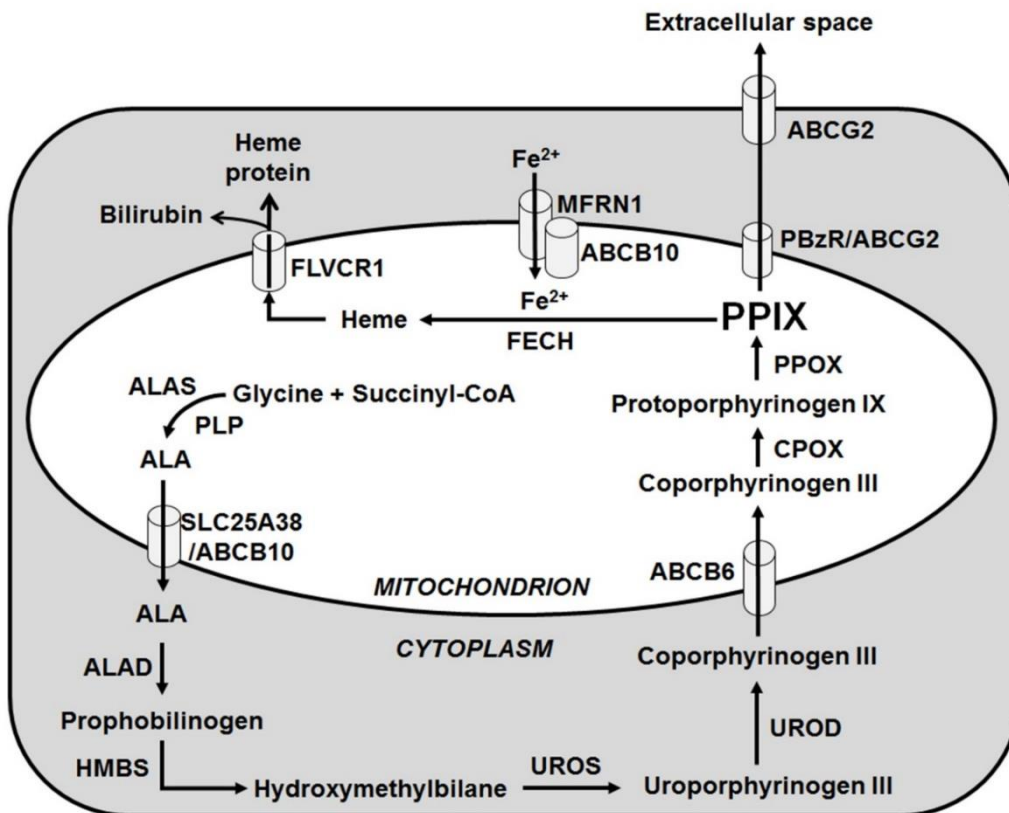


**Figure 1. PPIX/heme biosynthesis and disposition in mammalian cells.**

Multiple enzymes, cofactors, and transporters are involved in the pathway of PPIX and heme biosynthesis and in PPIX disposition. ALA,  $\delta$ -aminolevulinic acid; ALAS,  $\delta$ -aminolevulinic acid synthase; PLP, pyridoxal phosphate; ALAD, aminolevulinic acid dehydratase; HMBS, hydroxymethylbilane synthase; UROS, uroporphyrinogen III synthase; UROD, uroporphyrinogen decarboxylase; CPOX, coproporphyrinogen oxidase; PPOX, protoporphyrinogen oxidase; FECH, ferrochelatase; PPIX, protoporphyrin IX; SLC25A38, solute carrier family 25 member 38; ABCB6, ATP-binding cassette sub family B member 6; ABCB10, ATP-binding cassette sub family B member 10; MFRN1, mitoferrin 1; ABCG2, ATP-binding cassette sub-family G member 2; PBzR, peripheral benzodiazepine receptor; FLVCR1, feline leukemia virus subgroup c receptor 1.

## 1.2. PPIX biosynthesis

Biosynthesis of heme is an eight-step process that occurs partly in mitochondria and partly in the cytoplasm (**Figure 1**) [11]. All eight enzymes in this pathway are encoded in the nucleus and are synthesized in the cytoplasm. PPIX is the final intermediate in the heme synthesis pathway. PPIX is formed by protoporphyrinogen oxidase (PPOX) and converted to heme by FECH, both of which are mitochondrial enzymes. Biosynthesis of heme initiates in the mitochondrial matrix where one molecule of glycine combines with one molecule of succinyl-CoA to form  $\delta$ -aminolevulinic acid (ALA). This step is catalyzed by ALA synthase (ALAS; EC 2.3.1.37) in the presence of the cofactor pyridoxal phosphate [12, 13]. ALA formed in mitochondria is exported to the cytoplasm (**Figure 1**). The mechanism of ALA transport is not fully understood, but a role for solute carrier family 25 member 38 (SLC25A38) and ATP-binding cassette sub family B member 10 (ABCB10) has been suggested [14, 15]. Two molecules of ALA are condensed by ALA dehydratase (ALAD; EC 4.2.1.24, also known as porphobilinogen synthase) to form the monopyrrole porphobilinogen. Hydroxymethylbilane synthase (EC 2.5.1.61, also known as porphobilinogen deaminase) then assembles four molecules of porphobilinogen to form hydroxymethylbilane [16]. This reactive linear tetrapyrrole can spontaneously cyclize to form uroporphyrinogen I, which is not a heme precursor. The enzyme uroporphyrinogen synthase (EC 4.2.1.75) catalyzes hydroxymethylbilane ring closure with inversion of one of the pyrrole rings to form the heme precursor uroporphyrinogen III [17].

Uroporphyrinogen decarboxylase (EC 4.1.1.37) then removes carboxylic groups from the four acetic acid side chains of uroporphyrinogen III to form coproporphyrinogen III [18]. This

intermediate is then transported into mitochondria through ABCB6 [19, 20], where it is decarboxylated to protoporphyrinogen IX by coproporphyrinogen oxidase (CPOX; EC 1.3.3.3) [21]. Protoporphyrinogen IX is oxidized by PPOX (EC 1.3.3.4) with removal of six protons to form PPIX [21]. There are two major pathways for cellular PPIX disposition: synthesis of heme or excretion from the cell (**Figure 1**). PPIX in most tissues is efficiently converted to heme by FECH (EC4.99.1.1) in the presence of iron [22]. FECH activity is low in the oviduct of some birds, which allows PPIX to accumulate and serve as a brown pigment on eggshells [23]. Mitoferrin 1 (MFRN1) and ABCB10 are involved in providing iron to mitochondria for heme synthesis [24, 25]. In marrow reticulocytes, most PPIX remaining in small amounts after completion of heme and hemoglobin synthesis is chelated with zinc by FECH, and along with a smaller amount of metal-free PPIX is found in circulating erythrocytes. PPIX remaining in mitochondria may be transported into the extracellular space through ATP-binding cassette subfamily G member 2 (ABCG2) and peripheral benzodiazepine receptor (PBzR) [26-29] (**Figure 1**).

### **1.3. Regulation of PPIX biosynthesis through ALAS**

ALAS is the rate-limiting enzyme in PPIX production and heme synthesis. In mammals, ubiquitous and erythroid-specific forms of ALAS are encoded by separate genes on chromosomes 3 and X, respectively [30]. The ubiquitous form (ALAS1) is expressed in all tissues, including the liver. The erythroid-specific form (ALAS2) is only expressed in erythroid cells [31, 32]. Although heme is synthesized in all cells, approximately 85% is produced in the bone marrow, and most of the rest in the liver. Heme is a key regulator of hepatic ALAS1

**(Figure 2).** Heme directly binds to the upstream region of the *ALAS1* gene and prevents transcription [33-35]. In addition, heme destabilizes *ALAS1* mRNA and promotes degradation of mature *ALAS1* protein [36-38]. Furthermore, heme prevents transport of the precursor of *ALAS1* protein into mitochondria by binding to the terminal mitochondrial targeting sequence [39-41].

In addition, *ALAS1* biosynthesis is regulated by transcription factors and coactivators **(Figure 2)**. Fasting and feeding result in up- and down-regulation of *ALAS1* expression, respectively, by modulating the activity of proliferator-activated receptor- $\gamma$  coactivator 1 $\alpha$  (PGC-1 $\alpha$ ) [42-46]. Expression of proliferator-activated receptor- $\gamma$  coactivator 1 $\alpha$  is also regulated by a circadian oscillator Rev-erba [47, 48]. Thus, *ALAS1* expression is modulated by circadian rhythm. Most heme synthesized in the liver functions as a cofactor of cytochrome P450 enzymes (P450), which are abundant in liver, turn over rapidly and are critical for metabolism of many endogenous and exogenous chemicals. In response to P450 inducers, *ALAS1* is up-regulated by depletion of a “regulatory heme pool” in hepatocytes, and through nuclear receptors, such as the constitutive androstane receptor (CAR) and the pregnane X receptor (PXR) [49-51]. These receptors are important for regulation of both *ALAS1* and P450s in the liver by drugs and other chemicals. Therefore, ligands of these nuclear receptors can up-regulate *ALAS1* expression and increase PPIX and heme synthesis [49, 52].

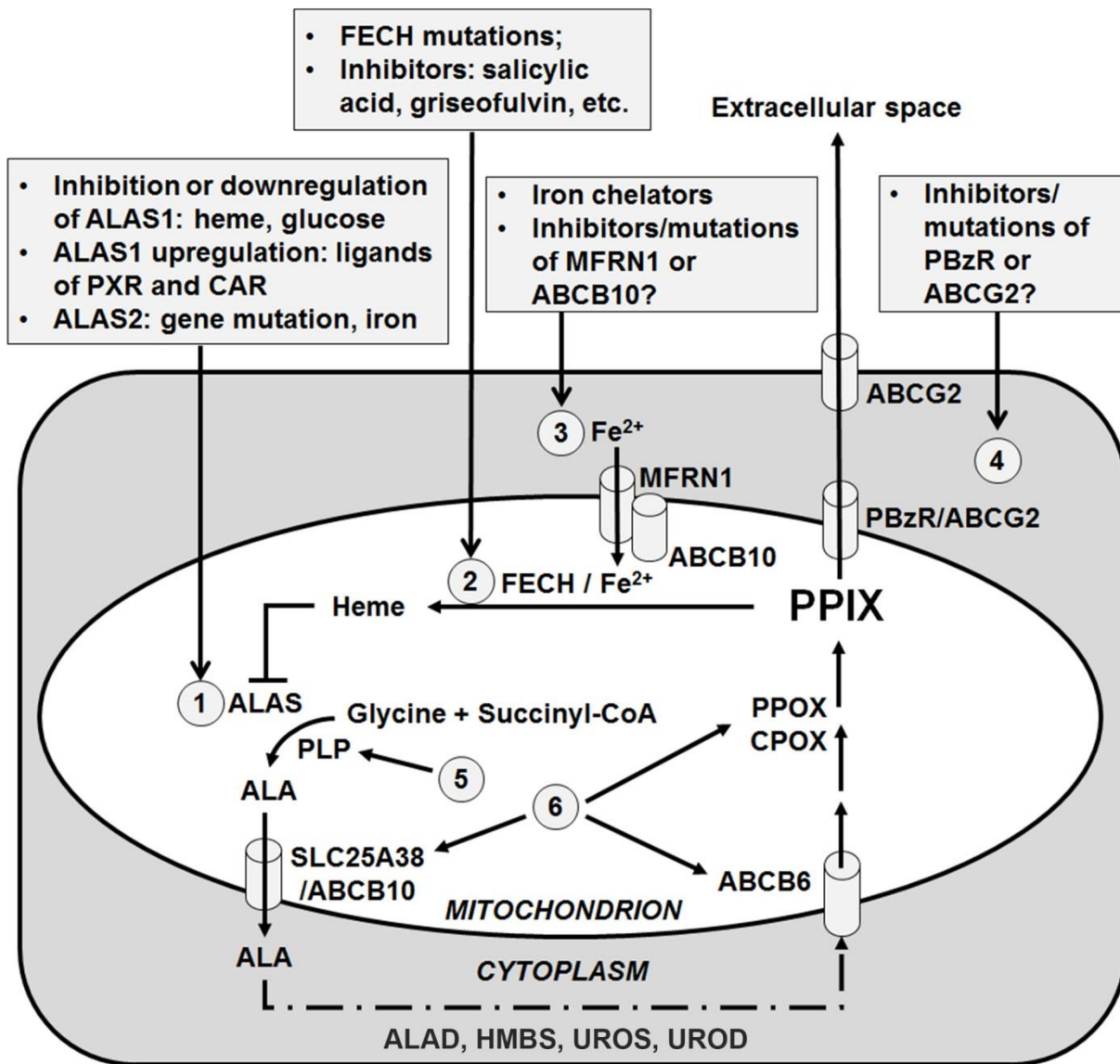


**Figure 4. Regulation of PPIX homeostasis.**

Genetic factors and xenobiotics can disturb PPIX homeostasis through effects on (1) ALAS, (2) FECH, (3) iron supply, (4) PPIX transporters, (5) PLP (the coenzyme of ALAS), and (6) the enzymes and transporters downstream of ALAS and upstream of FECH.

Transcription of *ALAS2*, unlike *ALAS1*, is regulated by erythroid specific transcription factors [37]. Regarding the post-transcription of *ALAS2*, it is regulated by iron. *ALAS2* mRNA possesses an iron regulatory element (IRE) in the 5'untranslated region, which responds to cellular iron content [53, 54]. In the absence of iron, the iron-free form of iron regulatory protein (IRP) binds to the IRE forming an IRE-IRP complex that prevents translation of *ALAS2* [55]. This inhibitory effect of IRE-IRP complex is prevented by iron sulfur clusters [56, 57]. These intricate regulatory mechanisms of *ALAS2* by erythroid-specific transcription factors coordinate PPIX synthesis with iron supply, allowing efficient synthesis of large amounts of heme while avoiding an oversupply of either PPIX or iron, which would have adverse effects. Heme does not alter transcription of the *ALAS2* gene or *ALAS2* mRNA stability [58]. However, heme may inhibit the translation of *ALAS2* mRNA and the import of precursor *ALAS2* protein into mitochondria [39, 59].

#### **1.4. Dysregulation of PPIX homeostasis**

PPIX can accumulate in disease states and from the effects of certain chemicals. There are multiple examples of dysregulation of PPIX homeostasis.

##### **1.4.1. ALA loading to bypass ALAS1.**

Because the rate-limiting step is bypassed, intermediates later in the pathway accumulate, including PPIX. PPIX is a photosensitizer, and ALA administration can result in enough PPIX accumulation in lesions in the skin and other tissues to be the basis for photodynamic therapy [60]. Tissue selectivity is enhanced by direct application of ALA (e.g. to skin lesions) and by

lesion-directed laser treatment. An ALA preparation is FDA-approved for this purpose. ALA loading in healthy humans also results in increased urinary excretion of coproporphyrin, particularly isomer III [61].

#### **1.4.2. Gain of function of ALAS2.**

X-linked protoporphyria (XLP) is a recently characterized, rare X-linked disease due to gain of function mutations of *ALAS2* [62, 63]. These mutations alter the C-terminal portion of the *ALAS2* gene [62], which enhances the function of ALAS2 such that amounts of PPIX produced exceed that needed by FECH for heme synthesis. Increased metal-free PPIX in erythrocytes and plasma causes a painful, mostly non-blistering type of photosensitivity. Zinc PPIX, a product of normal FECH activity, is also increased in this condition, but mostly remains in circulating erythrocytes and is less photosensitizing.

#### **1.4.3. Decreased ALAD activity.**

Deficient ALAD activity leads to accumulation of ALA and other pathway intermediates, including PPIX, in large amounts in erythroid cells. This enzyme is genetically deficient in ALAD deficiency porphyria (ADP, the most rare human porphyria), causing elevations in ALA in plasma and urine, coproporphyrin III in urine (as in ALA loading), and zinc PPIX in erythrocytes. The same findings occur in lead poisoning, suggesting that increases in coproporphyrin III and erythrocyte PPIX in lead poisoning result largely from inhibition of ALAD and a resulting oversupply of ALA. In hereditary tyrosinemia type I, succinylacetone

accumulates and potently inhibits ALAD, leading to similar biochemical findings and porphyria-like symptoms [64]. Photosensitivity does not occur in these conditions, because the excess PPIX is predominantly zinc PPIX, reflecting adequate FECH activity. ALAD can also be inhibited by styrene in animals and humans [65].

#### **1.4.4. Decreased PPOX activity.**

This penultimate enzyme in the heme biosynthetic pathway catalyzes the oxidation of protoporphyrinogen IX to PPIX with a loss of 6 protons. An inherited partial deficiency of PPOX in variegate porphyria (VP) causes hepatic accumulation of protoporphyrinogen IX, which is then oxidized nonenzymatically to PPIX. Chronic blistering photosensitivity is a common symptom in VP. Phenoxy acid herbicides are potent PPOX inhibitors, and cause PPIX accumulation and phototoxicity in exposed plants [66]. These chemicals also inhibit PPOX and cause protoporphyrinogen IX and PPIX accumulation in rodent hepatocytes [67].

#### **1.4.5. Decreased FECH activity.**

Loss of function *FECH* mutations are found in human erythropoietic protoporphyria (EPP) [68, 69]. The *FECH* gene is located on the long arm of chromosome 18 on locus 18q21 [70]. More than 120 different *FECH* mutations have been identified in EPP [69]. Decreased function of both *FECH* alleles is required to cause EPP. Most commonly a severe *FECH* mutation is inherited from one parent and a low expression (hypomorphic) *FECH* alteration that is common in the general population from the other parent [71]. *FECH* deficiency in EPP also impairs zinc

PPIX formation, so the excess PPIX that accumulates is mostly metal-free [72, 73].

Some xenobiotics and/or their metabolites inhibit FECH and cause PPIX accumulation.

Salicylic acid, a nonsteroidal anti-inflammatory drug, binds directly to FECH and inhibits its activity, and can inhibit heme synthesis in cultured cells [74]. Certain xenobiotics require P450s to produce metabolites that are FECH inhibitors. 3,5-Diethoxycarbonyl-1,4-dihydrocollidine (DDC) and the antifungal drug griseofulvin are examples of chemicals that are suicidal substrates of CYPs, and their metabolism in mouse liver produces *N*-methyl- and *N*-ethyl-protoporphyrin IX, which are potent FECH inhibitors [75, 76]. These chemicals are also potent inducers of hepatic ALAS1, which further contributes to PPIX accumulation [75]. Griseofulvin exacerbates acute hepatic porphyrias presumably by its inducing effect on ALAS1 and inhibition of FECH [77].

#### **1.4.6. Decreased iron availability.**

MFRN1 imports iron into mitochondria [24], and a deficiency of MFRN1 reduces iron supply for FECH, limits heme synthesis and leads to PPIX accumulation [78]. ABCB10 physically interacts with MFRN1 and increases the half-life of MFRN1 [25]. Deficiency of ABCB10 impairs mitochondrial iron import and causes PPIX accumulation [79]. At the same time, ABCB10 deficiency in mice results in iron accumulation in cytoplasm and leads to sideroblastic anemia [79].

Iron deficiency impairs heme formation because ferrous iron is a substrate for FECH. However,

zinc can substitute for iron, so with iron deficiency FECH catalyzes an increase in formation of zinc PPIX [80], which accumulates in reticulocytes and is increased in circulating erythrocytes. An increase in erythrocyte zinc PPIX is an early indicator of iron deficiency and precedes the development of anemia [73]. Iron chelators can bind to ferrous iron in the cytoplasm of cells such as hepatocytes and prevent iron from entering mitochondria, thus reducing FECH function and causing PPIX accumulation [81-83]. In rodent and chick embryo livers and isolated hepatocytes, iron chelation can limit heme synthesis sufficiently to potentiate induction of ALAS1 by drugs and steroids [84]. In lead and other heavy metal poisoning, disturbed iron hemostasis may account in part for zinc PPIX accumulation [85]. Impaired iron delivery to reticulocytes accounts in part for anemia of chronic disease, which is also associated with an increase in erythrocyte zinc PPIX [80].

#### **1.4.7. PPIX accumulation with normal PPOX and FECH activity and iron supply.**

Amounts of zinc PPIX under normal and abnormal conditions are higher in younger than older erythrocytes, so increased erythropoiesis and shortened erythrocyte life span will increase the average concentration of PPIX. Therefore, an increase in zinc PPIX in erythrocytes is expected in any erythrocytic disorder (e.g. hemolytic anemias), even if heme synthetic enzymes and iron availability are not impaired [86].

#### 1.4.8. PPIX transporters in PPIX accumulation.

Excess PPIX synthesized in mitochondria needs to be pumped out to the cytoplasm and then to the extracellular space (**Figure 2**). Transporters are required because the two carboxylate side chains of PPIX make the movement of PPIX across a lipid bilayer energetically unfavorable. PBzR locates in the outer membrane of mitochondria and its expression is increased during erythroid differentiation, suggesting that PBzR might be responsible for transporting PPIX [87, 88]. Overexpression of recombinant PBzR in *Escherichia coli* supported the role of PBzR in PPIX movement [26]. Apart from PBzR, ABCG2 also contributes to PPIX movement [27]. ABCG2 is primarily localized on extracellular membranes and responsible for PPIX efflux [28]. ABCG2 also locates in mitochondrial membranes and contributes to PPIX efflux from mitochondria [29]. ABCG2 deficient mice have a higher amount of PPIX in red blood cells (RBCs), liver, and the Harderian gland than wild-type mice [27, 89].

In summary, PPIX homeostasis is maintained by close coordination of multiple factors including ALAS, FECH, iron supply and transporters of iron and PPIX (**Figure 2**). These are targets for genetic and environmentally-induced disturbances in PPIX homeostasis. PPIX homeostasis is also disturbed by alterations in enzymes, coenzymes and transporters downstream of ALAS and upstream of FECH (**Figure 2**). For example, severe, homozygous or compound heterozygous deficiency of any enzyme in the heme biosynthetic pathway after ALAS leads to an increase in erythrocyte PPIX, which is zinc chelated if FECH activity is preserved. Heme synthesis is increased in the marrow in an effort to compensate for the severe hemolytic anemia seen in some of these disorders.

## **1.5. Clinical manifestations and management of PPIX toxicity**

Normally there is little accumulation of PPIX or other intermediates in the heme biosynthetic pathway. Because the bone marrow and liver are most active in PPIX and heme synthesis, under abnormal conditions, PPIX accumulation occurs either in the marrow and circulating erythrocytes or the liver [11, 90-92]. During erythroid maturation when hemoglobin synthesis is active, excess PPIX can be chelated with zinc, or be pumped out to plasma through ABCG2 [93]. In EPP and XLP, metal-free PPIX originates from the marrow and circulating erythrocytes and is delivered in plasma to the skin and liver [94, 95].

### **1.5.1. PPIX-mediated skin damage.**

Metal-free PPIX is an endogenously produced photosensitizer. An acute, painful and mostly nonblistering type of photosensitivity is the most common and significant clinical manifestation of increased metal-free PPIX in the protoporphyrias (EPP and XLP) [69]. To prevent symptoms, patients are forced to avoid light, which interferes with many professional and other every-day activities and impairs quality of life [69]. PPIX either in blood in the dermal vessels or after uptake into skin cells absorbs light energy and transfers this energy to oxygen, generating reactive oxygen species (ROS), which can lead to cytotoxicity through proteins, DNA and lipid damage [96]. These ROS can also cause local vasodilatation and edema by complement activation and mast cell degranulation [97]. Patients who remove themselves from exposure as soon as symptoms begin will recover quickly. Longer exposure can lead to more marked reactions with severe pain, redness, swelling and even blistering, as well as systemic reactions,

and may require several days or more for recovery [98]. Repeated reactions to sunlight can have residual effects, such as waxy thickening of the skin, especially over the knuckles, hands, nose and cheeks, and mild scarring [99]. Because sunlight exposure is avoided, EPP and XLP patients are often vitamin D deficient [100]. Mild microcytic anemia with evidence of iron deficiency is common in EPP and XLP and is poorly understood [101], since elemental iron absorption is not impaired [102].

Closely woven clothing, hats, and gloves are manufactured for patients with protoporphyria and other photosensitizing diseases. Pharmacological approaches have included pharmaceutical-grade  $\beta$ -carotene, narrow wave UVB phototherapy, cysteine, afamelanotide, antihistamines, and vitamin C (Table 1) [100, 103-113]. Minder et al. reviewed the treatment options for dermal photosensitivity in EPP in 2009 and concluded that the data were insufficient to prove efficacy of any treatments studied in EPP [114]. Since then, controlled trials have demonstrated improved light tolerance in EPP and XLP with afamelanotide, an alpha-melanocyte stimulating hormone analogue that increases skin melanogenesis [109-111, 115].

### **1.5.2. PPIX-mediated hepatobiliary disease.**

Because PPIX concentrations in bile are high in EPP and XLP, PPIX-containing gallstones are common and may require cholecystectomy at an early age [116-118]. PPIX-mediated liver damage, which occurs in less than 5% of patients with protoporphyria, is the most serious clinical manifestation and can be life threatening and require liver transplantation. The marrow is the major source of PPIX in EPP and XLP. Hepatic *de novo* synthesis is at best a minor

contributor (**Figure 3**). After uptake from plasma, hepatocytes transport PPIX into bile canaliculi. PPIX is stored and concentrated in the gallbladder and delivered to the small intestine during meals, and some may be reabsorbed in the small intestine and delivered back to the liver by an enterohepatic circulation. This is the only route for excretion of PPIX because it is a large, hydrophobic molecule that cannot be excreted by the kidneys [27, 89].

**Table 2. Pharmacological approaches for management of photosensitivity in EPP patients.**

Approaches	Mechanisms	Outcomes	References
$\beta$ -carotene	<ul style="list-style-type: none"> <li>Prevents penetration of sunlight</li> <li>Acts as a scavenger for reactive radicals</li> </ul>	<ul style="list-style-type: none"> <li>Effective in some patients;</li> <li>Causes yellowing of skin</li> </ul>	[103] [104]
Phototherapy <ul style="list-style-type: none"> <li>Narrow-band ultraviolet B</li> <li>Psoralen ultraviolet A</li> </ul>	<ul style="list-style-type: none"> <li>Increases skin pigmentation and thickness</li> <li>Induces UV tolerance</li> <li>Affects Langerhans cells</li> </ul>	<ul style="list-style-type: none"> <li>Effective in some patients;</li> <li>May potentiate erythema and skin photoaging</li> </ul>	[105] [106]
Cysteine	<ul style="list-style-type: none"> <li>Increase sunlight tolerance</li> </ul>	<ul style="list-style-type: none"> <li>Efficacy not established</li> </ul>	[107]
Afamelanotide	<ul style="list-style-type: none"> <li>Binds to the melanocortin 1 receptor</li> <li>Induces production of eumelanin that serves as a natural filter to reduce all wavelengths of light, quench UV light and decrease free radicals</li> </ul>	<ul style="list-style-type: none"> <li>Decreased photosensitivity and improved quality of life</li> </ul>	[108-114]
Antihistamines	<ul style="list-style-type: none"> <li>Histamine H-receptor antagonists</li> </ul>	<ul style="list-style-type: none"> <li>Limited efficacy</li> </ul>	[100]
Vitamin C	<ul style="list-style-type: none"> <li>Prevent oxidative damage from ROS</li> </ul>	<ul style="list-style-type: none"> <li>Limited efficacy</li> </ul>	[115]

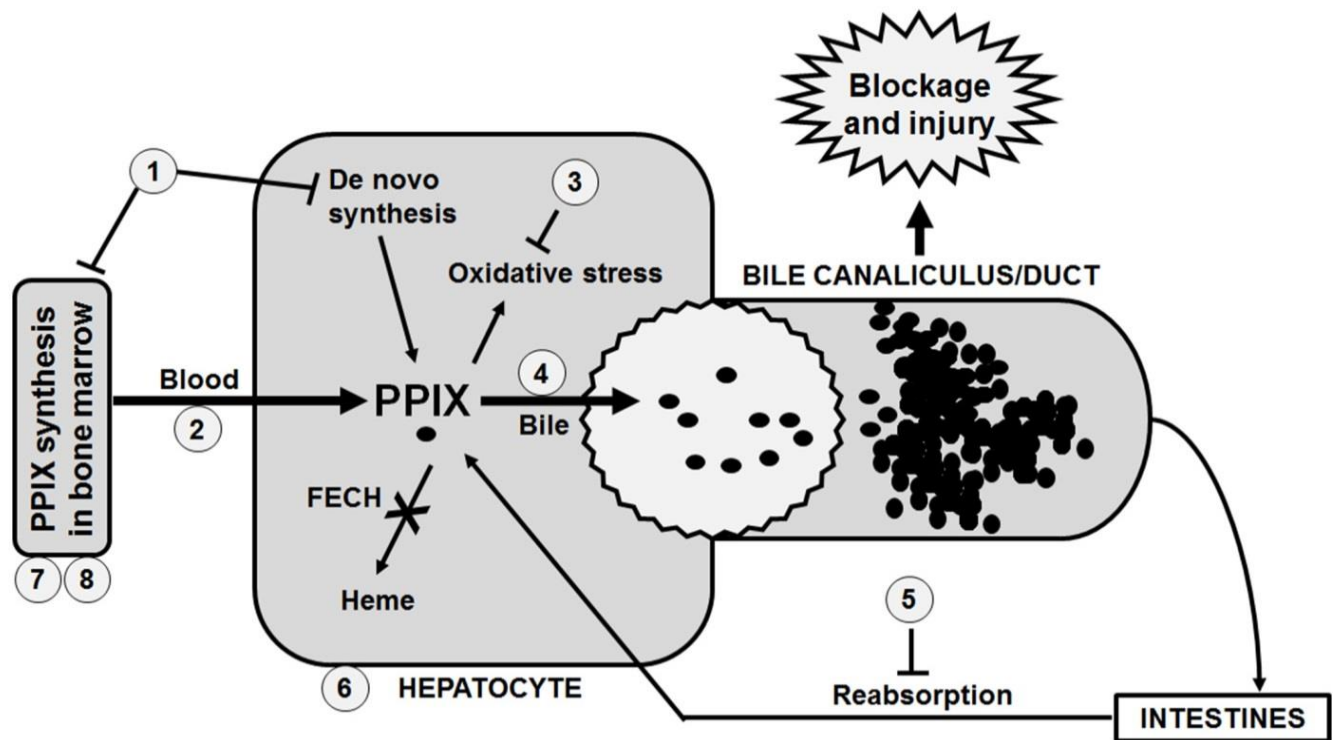


**Figure 7. Mechanisms of PPIX-mediated liver injury and strategies to manage this injury.**

PPIX-mediated hepatocyte and cholangiocyte damage initiates hepatobiliary injury in erythropoietic protoporphyria. Approaches to manage this condition have included (1) suppression of PPIX biosynthesis by hemin; (2) plasmapheresis; (3) vitamin E or *N*-acetyl cysteine to reduce oxidative stress; (4) ursodeoxycholic acid to increase bile flow and PPIX excretion; (5) activated charcoal or cholestyramine to prevent reabsorption of PPIX from the small intestine; (6) liver transplantation; (7) bone marrow transplantation to restore FECH function; and in preclinical models (8) gene therapy targeting FECH.

Large amounts of PPIX are hepatotoxic, damaging both hepatocytes and cholangiocytes. PPIX impairs bile flow when administered in large amounts to bile fistula rodents [119]. Once liver damage ensues, PPIX elimination by the liver is further compromised and levels of PPIX in plasma and erythrocytes can increase progressively, and bile composition becomes altered [120, 121]. Increased delivery of PPIX to the liver can lead to further inflammation and accelerated damage to hepatocytes and cholangiocytes. Liver damage can progress slowly, as indicated by mild and often unexplained abnormal liver function tests, or advance rapidly to hepatic failure with evidence of both acute and chronic liver disease [90, 122, 123]. Treatment with a combination of plasmapheresis to remove PPIX from plasma, hemin infusions to reduce marrow production of PPIX [124, 125], cholestyramine (or activated charcoal) to interrupt the enterohepatic circulation of PPIX [126], bile acids such as ursodeoxycholic acid to enhance bile formation and flow [127, 128], and vitamin E to reduce oxidative stress [129, 130] may achieve remission or slow the progression of liver disease and bridge the patient to hepatic transplantation. Such approaches are depicted in Figure 3. These measures are not always effective and have not been applied in sufficient numbers of patients with hepatopathy to allow rigorous evaluation of efficiency [90, 131]. New approaches to treatment and prevention of this severe complication of protoporphyria are needed.

Survival after liver transplantation for protoporphyric hepatopathy is comparable to that after other liver diseases [132]. However, as overproduction of PPIX by bone marrow continues, protoporphyric hepatopathy may recur [121, 132-135]. Marrow stem cell transplantation after a temporary remission of hepatopathy or liver transplantation can prevent recurrent liver damage [100, 130, 136, 137]. At present, identification in advance of patients at risk for development of

hepatopathy is not possible. Motor neuropathy, which is characteristic of the acute porphyrias but not EPP and XLP, can develop in patients with severe protoporphyric hepatopathy, suggesting that PPIX or a product of PPIX may be neurotoxic under some conditions [138]. Gene therapy targeting FECH, which is undergoing preclinical development, will, like bone marrow transplantation, restore FECH activity in the marrow [139, 140].

### **1.6. PPIX-based strategies for diagnosis and therapy**

PPIX can be activated by light to produce energy in the form of fluorescence and ROS. The photodynamic effect of hematoporphyrin, which is closely related to PPIX and formed by the acid hydrolysis of hemoglobin, was demonstrated in a self-experiment by Meyer-Betz in 1913 [141]. After self-injection of hematoporphyrin, he developed severe swelling of the face and other sun-exposed areas, similar to the phototoxic reactions seen in EPP and XLP. Use of PPIX as a photosensitizer for photodynamic therapy was explored after observing photodynamic effects in erythrocytes of EPP patients containing an excess amount of PPIX [142, 143]. Administration of ALA, which is more stable and readily taken up in tissues in whole animals, leads to dose-related PPIX accumulation in varying amounts in different tissues [144]. Exogenous ALA bypasses the regulatory control of PPIX by ALAS during heme biosynthesis and results in PPIX accumulation. In 1990, ALA was administered locally to generate endogenous PPIX for photodynamic treatment of basal cell carcinomas [60]. Afterwards, endogenous PPIX-based strategies have been used for many clinical applications [145-148]. Thus, ALA can be administered orally or locally as a stable precursor for PPIX. PPIX-based therapy is now approved by the Food and Drug Administration for treatment of bronchial and

esophageal cancers and early malignant lesions of the skin, bladder, breast, stomach, and oral cavity [9, 149-152].

Cancer cells accumulate a higher amount of PPIX than normal cells when treated with ALA [153]. Photoactivation of PPIX in cancer cells generates ROS, which can cause apoptosis and necrosis by attacking mitochondrial and cytoplasmic proteins and destroying cell membrane integration [154, 155]. ROS generated from PPIX also damages blood vessels leading to vascular occlusions, which deprives the tumor of oxygen and nutrients, thereby impairing tumor growth [156]. ROS can also elicit an immune response that suppresses tumor growth [157-160]. Photodynamic effects of PPIX have also been used for cancer diagnosis. PPIX emits red fluorescence when irradiated with light at wave lengths of 400-410 nm, making cancerous lesions that have higher concentrations or less overlying epithelium than surrounding tissue more visible [148].

In addition to cancer therapy and diagnosis, the photodynamic effects of endogenously generated PPIX have been used for the treatment of acne, sebaceous skin, rosacea, rhinophyma, Bowen's disease, androgenic alopecia, cosmetic enhancement, and photo rejuvenations [161, 162]. Furthermore, PPIX-based strategies have been explored against gram positive and negative bacteria, parasites, yeasts, and fungi [163-168].

## 1.7. Conclusions

PPIX homeostasis can be disturbed by effects on enzymes in the heme biosynthetic pathway (e.g. ALAS, PPOX and FECH), transporters of pathway intermediates and iron supply. In EPP and XLP, which are caused by loss of function FECH mutations and gain of function of ALAS2 mutations respectively, PPIX accumulates initially in the marrow and causes painful cutaneous phototoxicity. Excess PPIX in VP is derived from accumulation of protoporphyrinogen IX, the immediate precursor of PPIX. PPIX is water insoluble, and its excretion occurs through the liver and biliary system. An excessive amount of PPIX presented to the liver in EPP and XLP can cause hepatobiliary injury and liver failure. The photodynamic effect of PPIX produced endogenously after ALA administration can be used for cancer diagnosis and treatment. Approaches for management of EPP and XLP are advancing with emphasis on light protection, such as the development of an alpha-melanocyte stimulating hormone that increases skin melanogenesis. Therapies are needed to reduce endogenous PPIX levels in these conditions and to treat and prevent PPIX-mediated liver injury.

## **2. Chronic treatment with isoniazid causes protoporphyrin IX accumulation in mouse liver**

### **2.1. Introduction**

#### **2.1.1. An overview of tuberculosis and isoniazid.**

Tuberculosis (TB) is an airborne infection caused by the bacterium *Mycobacterium tuberculosis* which primarily affects lungs, but can attack other organs like the kidney, brain and spine. TB is one of the most predominant infectious diseases in the world [25]. In 2014 alone, approximately 9.6 million people contracted TB and 1.5 million people died because of it [25]. The majority of people who are infected with TB bacteria do not develop any symptoms, however, are known to have latent tuberculosis (LTBI). Around one-third of the world's population is believed to have LTBI [25]. Around 10% of patients with LTBI develop into an active form. TB is the major cause of death in patients with human immunodeficiency virus (HIV) and is responsible for one third of deaths caused by HIV.

Isoniazid (INH) is the drug of choice for the treatment of LTBI. Treatment of LTBI requires a six to nine months long INH course. INH is used alone or with other first-line drugs for TB

prevention. However, INH can cause hepatotoxicity and even liver failure [169, 170]. The manifestation of jaundice by INH can take around 1-25 weeks of treatment [171, 172]. In the majority of patients on INH treatment, there are no symptoms of liver injury but increased levels of ALT and AST are reported [169, 170]. In 1% of patients on INH treatment it led to severe liver injury [171, 173]. INH mainly causes hepatocellular injury with multilobular necrosis [171]. Mononuclear cell infiltration in the liver is also commonly seen in patients treated with INH [171]. Steatosis and cholestasis are rarely reported in patients treated with INH alone. However, co-treating INH with rifampicin (RIF) is reported to cause steatosis and cholestatic liver injury [174-176].

### **2.1.2. Porphyrinogenic effect of isoniazid.**

A previous study showed that co-treatment of INH and RIF caused the hepatic accumulation of PPIX and liver injury in the pregnane X receptor (PXR)-humanized mice [52]. RIF is a human PXR ligand that induces ALAS1, the rate-limiting enzyme regulating heme and porphyrin biosynthesis [50]. However, the role of INH in PPIX accumulation caused by co-therapy of INH and RIF remains unknown. Also, INH has been found to potentiate griseofulvin-induced hepatic porphyria [177]. Griseofulvin is a model drug used to develop hepatic porphyria by inhibiting FECH and inducing ALAS1 [75, 77, 178]. Furthermore, INH is used with extreme caution in patients with porphyrias, a group of disorders in the heme biosynthesis pathway [126].

### **2.1.3. Experimental design.**

Some reports suggest that INH can interact with the heme biosynthesis pathway [52, 126, 177]. Therefore, the current study was designed to explore the mechanism by which INH interacts with

the heme biosynthesis pathway. Wild-type mice were treated with INH in a time- dependent manner and dose-dependent manner. Untargeted metabolomics were used to analyse the effects on liver metabolome. The effect of INH on the expression and activity of ALAS1 and FECH was analysed. It is anticipated that INH will disrupt heme biosynthesis by dysregulating ALAS1 and FECH.

## **2.2. Material and Methods**

### **2.2.1. Chemicals and reagents.**

INH, PPIX, heme, delta-aminolevulinic acid (ALA), glycine, succinyl-CoA and N-methyl PPIX were purchased from Sigma-Aldrich (St. Louis, MO). All solvents for metabolite analysis were of the highest grade commercially available.

### **2.2.2. Animals and treatment.**

All animal experiments were performed in accordance with the Institutional Animal Care and Use Committee. FVB/NJ mice (male, six weeks old) were purchased from the Jackson Laboratory (Bar Harbor, ME) and were maintained in 12 h light/dark cycle. For the time-dependent effect of INH on the liver, mice were provided with drinking water supplemented with 400 mg/L INH for 0, 3, 7, 14 and 28 days. For the dose-dependent effect of INH on the liver, mice were treated with 0, 100, 200 and 400 mg/L INH in drinking water for 14 days. A slight decrease in water consumption was observed in 200 and 400 mg/L INH groups during INH treatment (Table 2). The computed human equivalent dosage was less than the maximum dosage

recommended in humans (5 mg/kg/day). After INH treatment, all mice were sacrificed. Liver, red blood cells (RBCs), serum, and bone marrow cells (BMCs) were collected for further analysis.

**Table 5. Water consumption of mice treated with isoniazid (INH).**

Mice were treated with 0, 100, 200 and 400 mg/L INH in drinking water for 14 days. All data are expressed as mean  $\pm$  SD (n = 4).

INH treatment (mg/L water)	Daily water intake (ml)	Body weight (g)	Daily water consumption vs body weight (ml/g)	Daily INH dosage (mg/Kg)	Human equivalent dosage (mg/Kg)
0	4.3 $\pm$ 0.3	27.7 $\pm$ 0.9	0.16	N.A.	N.A.
100	4.4 $\pm$ 0.5	24.7 $\pm$ 1.4	0.18	18	1.46
200	3.3 $\pm$ 0.1	26.2 $\pm$ 0.9	0.13	26	2.11
400	3.5 $\pm$ 0.1	24.7 $\pm$ 0.5	0.14	56	4.54

### 2.2.1. Biochemical and pathological analysis.

For the biochemical analysis, the serum alanine transaminase (ALT) level was measured using the standard protocol (Abcam, Cambridge, MA). For the pathological analysis, liver tissue was fixed in 4% formaldehyde phosphate buffer. The fixed liver tissue was subjected to dehydration

in serial alcohol and xylene concentration and finally embedded in paraffin. Four-micrometer serial sections were cut and stained with hematoxylin and eosin (H&E).

### **2.2.2. Metabolomic analysis.**

Liver metabolome was explored using a previously described method [178]. Briefly, 100 mg of liver samples were homogenized in 400  $\mu$ l water. In 100  $\mu$ l of liver homogenate, 200  $\mu$ l methanol was added and then vortexed two times for 1 min. The mixture was centrifuged at 15,000 g for 10 min and the supernatant was centrifuged again at 15,000 g for 10 min. The supernatant was collected and injected into ultra-performance liquid chromatography (UPLC)-quadrupole time-of-flight mass spectrometry (QTOFMS) for metabolite analysis. A Waters Acquity BEH C18 column (2.1  $\times$  100 mm, 1.7  $\mu$ m; Waters Corp, Milford, MA) was used for metabolite separation and the column temperature was maintained at 50  $^{\circ}$ C. QTOFMS (Waters Corp, Milford, MA) was operated in positive mode with electrospray ionization. The source temperatures was set at 150  $^{\circ}$ C and desolvation temperatures were set at 500  $^{\circ}$ C. Nitrogen was applied as cone and desolvation gas. Capillary voltage was set at 0.8 kV and cone voltage was set at 40 V. QTOFMS was calibrated with sodium formate and monitored by the intermittent injection of lockspray leucine enkephalin. MS data were acquired over a range of 50-1000 Da at a rate of 0.1 scans/second in centroid format.

### **2.2.3. Data analysis**

MassLynx 4.1 was used to acquire mass spectra in centroid format from m/z 50 to 1000. Using progenesis QI software (Waters) through deconvolution, recognition, peak alignment,

deisotoping, and integration, a multivariate data matrix containing ion identity (retention time and m/z), sample identity, and ion abundance was generated. Each ion's intensity was computed by normalizing each ion counts with the total ion counts in the chromatogram. Next, the data matrix was further exported into SIMCA-P+ software (Version 13, Umetrics, Kinnelon, NJ). To increase the importance of low abundance ions without amplification of noise, the data was transformed using mean-centering and pareto-scaling. To analyze the inter-relationship among different treatment groups a principal component analysis (PCA) was performed. Orthogonal partial least-squares discriminant analysis (OPLS-DA) was performed to maximize the class discrimination and an S-plot was generated. The metabolites with significant differentiation between the groups were considered as potential metabolites for further analysis. The identities of the ions were searched in metabolomics databases including: METLIN, HMDB and Lipid MAPS and further confirmed by comparing the retention time and MS/MS spectrum with commercially available standards.

#### **2.2.4. PPIX quantification.**

To extract PPIX from RBCs and BMCs,  $10^7$  cells were sonicated in 100  $\mu$ l of methanol and water (v/v, 4:1). To extract PPIX from serum, 80  $\mu$ l methanol was added to 20  $\mu$ l of serum and vortexed twice. To extract PPIX from the liver, 100  $\mu$ l methanol and 100  $\mu$ l acetonitrile was added to 100  $\mu$ l of homogenate prepared for metabolite extraction. The mixture was vortexed and then centrifuged at 15,000 g for 10 min. Analysis of PPIX was conducted using UPLC-QTOFMS. One microliter of the sample was injected onto the UPLC-QTOFMS system for analysis of PPIX. Chromatographic separation of PPIX was achieved on an Aquity BEH C18 column (2.1  $\times$  50 mm, 1.7  $\mu$ m, Waters). The flow rate of the mobile phase was 0.40 ml/min and

the column temperature was maintained at 50 °C. The mobile phase A (MPA) 2mM NH<sub>4</sub>HCO<sub>3</sub> was in water containing 0.05% of ammonia water, and the mobile phase B (MPB) 2mM NH<sub>4</sub>HCO<sub>3</sub> was in water/acetonitrile (5:95, v/v) containing 0.05% of NH<sub>4</sub>OH solution. The gradient began at 30% MPB, followed by 2.5-min linear gradient to 65% MPB, then increased to 90% MPB in 0.5 min and held for 2 min, finally decreasing to 30% MPB for column equilibration. The QTOFMS system was operated in positive resolution mode (resolution ~ 20,000). The source and desolvation temperatures were set at 150 °C and 500 °C, respectively. Nitrogen was applied as cone and desolvation gas. Capillary and cone voltages were set at 0.8 kV and 40 V. QTOFMS was calibrated using sodium formate and monitored by the intermittent injection of lockspray leucine enkephalin. The MS scan of m/z 563.27 was used for PPIX quantification. The data were acquired using Masslynx 4.1 and quantified by QuanLynx.

#### **2.2.5. FECH activity assay.**

FECH activity assay was performed using the previously described methods [179-181]. In brief, 5 µg of liver mitochondria was added to 100 µl of 50 µM PPIX (100 mM Tris-HCl, pH 8.0, 1 mM DTT, 0.1% (v/v) Triton X-100). To initiate a reaction, an equal volume of 100 µM iron citrate prepared in 100 mM Tris-HCl (pH 8.0) was added. Incubations were carried out at 37 °C for 1 hr in the dark. Twice the volume of methanol was added to stop the reaction. The mixture was vortexed for 1 min and then centrifuged at 15,000 g for 10 min. The supernatant was collected for analysis of heme using UPLC-QTOFMS. One microliter of the sample was injected onto the UPLC-QTOFMS system for analysis of PPIX. Chromatographic separation of heme was achieved on an Aquity BEH C18 column (2.1 × 50 mm, 1.7 µm, Waters). The flow rate of the mobile phase was 0.40 ml/min and the column temperature was maintained at 50 °C. The

mobile phase A (MPA) 2mM  $\text{NH}_4\text{HCO}_3$  was in water containing 0.05% of ammonia water, and mobile phase B (MPB) 2mM  $\text{NH}_4\text{HCO}_3$  was in water/acetonitrile (5:95, v/v) containing 0.05% of  $\text{NH}_4\text{OH}$  solution. The gradient began at 30% MPB, followed by 2.5-min linear gradient to 65% MPB, then increased to 90% MPB in 0.5 min and held for 2 min, finally decreasing to 30% MPB for column equilibration. The QTOFMS system was operated in positive resolution mode (resolution  $\sim 20,000$ ). The source and desolvation temperatures were set at 150 °C and 500 °C, respectively. Nitrogen was applied as cone and desolvation gas. Capillary and cone voltages were set at 0.8 kV and 40 V. QTOFMS was calibrated with sodium formate and monitored by the intermittent injection of lockspray leucine enkephalin. The MS scan of  $m/z$  616.17 was used for heme quantification. The data were acquired using Masslynx 4.1 and quantified by QuanLynx.

#### **2.2.6. ALAS activity assay.**

ALAS activity was analyzed using the mitochondria isolated from the liver of mice treated with INH. The assay was conducted using a previous protocol with slight modification [182]. Briefly, 50  $\mu\text{g}$  of mitochondria was incubated in 100  $\mu\text{l}$  glycine buffer (35 mM Tris-HCl, pH 7.4, 30 mM  $\text{Na}_2\text{HPO}_4$ , 8 mM  $\text{MgCl}_2$ , 0.2 mM pyridoxal phosphate, 25  $\mu\text{M}$  succinylacetone, 5 mM EDTA and 150 mM glycine) for 1 h at 37 °C. The product of ALAS was analyzed using UPLC-QTOFMS as described previously [183]. Samples were derivatized by adding 150 $\mu\text{L}$  of solution A: water, 37% formaldehyde, ethanol, and acetyl acetone (107:5:15:23). The mixture was vortexed a few times and heated at 100 °C for 5 min. Afterwards the mixture was kept on ice in the dark until final processing for separation. The derivitized peak corresponding to ALA was separated by the UPLC system on a BEH C18 1.7- $\mu\text{M}$ , 2.1 $\times$ 100-mm column. The solvent system

was 0.2% formic acid in water and acetonitrile with a flow rate of 0.4 mL/min in a 12-min run with a gradient optimized for peak separation. For QTOF system, desolvation gas and cone gas nitrogen was used with a flow rate of 650 and 50 L/h, respectively, and for collision gas argon was used with a flow rate of 0.2 mL/min. The source temperature was set at 120°C and desolvation temperature was at 450°C. QTOFMS was calibrated with sodium formate and monitored by the intermittent injection of lockspray leucine enkephalin. The data were acquired using Masslynx 4.1 and quantified by QuanLynx.

#### **2.2.7. Western blotting.**

Liver homogenates were used for analysis of ALAS1 and FECH proteins. Briefly, 50 µg of proteins per sample were resolved using 10% SDS-polyacrylamide gels and transferred to an Immobilon-P membrane (Millipore, Bedford, MA). The membrane was incubated with anti-ALAS1 (1:5000, Abcam, ab84962) and anti-FECH (1:1000, Santa Cruz, sc-377377) antibodies, respectively. Subsequently, the membrane was incubated with DyLight 800 4X PEG conjugated goat anti-rabbit (1:10,000, Thermo Scientific, SA5-35571) and DyLight 680 conjugated goat anti-mouse (1:10,000, Thermo Scientific, 35519) secondary antibodies. Protein was visualized using the Odyssey infrared imaging system (LICOR, Lincoln, NE) and was quantified using the Odyssey infrared imaging system application software. K-562 whole cell lysate (Santa Cruz, sc-2203) was used as a positive control of both ALAS1 and FECH. GAPDH was used as a loading control.

### **2.2.8. Real-time PCR.**

RNA in the liver was isolated using Trizol®. cDNA was reverse transcribed from total RNA using Superscript3 (Invitrogen, Carlsbad, CA). Real-time quantification of mRNA was conducted using the QuantStudio™ 6 Flex real-time PCR system (Applied Biosystems, Foster City, CA) and the SYBR Green PCR master mix. The target mRNA expression was normalized against cyclophilin expression.

### **2.2.9. Statistical analysis.**

All the data were expressed as means  $\pm$  SD. Statistical significance between two groups was determined by two-tailed Student's t-test. Statistical significance among three or four groups was determined by Analysis of variance (ANOVA), followed by a Tukey post hoc test for multiple comparisons in reference to the control group. A P value less than 0.05 was considered as statistically significant.

## **2.3. Results**

### **2.3.1. Effect of INH on liver injury.**

Treatment for LTBI requires a 6-9 months INH course. Therefore, we treated mouse with the maximum recommended human equivalent dose of 400mg/L INH in drinking water. Mice were sacrificed after 0,3,7,14, and 28 days of INH treatment. Liver histological analysis showed that chronic treatment with INH did not cause liver injury in mice (**Figure 4A, 4B, 4C, 4D and 4E**).

Liver injury marker serum ALT levels increased over time but the levels of serum ALT levels

were in normal range (**Figure 4F**). These results clearly showed that chronic INH treatment did not cause liver injury.

### **2.3.2. Effect of INH on PPIX homeostasis in the liver.**

Untargeted metabolomic analysis showed liver metabolome was dramatically altered after INH treatment. The PCA analysis clearly separated the untreated group from the INH-treated groups (**Figure 5A**). The S-plot generated from OPLS-DA showed the ion contribution to the group separation of the untreated and treated groups (**Figure 5B**). The number 1 ranking ion was identified as PPIX (**Figures 5B, 6A and 6B**). The structure of PPIX was confirmed by comparing the extracted ion chromatograph and the MS/MS spectra with the standard PPIX (**Figure 6A and 6B**). It was further confirmed that INH-mediated PPIX accumulation in the liver is time-dependent (**Figure 6C**) and dose-dependent (**Figure 6D**). These data suggest that INH disturbs PPIX synthesis and/or metabolism.

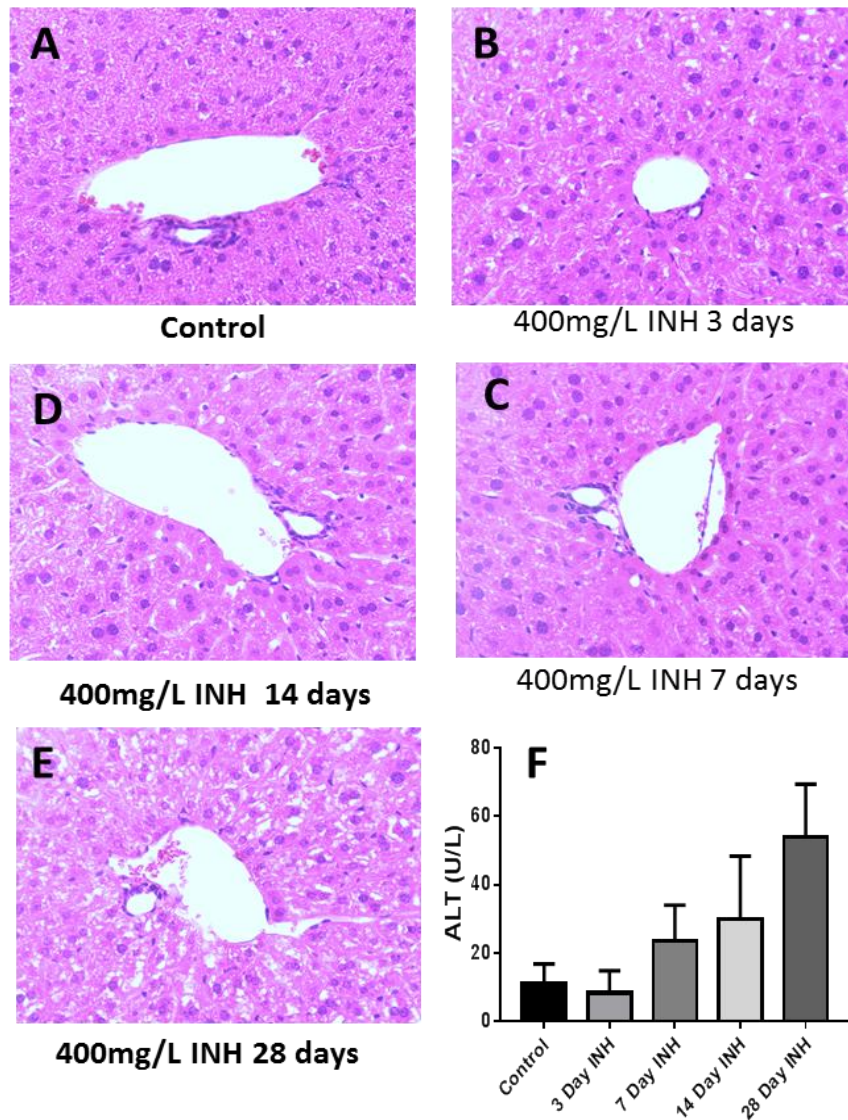


**Figure 10. Evaluation of liver damage in mice treated with INH.**

(A-E) Histological analysis of the liver in mice treated with 400 mg/L INH in drinking water for 0 (A) 3 (B), 7 (C), 14 (D) and 28 (E) days. H&E staining, 200 X. (F) Serum activity of ALT in mice treated with INH for 0-28 days. All data were expressed as means  $\pm$  SD (n = 3 or 4). No statistical difference was observed from day 0 to day 28.

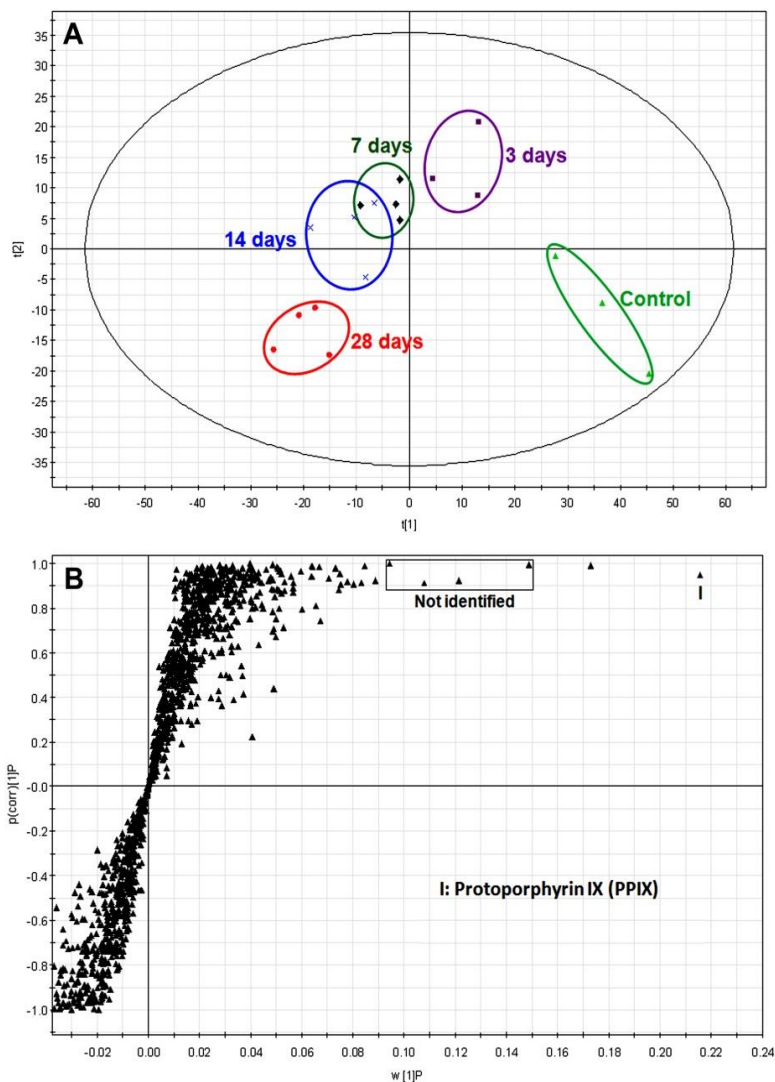


**Figure 13. Effect of INH on mouse liver metabolome.**

The mice were treated with 400 mg/L INH in drinking water for 0-28 days. Liver samples were analyzed by UPLC-QTOFMS in positive mode. (A) Separation of liver samples from the control and INH-treated mice in a PCA score plot. The  $t[1]$  and  $t[2]$  values represent the score of each sample in principle component 1 and 2, respectively. (B) Loading S plots of liver samples generated by OPLS-DA analysis. The  $x$ -axis is a measure of the relative abundance of ions, and the  $y$ -axis is a measure of the correlation of each ion to the model. The number 1 ranking ion was identified as PPIX

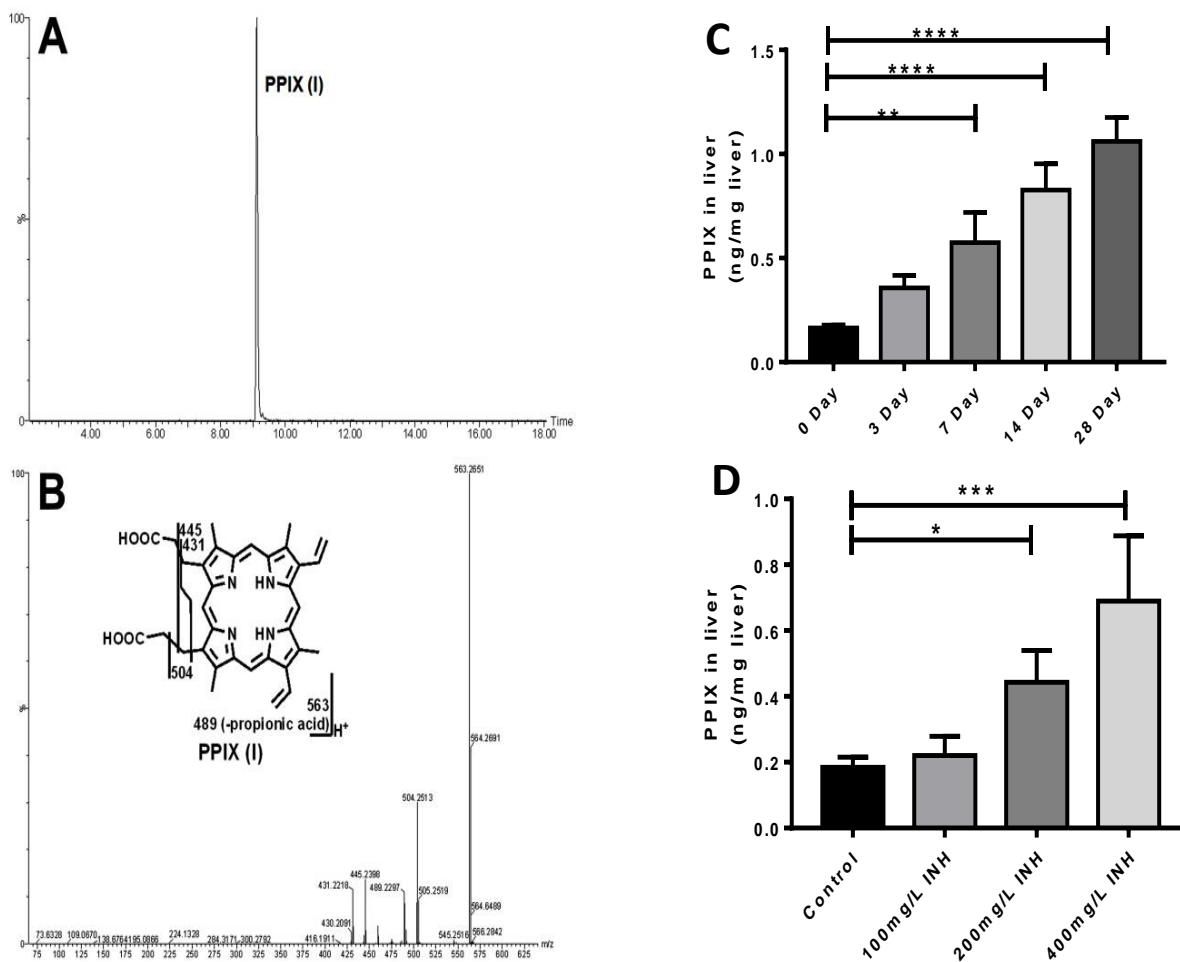


**Figure 16. Identification and quantification of PPIX.**

(A) Extracted chromatogram of PPIX. (B) MS/MS of PPIX. (C) Time-dependent accumulation of PPIX in the liver of mice treated with 400 mg/L INH in drinking water for 0–14 days. (D) Dose-dependent accumulation of PPIX in the liver of mice treated with 0, 100, 200, or 400 mg/L INH in drinking water for 14 days. \* $P < 0.05$ , \*\*\* $P < 0.001$  vs control (n = 3 or 4).

### **2.3.1. Effect of INH on PPIX levels in BMCs, serum and RBCs.**

Because bone marrow is the major resource of PPIX production,[11] we next investigated the effect of INH on PPIX levels in BMCs, serum and RBCs. We find that treatment with INH does not alter PPIX levels in BMCs, serum or RBCs (**Figure 7**), indicating that INH has no effect on PPIX synthesis and/or metabolism in the bone marrow. In addition, we excluded the possibility of INH-mediated erythrocytes congestion in the liver by analyzing liver histology (**Figure 4**) and hemoglobin (**Figure 8**).

### **2.3.2. Effect of INH on FECH expression and function in the liver.**

To determine the mechanism of PPIX accumulation in the liver, we investigated the effect of INH and its major metabolites on the function of FECH, the enzyme that converts PPIX into heme [11]. We found that INH and its major metabolites have no inhibitory effect on FECH activity (**Figure 9**); suggesting that INH-mediated PPIX accumulation in the liver is not due to the direct inhibition of INH or its metabolites on FECH. We further examined the effect of INH on FECH expression in the liver. We found that INH has no effect on the mRNA expression of FECH in mouse liver (**Figure 10**). Interestingly, treatment of INH decreased the level of FECH protein, which is time-dependent (**Figure 11A and 11B**) and dose-dependent (**Figure 11C and 11D**).

### **2.3.3. Effect of INH on ALAS1 expression and function in the liver.**

ALAS1 is the rate-limiting enzyme in hepatic PPIX synthesis [11, 184]. We found that treatment with INH has no statistically significant effect on mRNA expression of ALAS1 (**Figure 12A and**

12B). However, the levels of ALAS1 protein were significantly increased after INH treatment in both time-dependent (Figure 12C and 12D) and dose-dependent (Figure 12E and 12F) manners. Furthermore, treatment with INH increased ALAS1 activity in mouse liver (Figure 12G).

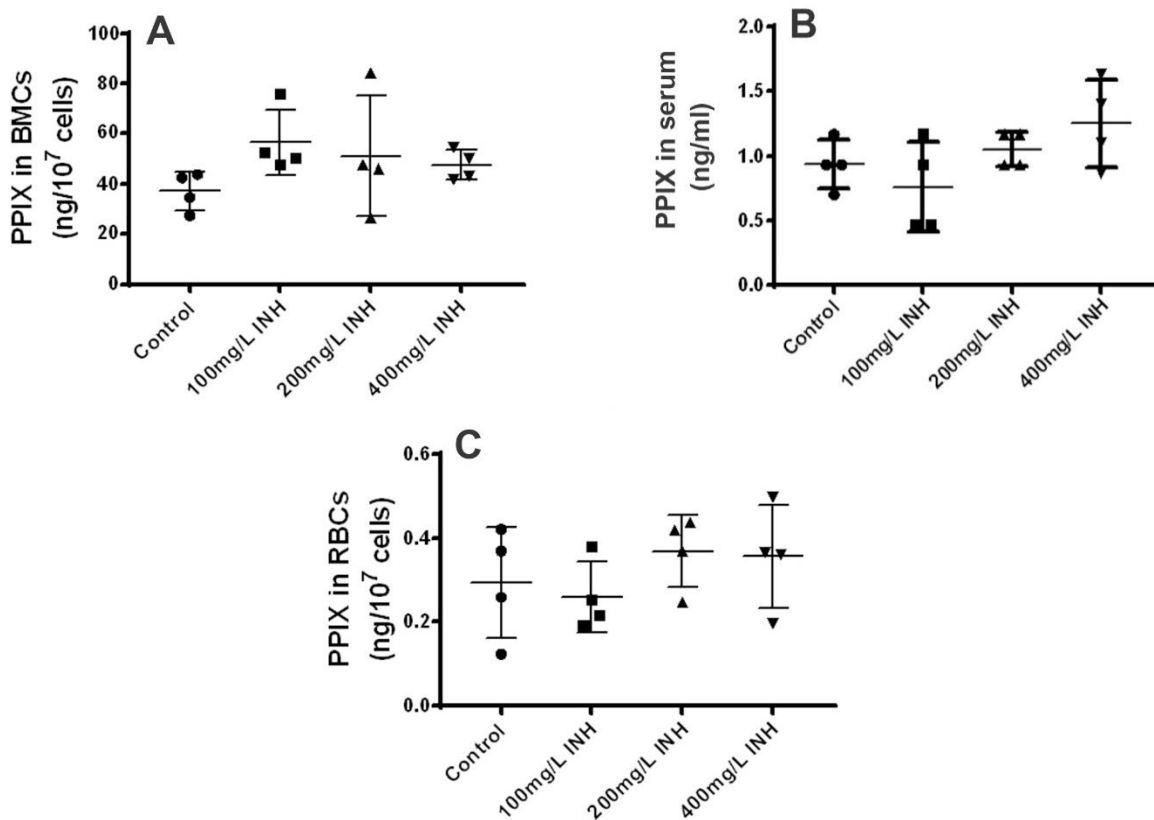


**Figure 19. Effect of INH on PPIX levels in bone marrow cells (BMCs), serum and red blood cells (RBCs).**

The mice were treated with 0, 100, 200, or 400 mg/L INH in drinking water for 14 days. All samples were analyzed by UPLC-QTOFMS in positive mode. (A) PPIX in BMCs. (B) PPIX in serum. (C) PPIX in RBCs. All data were expressed as the mean  $\pm$  SD (n = 4).

**Figure 20. Hemoglobin in the liver of mice treated with INH. Figure 21. Effect of INH on PPIX levels in bone marrow cells (BMCs), serum and red blood cells (RBCs).**

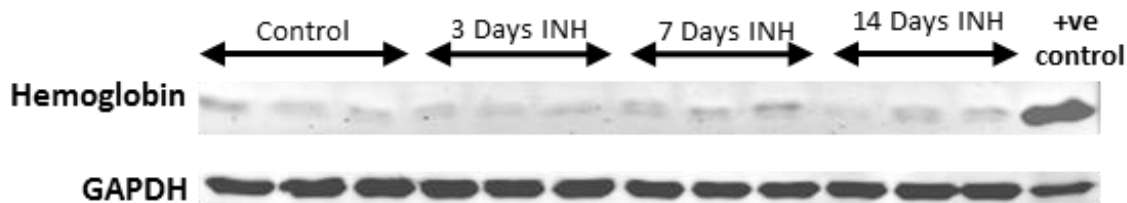


**Figure 22. Hemoglobin in the liver of mice treated with INH.**

Mice were treated with 400 mg/L INH in drinking water for 0-14 days. Hemoglobin was analyzed using western blotting. GAPDH was used as loading control.

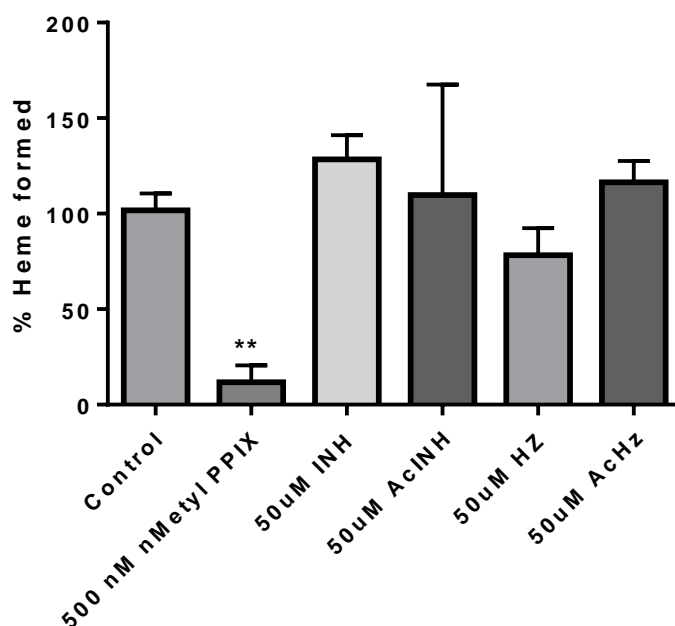


**Figure 25. Effect of INH and its metabolites on FECH activity.**

Liver mitochondria of WT mice were used for analysis of FECH activity. All data were expressed as means  $\pm$  SD (n=3). The data in control group was set as 100%. \*\* $P < 0.01$  vs control. N-methyl PPIX was used as a positive control. AcINH, acetyl isoniazid; Hz, hydrazine; AcHz, acetyl hydrazine.

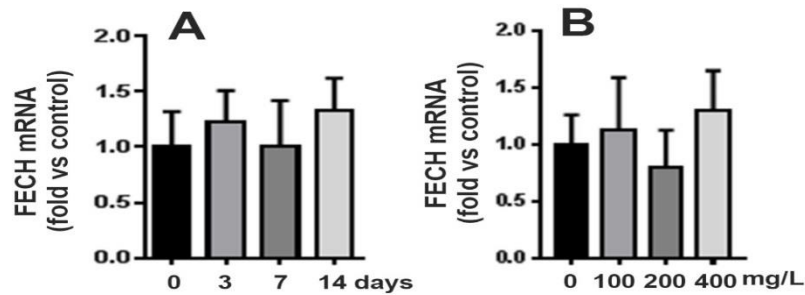


**Figure 310. Effect of INH on FECH mRNA expression in mouse liver.**

The liver samples were analyzed using qPCR. (A) FECH mRNA expression in the liver of mice treated with 400 mg/L INH in drinking water for 0-14 days. (B) FECH mRNA expression in the liver of mice treated with 0, 100, 200 and 400 mg/L INH in drinking water for 14 days. All data were expressed as mean  $\pm$  SD (n = 4). The data in the control group

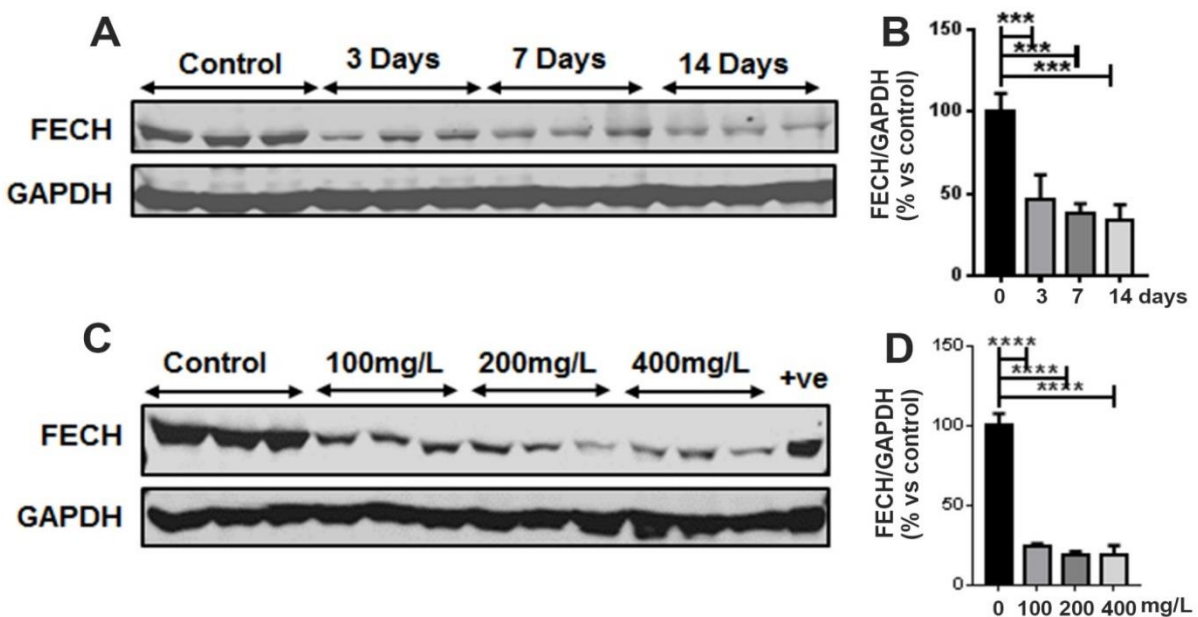
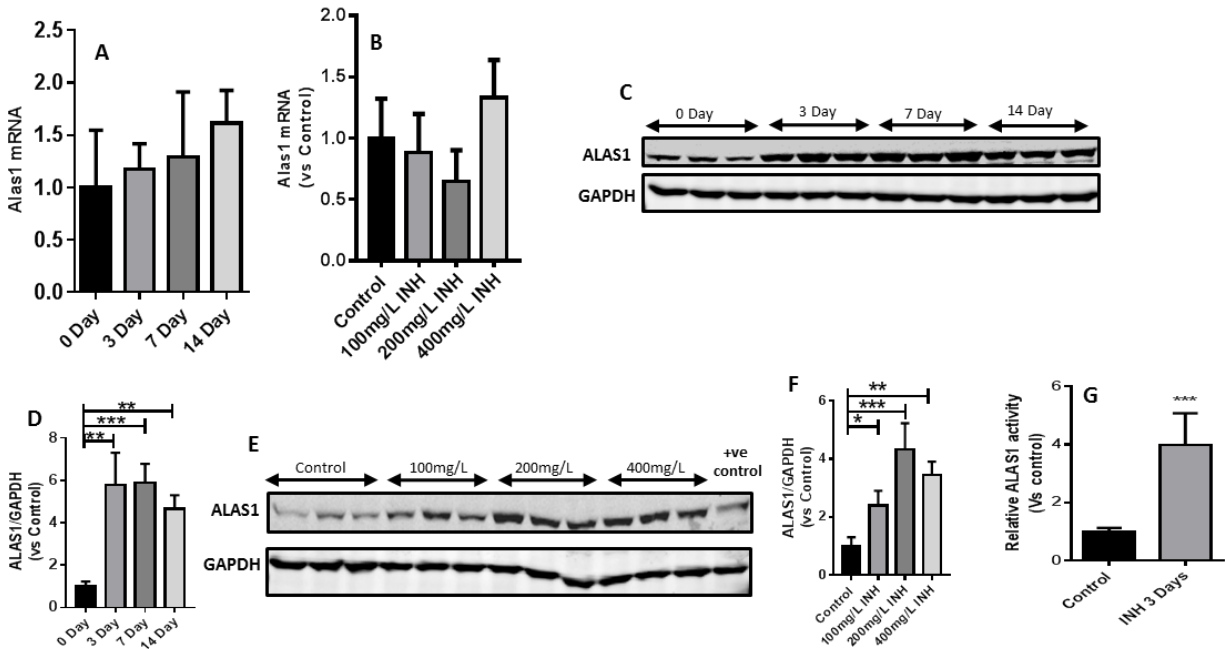


**Figure 31. Effect of INH on FECH expression in the liver.**

FECH protein was analyzed by western blotting. GAPDH was used as loading control. (A and B) FECH expression in liver of mice treated with 400 mg/L INH in drinking water for 0-14 days. (C and D) FECH expression in liver of mice treated with 0, 100, 200 or 400mg/L INH in drinking water for 14 days. All data were expressed as mean  $\pm$  SD (n=3). The data in control group were set as 100%. \*\*\* $P$  < 0.001, \*\*\*\* $P$  < 0.0001 vs control.

**Figure 32. Effect of INH on ALAS1 expression and activity in the liver.** **Figure 33. Effect of INH on FECH expression in the liver.**



## 2.4. Discussion

In the current study, we explored the effect of INH on mouse liver metabolome using untargeted metabolomics. We found that INH causes PPIX accumulation in the liver through ALAS1 induction and FECH downregulation. This discovery explains why INH potentiates drug-induced hepatic porphyria, such as rifampicin and griseofulvin [52, 177]. In addition, this study provides a mechanistic understanding of contraindication of INH in patients with porphyrias [126]. Furthermore, this project provides a novel insight into the mechanism of INH-induced liver injury. PPIX is mainly produced in the bone marrow and secondly in the liver [11, 184]. PPIX produced in the bone marrow is transported to serum through RBCs and then up taken by hepatocytes [90]. Therefore, we first examined the effect of INH on PPIX levels in bone marrow, RBCs, and serum. We found that treatment with INH has no significant effect on PPIX levels in BMCs, RBCs and serum, suggesting INH-mediated PPIX accumulation in the liver is not through the bone marrow. We next investigated the effect of INH on ALAS1 and FECH, the enzymes that are involved in PPIX synthesis and metabolism, respectively [185-187]. We found that INH and its metabolites have no inhibitory effect on FECH activity, suggesting that INH-mediated PPIX accumulation in the liver is not due to the direct inhibition of FECH. Interestingly, INH significantly decreases the FECH protein level without affecting the FECH mRNA level in the liver. We also found that INH had no significant effect on mRNA expression of ALAS1 in the liver but the protein expression of ALAS1 was significantly induced after INH treatment. This is similar to INH-mediated upregulation of CYP2E1, in which INH increases the CYP2E1 expression at the protein level but not at the mRNA level [188-190]. These data suggest that INH stabilizes the ALAS1 protein and increases PPIX production.

Hepatic accumulation of PPIX causes liver injury [90, 131, 184]. Accumulation of PPIX in the liver is associated with increased protein oxidation, decreased proteasome activity, and disruption of mitochondrial function [184, 191]. In addition, PPIX inhibits cytochrome P450 in the liver, which can suppress drug elimination and potentially increase drug toxicity [192]. Furthermore, PPIX is mainly excreted through the biliary system. Excessive PPIX in bile can cause bile duct blockage and cholestatic liver injury [193]. Although INH causes PPIX accumulation in the liver, we did not observe severe liver damage. We expect that co-factors that induce ALAS1 will potentiate INH-mediated liver injury. This is supported by the facts that many ALAS1 inducers can potentiate INH hepatotoxicity [52, 194]. These data suggest that INH can disrupt the metabolic pathway of PPIX and increase the risk of liver damage. Moreover, INH may also disrupt the metabolic pathways of other endobiotics and lead to liver damage.

In summary, this study found that INH causes PPIX accumulation in the liver in part through ALAS1 induction and FECH downregulation. This study also highlights that drugs can interact with metabolic pathways of endobiotics and increase the risk of hepatotoxicity.

### **3. Deficiency of ATP-binding cassette sub-family G member 2 attenuates protoporphyrin IX -mediated liver injury**

#### **3.1. Introduction**

##### **3.1.1. ATP-binding cassette sub-family G member 2 (ABCG2).**

ABCG2 is one of the G subfamily members in the ATP-binding cassette (ABC) protein superfamily. The ABC protein superfamily mainly consists of active transporters that require ATP to pump molecules across the lipid bilayers [195]. Unlike other G subfamily transporters, ABCG2 is a broad range transporter which exports substrate including anions, cations, hydrophobic compounds, and phase II drug conjugates [196-198]. The broad substrate range of ABCG2 helps in protecting against xenobiotics' toxicity specifically in the liver, intestine, blood-brain barrier, and placenta.

ABCG2 is distributed throughout the body to play significant physiological roles in absorption, distribution, metabolism, and excretion (ADME) of xenobiotics. In the small intestine, ABCG2 is expressed on the apical membrane of enterocytes to pump out the absorbed xenobiotic [199]. In the blood-brain barrier and blood-placenta barrier, ABCG2 limits distribution of xenobiotics in the brain and developing fetus, respectively [200, 201]. In the testis, ABCG2 is highly expressed in interstitial cells and Sertoli/Leydig cells to export 2-Amino-1-methyl-6-phenylimidazo[4,5-b]pyridine (PhIP), N-hydroxyl PhIP, dantrolene, and prazosin [202, 203].

ABCG2 is highly expressed in human mammary glands and is strongly induced during lactation to transport vitamins and alter fat and protein content in milk [204-206]. In the kidney, ABCG2 is localized in the cortical tubule, to facilitate in excretion and elimination of xenobiotics [207]. In the liver, ABCG2 is expressed on the canalicular membrane of hepatocytes for biliary excretion of xenobiotics [207]. ABCG2 prevents accumulation by excreting a wide range of xenobiotics such as chemotherapeutics, tyrosine kinase inhibitors, nucleoside, and nucleotide analogs [208, 209]. Apart from xenobiotics, ABCG2 is responsible for pumping endobiotics such as sulfated steroids, unconjugated estradiol, and bile acid cholate [210, 211].

### **3.1.2. Role of ABCG2 in PPIX homeostasis.**

The role of ABCG2 in PPIX transport was first identified using *Abcg2* knockout (*Abcg2*-null) mice generated to investigate the physiological role of ABCG2 in pheophorbide, a chlorophyll-derived dietary toxin [27]. In the liver, ABCG2 excretes PPIX from the hepatocytes into the bile. Thus, PPIX accumulation was slightly higher in the liver of *Abcg2*-null mice as compared to their wild-type counterpart and biliary excretion of intravenously administered PPIX was significantly reduced in *Abcg2*-null mice [89]. Another study showed that in erythroid progenitor cells from mice, ABCG2 is expressed on the cell surface and is upregulated during erythroid differentiation to prevent accumulation of PPIX [93]. Also, RBCs from *Abcg2*-null mice contained around tenfold higher levels of PPIX as compared to control [27]. Patients with *Abcg2*-null genotype also had around a two-fold higher PPIX levels in RBC [212]. Overexpression of *Abcg2* in K562 cells resulted in a significantly lower retention of exogenously provided PPIX or endogenously induced PPIX by ALA treatment but KO143, a specific ABCG2 inhibitor prevented the export of PPIX [93].

### **3.1.3. Animal models used to study PPIX-mediated liver injury.**

Both genetic and drug-induced mouse models are used to examine PPIX-mediated liver injury. We previously reported that treating pregnane X receptor-humanized (hPXR) mice with RIF, and INH co-treatment caused accumulation of PPIX in the liver to cause severe liver injury [52]. RIF is an hPXR inducer which upregulates *Alas1* to potentiate PPIX biosynthesis [50]. Isoniazid induces PPIX accumulation by stabilizing *ALAS1* and decreasing *FECH* [213]. Together INH and RIF induce significant buildup of PPIX in the liver. INH and RIF-induced PPIX accumulation in hPXR mice led to the formation of bile plugs with a significant increase in cholestatic liver injury [52].

DDC and griseofulvin (GSF) are commonly used drugs to generate hepatic porphyria models [75, 214, 215]. Both DDC and GSF cause PPIX accumulation by inducing *ALAS1* expression that results in an increase in PPIX synthesis and inhibition of *FECH* activity that prevents metabolism of PPIX [46, 216-218]. Like EPP patients, mice treated with DDC or GSF also developed bile plugs and increased ductular reaction and pericholangitis [75, 214, 215]. However, DDC or GSF-induced porphyria exhibit a phenotype similar to the EPP patients but was limited to hepatic manifestation only. Also, a mechanism for the development of DDC or GSF induced hepatitis porphyria is different for EPP patients. DDC or GSF-induced PPIX accumulation requires metabolism of DDC or GSF by P450 enzymes; whereas, in EPP patients PPIX accumulation is caused by *FECH* deficiency [216, 217].

The genetic EPP mouse model was generated by Dr. J.C. Deybach's team using chemical mutagen ethylnitrosourea [219]. Similar to EPP patients, genetic EPP mouse model is characterized by photosensitivity, hemolytic anemia, cholestasis, jaundice, and severe hepatic dysfunction [219]. The genetic EPP mouse model contains an inherited Fech mutation (Fech-mut or Fech<sup>m1Pas</sup>/Fech<sup>m1Pas</sup>) which causes a decrease in FECH activity by 90% [220]. Decreased Fech activity results in increased PPIX levels in RBCs, serum, and liver. Unlike humans, hepatic dysfunction always occurs in this mouse model. The genetic EPP mouse model mimics the severe form of the hepatic disease in EPP and has been used extensively to demonstrate the effectiveness of genetic and cellular therapy [221-225].

#### **3.1.4. Experimental Design.**

The objective of this study was to develop a strategy to manage the PPIX-mediated liver injury. Excreted PPIX in the bile precipitates to physically block bile flow and results in cholestatic liver injury [90]. ABCG2 is the key transporter that contributes to the efflux of PPIX from hepatocytes to the biliary system. We anticipate ABCG2 deficiency will decrease PPIX flow into bile preventing liver injury. To evaluate the role of ABCG2 on RIF and INH-induced liver injury, we generated hPXR/Abcg2-null mice and treated them with RIF and INH. To further validate the role of ABCG2 in PPIX-mediated liver injury, Abcg2-null mice were treated with DDC and GSF and the liver injury was evaluated. We also generated a genetic EPP mouse model with Abcg2 deficiency (Fech-mut/Abcg2-null) to assess the effect of Abcg2 deficiency in EPP condition. We anticipate that Abcg2 deficiency in hepatocytes will cause PPIX accumulation in hepatocytes and the liver will detoxify PPIX for elimination.

## **3.2. Material and Methods**

### **3.2.1. Chemicals.**

ALA, RIF, INH, DDC, and GSF were purchased from Sigma-Aldrich (St. Louis, MO). 5-Aminolevulinic-2,2-d<sub>2</sub> acid (D<sub>2</sub>-ALA) was purchased from C/D/N Isotopes Inc. (Pointe-Claire, Quebec, Canada). All solvents for metabolite analysis were of the highest grade commercially available.

### **3.2.2. Animal treatment.**

All mice were kept under standard 12-h light/dark cycle. The handling of mice was in accordance with study protocols approved by the Institutional Animal Care and Use Committee. *Abcg2*-null mice and FVB/NJ (WT) were purchased from Taconic Biosciences, Inc (Hudson, NY), and were used to determine the role of ABCG2 in DDC or GSF-induced liver injury. WT and *Abcg2*-null mice (2-4 months old, male) were fed with control, DDC (100 mg/Kg diet) or GSF (2.5 g/Kg) diet. After two weeks of treatment, mice were sacrificed and blood and liver samples were collected for evaluation of the liver injury.

### **3.2.3. Development and treatment of hPXR/*Abcg2*-null mice.**

To determine the role of ABCG2 in RIF and INH-induced hepatic porphyria in hPXR mice, we generated hPXR mice on the background of *Abcg2*-null mice (hPXR/*Abcg2*-null). Briefly, these mice were generated by crossing hPXR mice with *Abcg2*-null mice. hPXR/*Abcg2*-null mice were verified by genotyping hPXR, mouse *Pxr*, and mouse *Abcg2*. Afterward, hPXR and hPXR/*Abcg2*-null mice (2-4 months old, male) were fed with RIF (100 mg/Kg diet) and INH

(400 mg/L drinking water). After four weeks of treatment, blood and liver samples were collected for evaluation of the liver injury.

#### **3.2.4. Development of Fech-mut (Fech<sup>m1pas</sup>/Fech<sup>m1pas</sup>)/Abcg2-null mice.**

To determine the role of ABCG2 in genetic erythropoietic protoporphyria we generated Fech-mutant (mut) (Fech<sup>m1pas</sup>/Fech<sup>m1pas</sup>) on the background of Abcg2-null mice (Fech-mut/Abcg2-null). Fech-mut mice were purchased from the Jackson Laboratory (Bar Harbor, ME). Fech-mut/Abcg2-null mice were generated by crossing Fech-mut mice with Abcg2-null mice.

Heterozygotes (Fech/Fech<sup>m1pas</sup>/Abcg2<sup>+/-</sup>) obtained were backcrossed with Fech-mut for five generations. Fech-mut/Abcg2-null and Fech-mut mice used for the study were obtained by self-crossing Fech-mut /Abcg2<sup>+/-</sup> mice. Mice were verified by genotyping of Fech point mutation and mouse Abcg2. Two-month-old Fech-mut/Abcg2-null and Fech-mut mice were used to collect liver, spleen, and blood for evaluation of the liver injury. For metabolomics analysis, Fech-mut/Abcg2-null and Fech-mut mice were treated with 50 mg/kg 5-aminolevulinic-2,2-D<sub>2</sub> acid (D<sub>2</sub>-ALA) intraperitoneally and sacrificed after 2 h.

#### **3.2.5. Biochemical and histological analysis.**

ALT, AST and ALP in serum were analyzed according to the procedures of standard assay kits. For histological analysis, liver tissues were fixed in 4% formaldehyde phosphate buffer. Fixed liver tissues were subjected to dehydration in serial concentrations of alcohol and xylene and finally embedded in paraffin. A four-micrometer section of liver tissues was cut and stained with hematoxylin and eosin (H&E).

### 3.2.6. Metabolite analysis.

Liver metabolome was explored using a previously described method [178]. Briefly, 100 mg of liver samples were homogenized in 500  $\mu$ l water. In 100  $\mu$ l of liver homogenate, 200  $\mu$ l methanol was added and then vortexed two times for 1 min. Bile metabolome was explored by adding 1  $\mu$ l of bile into 99  $\mu$ l of acetonitrile:methanol:water (1:1:1) and the mixture was vortexed hard two times for 1 min. Feces metabolome was explored using homogenizing 100 mg feces in 1ml of water. In 100  $\mu$ l of fecal homogenate, 200  $\mu$ l methanol was added and then vortexed two times for 1 min. The mixture was centrifuged at 15,000 g for 10 min and the supernatant was centrifuged again at 15,000 g for 10 min. The supernatant was collected and injected into ultra-performance liquid chromatography (UPLC)-quadrupole time-of-flight mass spectrometry (QTOFMS) for metabolite analysis. A Waters Acquity BEH C18 column (2.1  $\times$  100 mm, 1.7  $\mu$ m; Waters Corp, Milford, MA) was used for metabolite separation. The column temperature was maintained at 50  $^{\circ}$ C. QTOFMS (Waters Corp, Milford, MA) was operated in positive mode with electrospray ionization. The source and desolvation temperatures were set at 150  $^{\circ}$ C and 500  $^{\circ}$ C, respectively. Nitrogen was applied as cone and desolvation gas. Capillary voltage was set at 0.8 kV and cone voltages were set at 40 V. QTOFMS was calibrated with sodium formate and monitored by the intermittent injection of lockspray leucine enkephalin. MS data were acquired over a range of 50-1000 Da at a rate of 0.1 scans/second in centroid format. For data analysis, MassLynx 4.1 was used to acquire mass spectra in centroid format. A multivariate data matrix containing sample identity, ion identity (m/z and retention time) and ion abundance was generated and was exported into SIMCA-P+ (Version 13, Umetrics, Kinnelon, NJ). The data were further analyzed to perform principal component analysis (PCA) and orthogonal partial

least-squares discriminant analysis (OPLS-DA). Using OPLS-DA, S-plot was generated and was used to identify PPIX-metabolites.

### **3.2.7. PPIX and protoporphyrin-1-*O*-acyl-glucouronide quantification.**

PPIX and protoporphyrin-1-*O*-acyl-glucouronide (PPIX-glu) concentrations were measured using UPLC-QTOFMS (Waters Corp, Milford, MA). A serum sample was prepared by adding 70  $\mu$ l of methanol to 30  $\mu$ l of serum, followed by vortexing for 30 s and centrifugation at 15,000 g for 10 min. A liver and spleen sample was homogenized in water (100 mg of liver in 500  $\mu$ l of water) on the ice. Two hundred  $\mu$ l of acetonitrile:methanol (1:1, v/v) was added to 100  $\mu$ l of each homogenate, and followed by vortexing and centrifugation at 15,000 g for 10 min. A RBC sample was prepared by adding 80  $\mu$ l of methanol and 20  $\mu$ l of water to  $10^7$  RBCs, followed by sonication, vortexing, and centrifugation (15,000 g for 10 min). Each supernatant was transferred to an autosampler vial. One microliter of the sample was injected onto the UPLC-QTOFMS system for analysis of PPIX. Chromatographic separation of PPIX was achieved on an Aquity BEH C18 column (2.1  $\times$  50 mm, 1.7  $\mu$ m, Waters). The flow rate of the mobile phase was 0.40 ml/min and the column temperature was maintained at 50  $^{\circ}$ C. The mobile phase A (MPA) 2mM  $\text{NH}_4\text{HCO}_3$  was in water containing 0.05% of ammonia water, and the mobile phase B (MPB) 2mM  $\text{NH}_4\text{HCO}_3$  was in water/acetonitrile (5:95, v/v) containing 0.05% of  $\text{NH}_4\text{OH}$  solution. The gradient began at 30% MPB, followed by 2.5-min linear gradient to 65% MPB, then increased to 90% MPB in 0.5 min and held for 2 min, finally decreasing to 30% MPB for column equilibration. The QTOFMS system was operated in positive resolution mode (resolution  $\sim$  20,000). MS scan of m/z 563.27 for PPIX and 739.30 for PPIX-glu quantification was set. The data were acquired using Masslynx 4.1 and quantified by QuanLynx. MS data were acquired

using Masslynx version 4.1 software and the peak area was quantified using QuanLynx program (Waters Corp, Milford, MA).

### **3.2.8. Synthesis of protoporphyrin-1-*O*-acyl-glucouronide (PPIX-glu).**

To confirm the structure of PPIX-glucuronic acid, we synthesized this metabolite with a two-step procedure shown in **(Figure 20E)** [226]. Briefly, the PPIX was first activated using HATU (1-[bis(dimethylamino)methylene]-1H-1,2,3-triazolo[4,5-b] pyridinium 3-oxid hexafluorophosphate) in the presence of N-methyl morpholine (NMM), then reacted with D-glucuronic acid. To a solution of PPIX (281 mg, 0.5 mmol) and HATU (274 mg, 0.72 mmol) in anhydrous DMF (15 ml), was added NMM (75  $\mu$ l, 0.63 mmol) at room temperature. The solution was stirred for 14 h. Glucuronic acid (168 mg, 0.86 mmol) was added followed by NMM (150  $\mu$ l, 1.26 mmol), and the solution was stirred at room temperature for 14 h. The reaction mixture was injected to UPLC-QTOFMS to confirm the structure of PPIX-glu. The PPIX-glu found in the mouse liver and gall bladder has an identical retention time and MS/MS fragments to the synthetic standard.

### **3.2.9. Statistical analysis.**

Statistical significance between two groups was determined using a two-tailed Student's t-test. Statistical significance among more than two groups was determined by analysis of variance (ANOVA), followed by the Tukey post hoc test for multiple comparisons in reference to the control group. A P value less than 0.05 was considered as statistically significant.

### 3.3. Results

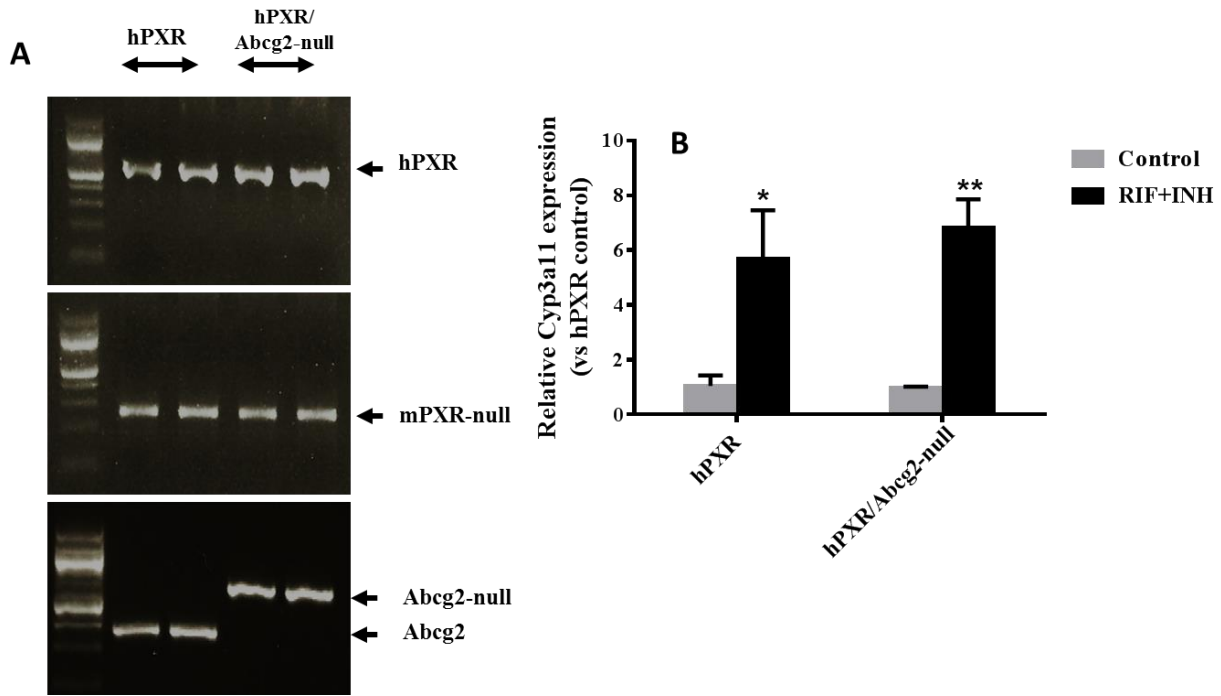


**Figure 13. Generation of hPXR/Abcg2-null mice. (a)** Genotyping results of hPXR and hPXR/Abcg2-null mice. **(b)** Cyp3a11 mRNA was quantified by qPCR. All data are expressed as means  $\pm$  S.D. (n = 4). The data in the control group of hPXR mice was set as 1. \*P < 0.05, \*\*P < 0.01. RIF: rifampicin; INH: isoniazid

#### 3.3.1. Abcg2 deficiency prevents RIF and INH-induced hepatotoxicity.

hPXR/Abcg2-null mice were generated by crossing hPXR mice and Abcg2-null mice.

hPXR/Abcg2-null mice are positive for human PXR but negative for mouse Abcg2 (**Figure 13A**).

To develop the liver injury model, hPXR, and hPXR/Abcg2-null mice were co-treated with RIF and INH for 28 days. Like hPXR mice, Cyp3a11 expression was significantly induced in

hPXR/Abcg2-null mice after the co-treatment of RIF and INH, suggesting hPXR is functional in

hPXR/Abcg2-null mice (**Figure 13B**). As expected, hPXR mice developed significant liver

injury after RIF and INH treatment (**Figure 14**). Moreover, hPXR mice co-treated with RIF and INH had a significant increase in serum ALT, AST and ALP activities. Increased ALP activities suggested cholestasis, and histological analysis showed bile plugs with portal inflammation. Surprisingly, serum ALT, AST and ALP levels in hPXR/Abcg2-null mice co-treated with RIF and INH were in the normal range (**Figure 14A, 14B, and 14C**). Histological analysis also showed bile plugs were absent in hPXR/Abcg2-null mice co-treated with RIF and INH (**Figure 14D**). These results indicate that ABCG2 is crucial for RIF and INH-induced liver injury.

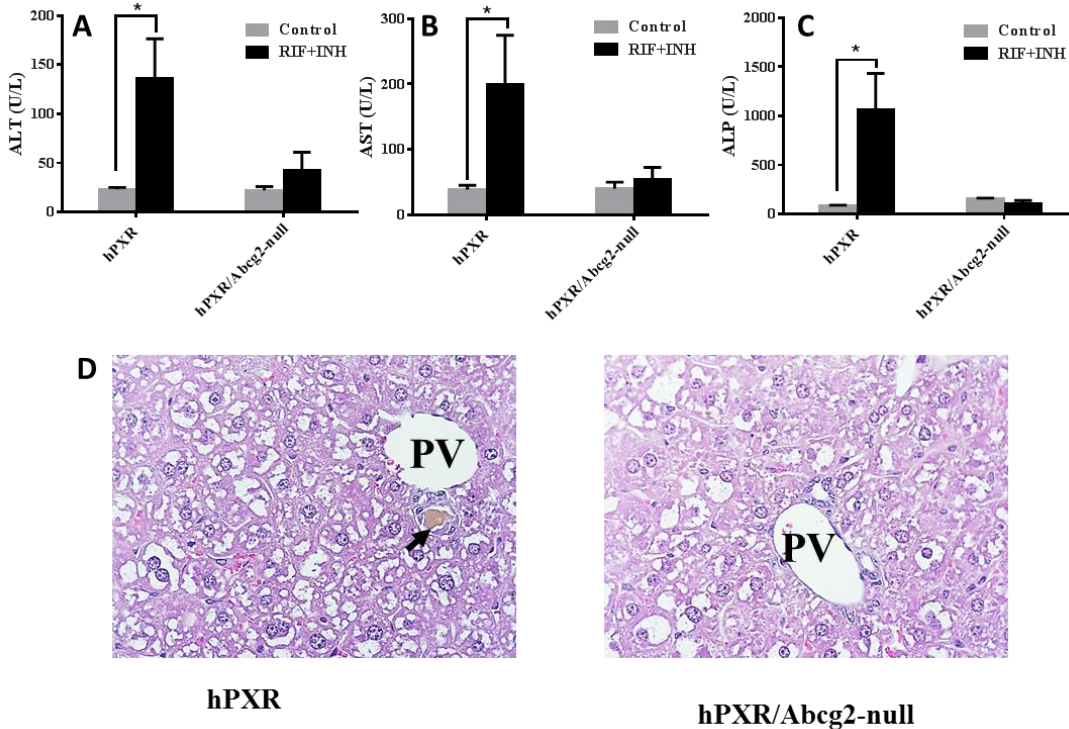


**Figure 14. hPXR/Abcg2-null mice are protected from RIF and INH induced liver injury.**

hPXR and hPXR/Abcg2-null mice were treated with RIF and INH for 28 days. **(A)** Serum activity of ALT. **(B)** Serum activity of AST. **(C)** Serum activity of ALP. **(D)** Histological analysis of liver, H&E staining, 400 X. Arrows point to bile plugs. All data are expressed as means  $\pm$  S.D. (n = 4). \*P < 0.05. RIF: rifampicin; INH: isoniazid; PV: portal vein; BD: bile duct.

### 3.3.2. Abcg2 deficiency prevents DDC-induced liver injury.

Next, we treated WT and Abcg2-null mice with DDC in the diet. After 14 days of DDC treatment, the liver/body weight ratio increased by more than 2-fold in WT mice as compared to the untreated group (**Figure 15A**). Similar to previously published reports, in WT mice DDC treatment caused severe liver injury and significantly increased serum ALT levels to 600 U/L and AST to more than 200 U/L (**Figure 15B and 15C**). The significant cholestatic injury was observed in DDC treated WT mice, and serum ALP levels were increased by more than 1000 U/L with a large number of bile plugs with inflammation confirming cholestasis (**Figure 15D and 15E**). Similar to hPXR/Abcg2-null mice treated with RIF and INH, we found that DDC-induced liver injury was abolished in Abcg2-null mice. We also found that the liver/body weight ratio was unchanged in Abcg2-null mice after DDC treatment (**Figure 15A**). Furthermore, the serum ALT, AST and ALP levels in DDC-treated Abcg2-null mice were in the normal range (**Figure 15B, 15C, and 15D**). Histological analysis also confirmed the absence of bile plugs in DDC-treated Abcg2-null mice (**Figure 15E**). Thus, data clearly indicate that ABCG2 is essential for the development of PPIX-mediated liver injury and loss of ABCG2 prevents the accumulation of PPIX in the bile duct and protects the liver.

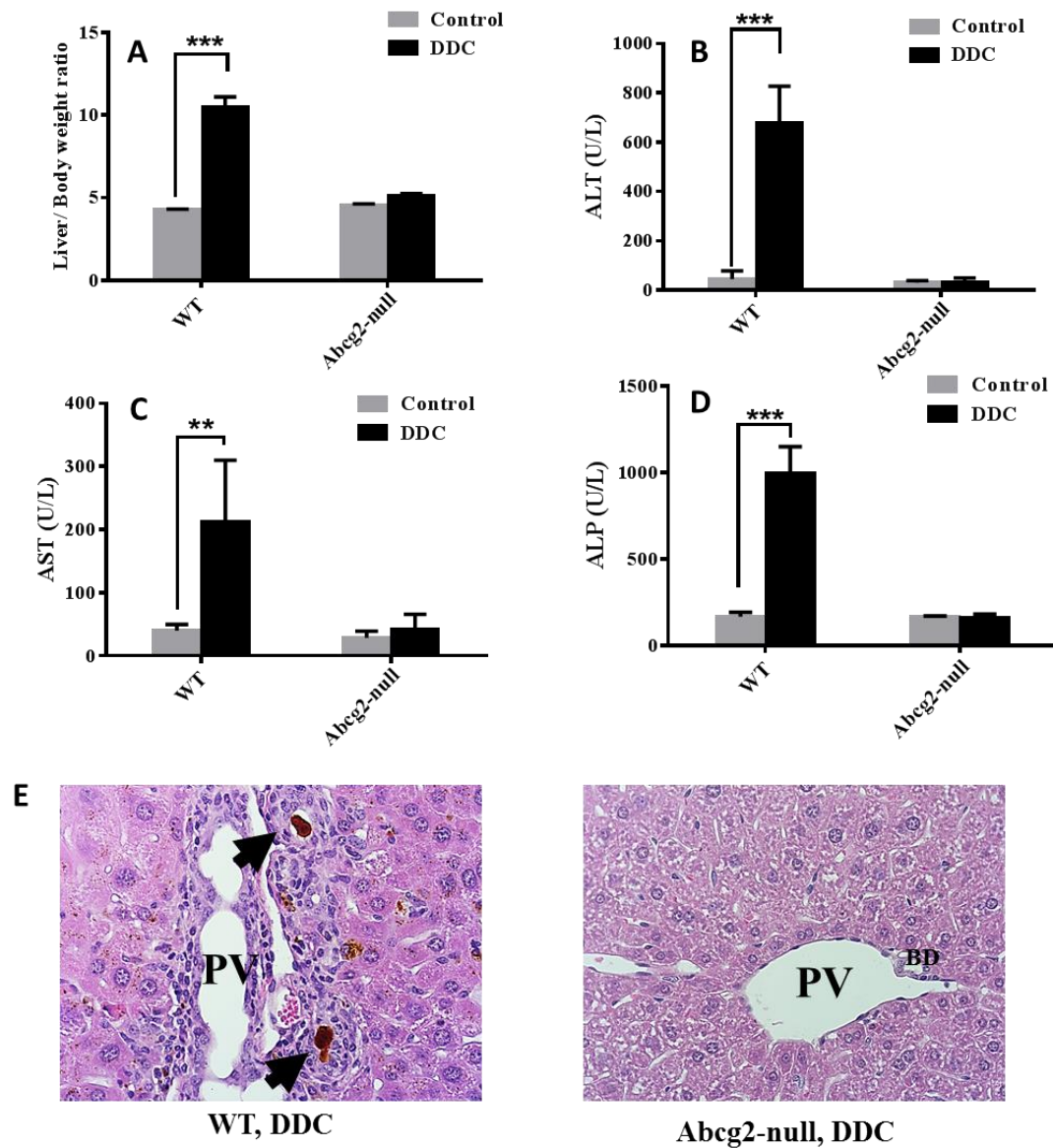


**Figure 15. Abcg2-null mice are protected from DDC-mediated liver injury.** WT and Abcg2-null mice were treated with control, DDC diet for 14 days. **(A)** Liver/Body weight ratio. **(B)** Serum activity of ALT. **(C)** Serum activity of AST. **(D)** Serum activity of ALP. **(E)** Histological analysis of liver, H&E staining, 400 X. Arrows point to bile plugs. All data are expressed as means  $\pm$  S.D. (n = 4). \*\*P < 0.01, \*\*\*P < 0.001. WT: Wild type; DDC: 3,5-diethoxycarbonyl-1,4-dihydrocollidine; PV: portal vein; BD: bile duct.

### 3.3.3. Abcg2 deficiency prevents GSF-induced liver injury.

We further confirmed the role of ABCG2 in PPIX-mediated liver damage by treating WT and Abcg2-null mice with GSF diet for 14 days. GSF treatment increased the liver/body weight ratio by more than 3-fold in WT mice (**Figure 16A**). In GSF treated WT mice, serum ALT increased by more than 1000 U/L as well as the levels of AST increased by more than 600 U/L (**Figure 16B and 16C**). GSF treatment caused severe cholestasis in WT mice; serum ALP increased more than 3000 U/L (**Figure 16D**). Liver histological analysis of WT mice treated with GSF, revealed an abundance of bile plugs (**Figure 16E**). However, with DDC treatment, the liver injury was abolished in GSF treated Abcg2-null mice. Although the GSF treatment increased the liver/body weight ratio by 1.4-fold in Abcg2-null mice, the serum ALT, AST and ALP levels were in normal range (**Figure 16A, 16B, 16C, and 16D**). The liver histological analysis also showed no damage to bile ducts in Abcg2-null mice treated with GSF (**Figure 16E**). Thus confirming Abcg2-null mice were resistant to hepatic porphyria and ABCG2 is a key modulator in hepatic porphyria.

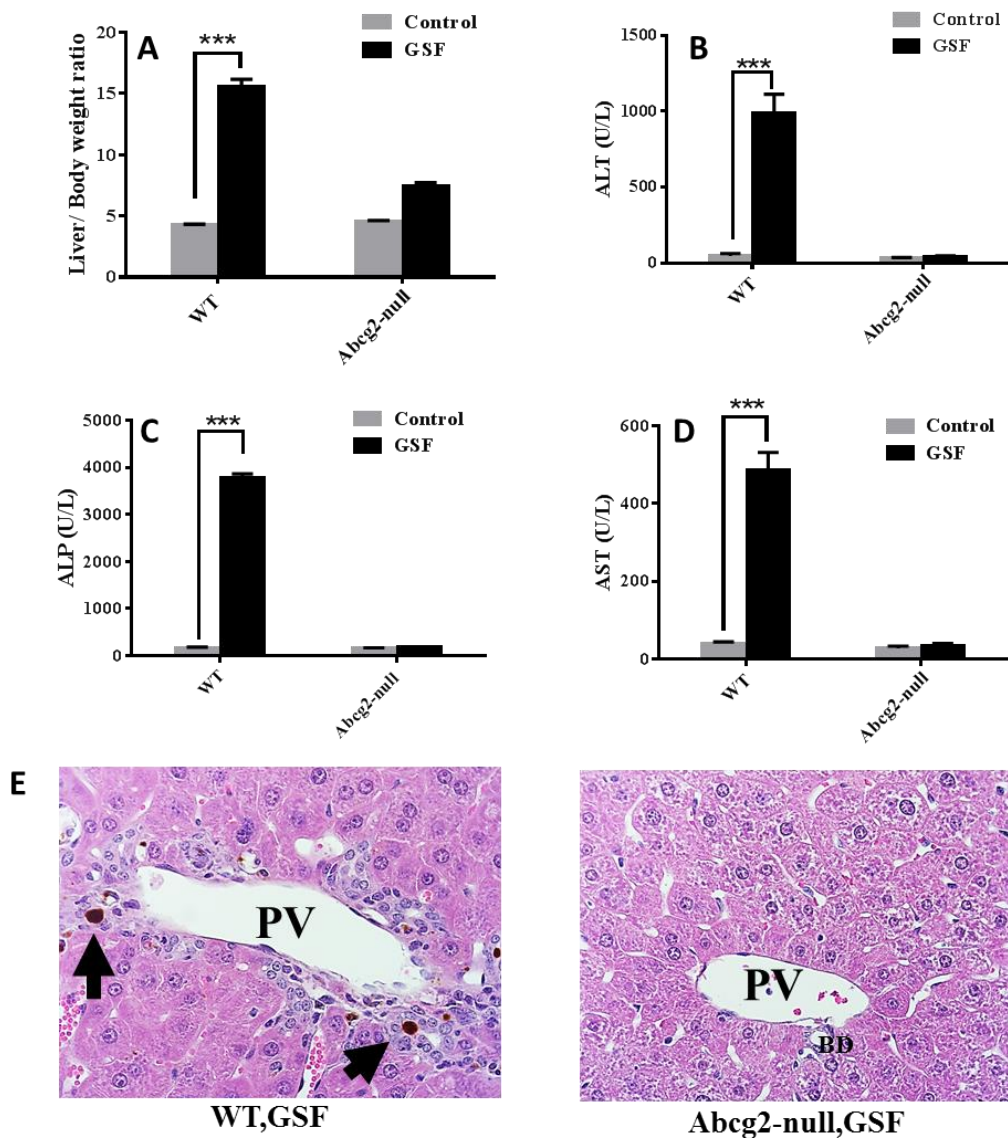


**Figure 16. Abcg2-null mice are protected from GSF-mediated liver injury.**

WT and Abcg2-null mice were treated with control, GSF diet for 14 days. (A) Liver/Body weight ratio. (B) Serum activity of ALT. (C) Serum activity of AST. (D) Serum activity of ALP. (E) Histological analysis of liver, H&E staining, 400 X. Arrows point to bile plugs. All data are expressed as means  $\pm$  S.D. (n = 4). \*\*\*P < 0.001. WT: Wild type; GSF: Griseofulvin; PV: portal vein; BD: bile duct.

#### **3.3.4. Abcg2 deficiency in a genetic EPP mouse model abolishes PPIX-mediated liver injury.**

To further validate the role of ABCG2 in EPP mediated liver injury, we generated Fech-mut/Abcg2-null mice by crossing Fech-mut mice and Abcg2-null mice (**Figure 17A**). Unlike drug-induced porphyria models, in EPP patients PPIX accumulation is caused by defective FECH. Like EPP patients, Fech-mut mice have significantly decreased FECH activity and extensive liver damage caused by PPIX accumulation [219, 220]. Six-week-old Fech-mut mice developed significant liver injury and had significantly increased serum ALT, AST, and ALP levels (**Figure 17B, 17C, and 17D**). Bile plugs with biliary inflammation were also observed in the Fech-mut liver (**Figure 17E**). However, ABCG2 deficiency abolished the liver injury in Fech-mut/Abcg2-null mice (**Figure 17B, 17C, and 17D**). Liver histological analysis of Fech-mut/Abcg2-null mice also showed no portal damage and bile plugs (**Figure 17E**).

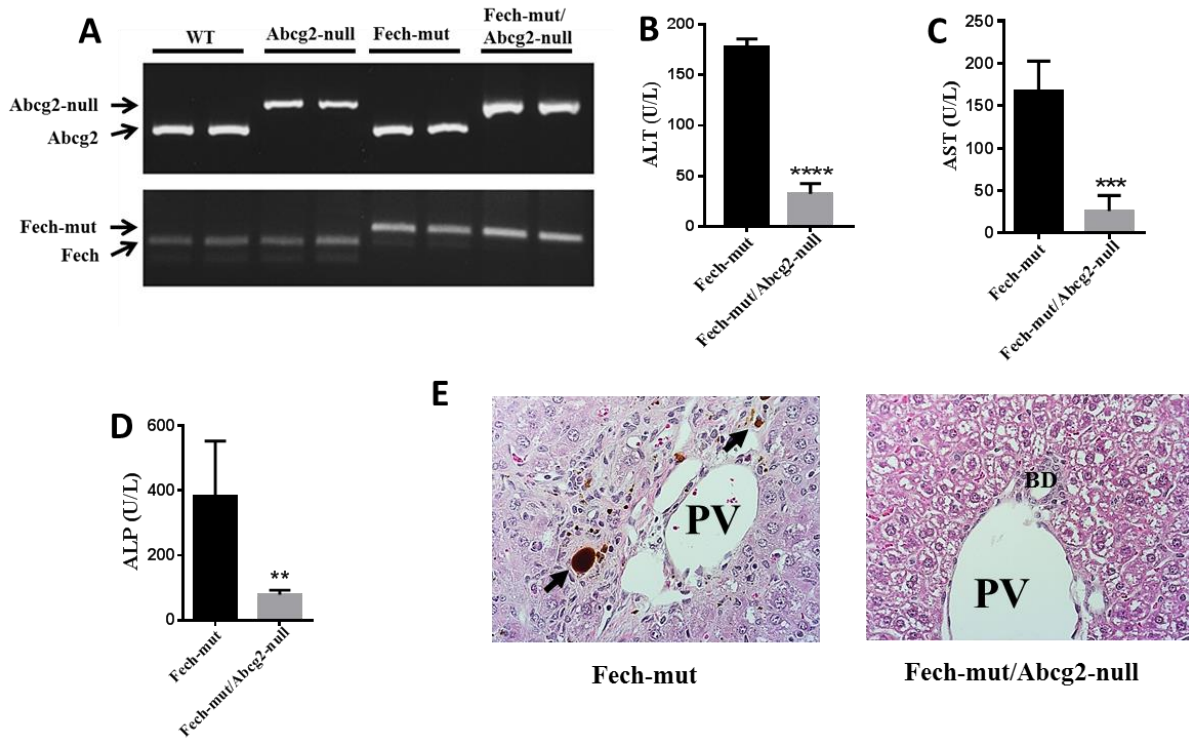


**Figure 17. Fech-mut/Abcg2-null mice are protected from PPIX-induced liver injury. (A)** Genotyping results of Fech-mut and Fech-mut/Abcg2-null mice. **(B)** Serum activity of ALT. **(C)** Serum activity of AST. **(D)** Serum activity of ALP. **(E)** Histological analysis of liver, H&E staining, 400 X. Arrows point to bile plugs. All data are expressed as means  $\pm$  S.D. (n = 4,5). \*\*P < 0.01, \*\*\*P < 0.001, \*\*\*\*P < 0.0001. PV: portal veins; BD: bile duct.

### 3.3.5. Abcg2 deficiency in erythroid progenitor cells of Fech-mut/Abcg2-null mice redistributes PPIX from bone marrow.

Next, we evaluated the role of Abcg2 deficiency on PPIX homeostasis from bone marrow. We found that Abcg2-deficiency in Fech-mut/Abcg2-null mice prevented the excretion of PPIX from RBCs to serum, causing 6-fold increase in RBCs PPIX levels and 80% less PPIX in the serum of

Fech-mut/Abcg2-null mice as compared to Fech-mut mice (**Figure 18A and 18B**). Older RBCs are degraded by spleen and liver for heme recycling. We found that the PPIX level in the spleen of Fech-mut/Abcg2-null mice significantly increased as compared to Fech-mut mice (**Figure 18C**). The liver collects excess PPIX in the serum for fecal excretion. However, decreased serum PPIX resulted in decreased PPIX accumulation in the liver of Fech-mut/Abcg2-null mice as compared to Fech-mut mice (**Figure 18D**). Thus, ABCG2 deficiency prevents the escape of PPIX from RBCs into serum, and part of PPIX formed from bone marrow in Fech-mut/Abcg2-null mice is sequestered in the spleen, decreasing PPIX collected by the liver.

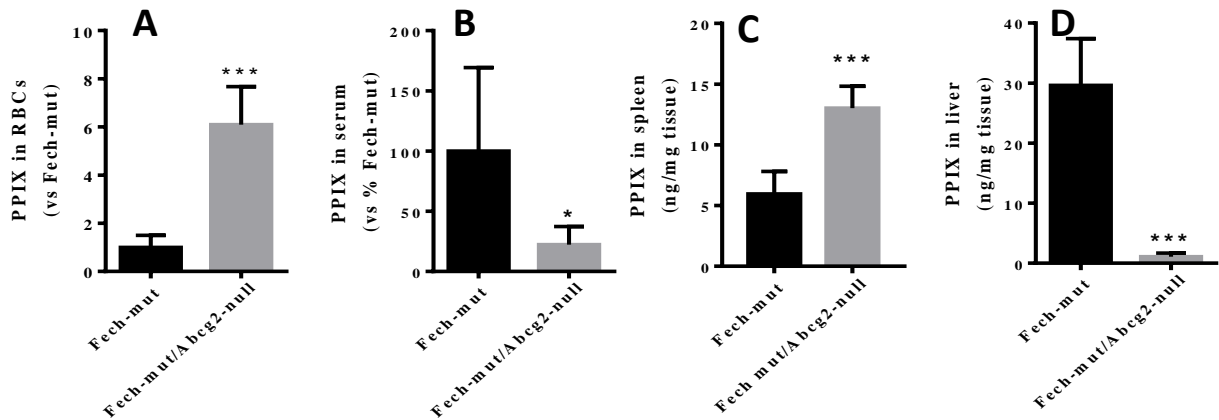


**Figure 18. Redistribution of PPIX produced by bone marrow in Fech-mut/Abcg2-null mice.**

All samples were analyzed by UPLC-QTOFMS in positive mode. PPIX in (A) RBCs, (B) serum, (C) spleen and (D) liver of Fech-mut and Fech-mut/Abcg2-null mice (n=4,5). \*\*P < 0.01, \*\*\*P < 0.001.

### 3.3.6. ABCG2 deficiency in the liver causes PPIX accumulation in hepatocytes.

Although PPIX redistribution decreased PPIX in the liver of Fech-mut/Abcg2-null mice, the accumulation of PPIX due to the treatment of DDC or GSF resulted in the disruption of PPIX homeostasis in the liver. Thus, to investigate PPIX distribution in the case of porphyria and Abcg2-deficiency, we treated Fech-mut/Abcg2-null and Fech-mut mice with 50mg/kg D<sub>2</sub>-ALA intraperitoneally, and samples were collected after 2 h. ALA is a PPIX precursor and in the liver, thus D<sub>2</sub>-ALA is readily converted into D<sub>16</sub>-PPIX (Figure 19A). As expected in Fech-mut/Abcg2-null mice, Abcg2-deficiency in hepatocytes prevented the excretion of PPIX formed causing 4-fold accumulation of D<sub>16</sub>-PPIX in the liver of Fech-mut/Abcg2-null mice as compared to Fech-mut mice (Figure 19B).

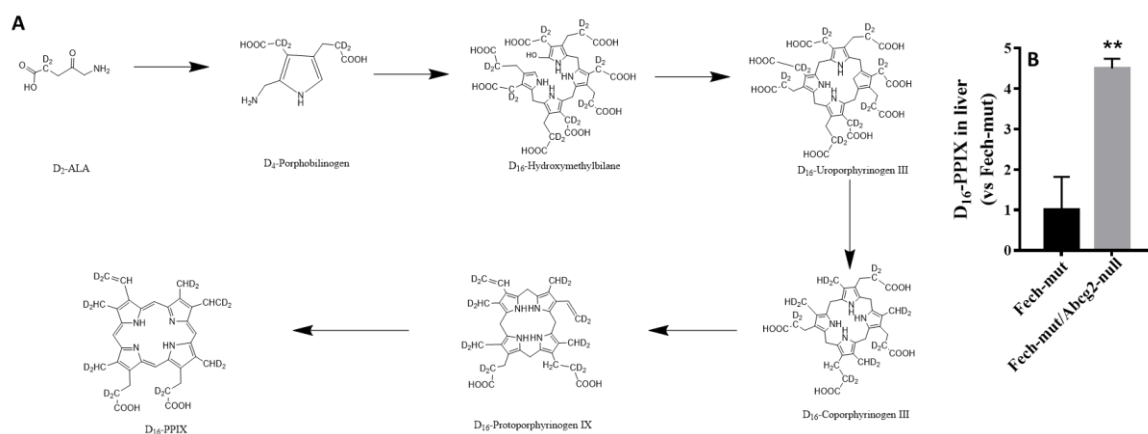


**Figure 19. Formation of D<sub>16</sub>-PPIX in Fech-mut and Fech-mut/Abcg2-null mice liver. (A)** A schematic showing conversion of D<sub>2</sub>-ALA into D<sub>16</sub>-PPIX. **(B)** Quantified PPIX level in liver collected 2h after D<sub>2</sub>-ALA treatment from Fech-mut and Fech-mut/Abcg2-null mice (n=3).

\*\**P*<0.01.

### 3.3.7. ABCG2 deficiency in the liver induces PPIX metabolism to PPIX metabolites.

The liver is a major metabolizing organ which detoxifies molecules for excretion. Thus we performed metabolomic analysis from liver samples of D<sub>2</sub>-ALA treated Fech-mut/Abcg2-null and Fech-mut mice. Clusters of D<sub>2</sub>-ALA treated Fech-mut/Abcg2-null and Fech-mut mice were separated in PCA analysis of liver metabolome (**Figure 20A**). Using OPLS-DA analysis of liver metabolome, the S-plot was generated and depicted ion contribution comparing the D<sub>2</sub>-ALA treated Fech-mut/Abcg2-null and Fech-mut mice groups (**Figure 20B**). We discovered that a novel D<sub>16</sub>-protoporphyrin-1-O-acyl-glucouronide (D<sub>16</sub>-PPIX-glu) conjugate increased in the liver of D<sub>2</sub>-ALA treated Fech-mut/Abcg2-null mice as compared to Fech-mut mice (**Figure 20B**). The structure of D<sub>16</sub>-PPIX-glu conjugate was predicted from the MS/MS spectra (**Figure 20C**). The structure of D<sub>16</sub>-PPIX-glu conjugate was further confirmed by comparing the MS/MS spectra of synthesized protoporphyrin-1-O-acyl-glucouronide (PPIX-glu) conjugate (**Figure 20E and 20F**). After quantifying the D<sub>16</sub>-PPIX-glu conjugate from the liver tissues of D<sub>2</sub>-ALA treated Fech-mut/Abcg2-null and Fech-mut mice, we found that its levels increased very significantly in the liver of Fech-mut/Abcg2-null mice compared to Fech-mut mice (**Figure 20G**).



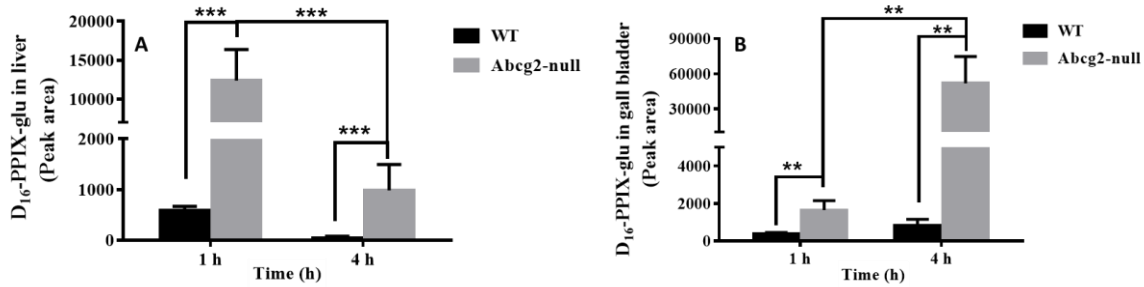


**Figure 21. D16-protoporphyrin-1-O-acyl-glucouronide in WT and Abcg2-null mice.**

WT and Abcg2-null mice were treated with D<sub>2</sub>-ALA for 1 h and 4 h. Liver and gall bladder samples were analyzed by UPLC-QTOFMS in positive mode. (A) Quantified D<sub>16</sub>-PPIX-glu in liver. (B) Quantified D<sub>16</sub>-PPIX-glu in gall bladder (n=4). \*\*P<0.01, \*\*\*P<0.001. WT, wild type; D<sub>16</sub>-PPIX-glu, D<sub>16</sub>-protoporphyrin-1-O-acyl-glucouronide.

Next, we treated Abcg2-null mice with D<sub>2</sub>-ALA and samples were collected post 1 and 4 h of the treatment. We observed that the levels of D<sub>16</sub>-PPIX-glu conjugate significantly increased in the liver of Abcg2-null mice as compared to WT mice (**Figure 21A**). We further showed PPIX-glu conjugate/PPIX levels were also significantly increased in the liver of hPXR/Abcg2-null mice treated with RIF and Abcg2-null mice treated with DDC or GSF (**Figure 22**). Thus, Abcg2 deficiency in hepatocytes significantly increased PPIX conjugation pathway.

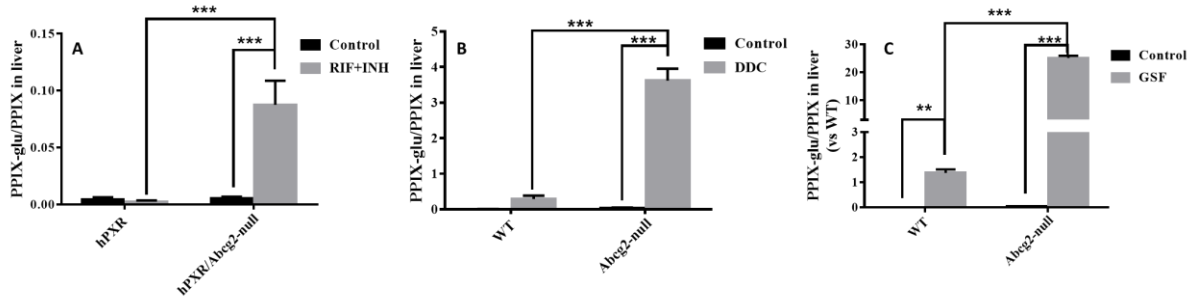


**Figure 22. Protoporphyrin-1-O-acyl-glucounone in the liver of drug-induced porphyria models.**

All samples were analyzed by UPLC-QTOFMS in positive mode. (A) PPIX- glu/PPIX in liver of hPXR and hPXR/Abcg2-null mice treated with RIF and INH for 28 days (n=4) (B) PPIX- glu/PPIX in liver of WT and Abcg2-null mice treated with DDC for 14 days (n=4). (C) PPIX- glu/PPIX in liver of WT and Abcg2-null mice treated with GSF for 14 days (n=4) \*\*P<0.01, \*\*\*P<0.0001. WT, wild type; PPIX-glu, protoporphyrin-1-O-acyl-glucounone; RIF, rifampicin; INH, isoniazid; DDC, 3,5-diethoxycarbonyl-1,4-dihydrocollidine; GSF, griseofulvin.

### 3.3.8. PPIX-glu conjugate is excreted into bile for fecal elimination

Next, to evaluate the elimination of PPIX-glu conjugate from the liver, we quantified D<sub>16</sub>-PPIX-glu in the gall bladder of WT and Abcg2-null mice treated with D<sub>2</sub>-ALA and samples were collected 1 h and 4 h post treatment. Interestingly, D<sub>16</sub>-PPIX-glu conjugate decreased in the liver with time but significantly increased with time in the gall bladder of Abcg2-null mice, suggesting the PPIX-glu conjugate was excreted in bile for excretion (**Figure 21A and 21B**). Also, D<sub>16</sub>-PPIX-glu conjugate was increased in the gall bladder of Fech-mut/Abcg2-null mice 2 h after D<sub>2</sub>-ALA treatment (**Figure 23A**). We also treated Fech-mut/Abcg2-null and Fech-mut

mice with D<sub>2</sub>-ALA and collected feces 18 h post D<sub>2</sub>-ALA treatment. We saw that the levels of D<sub>16</sub>-PPIX-glu conjugate significantly increased in the feces of Fech-mut/Abcg2-null mice compared to Fech-mut mice further confirming fecal elimination of PPIX-glu conjugate. Thus, in mice with Abcg2 deficiency, PPIX-glu conjugate is eliminated through the bile for fecal elimination.

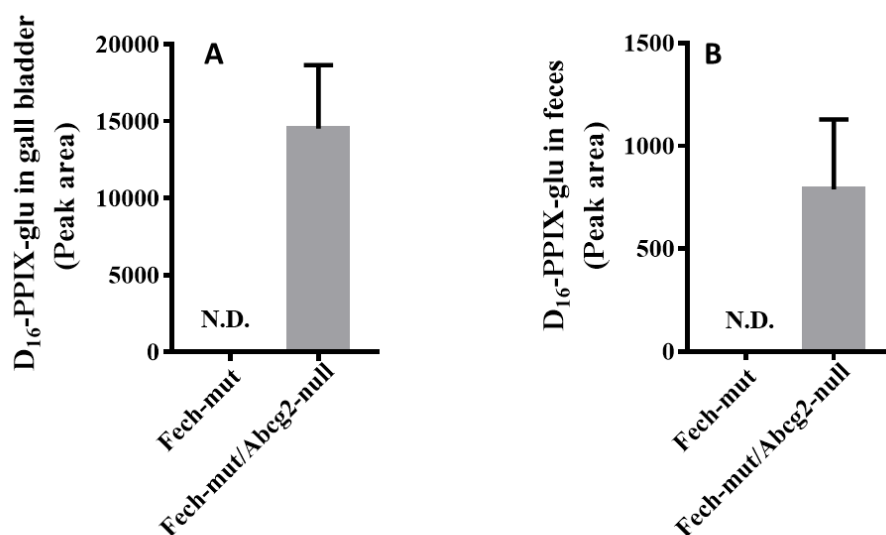


**Figure 23. D<sub>16</sub>-Protoporphyrin-1-O-acyl-glucouronide in the gall bladder and feces of the genetic porphyria models.**

All the samples were analyzed by UPLC-QTOFMS in positive mode. (A) D<sub>16</sub>-PPIX-glu quantified from the gall bladder collected 2 h after D<sub>2</sub>-ALA treatment in Fech-mut and Fech-mut/Abcg2-null mice (n=3). (B) D<sub>16</sub>-PPIX-glu quantified from the feces collected 18h after D<sub>2</sub>-ALA treatment in Fech-mut and Fech-mut/Abcg2-null mice (n=3). All data are expressed as means ± S.D.\*P<0.05. D<sub>16</sub>-PPIX-glu: D<sub>16</sub>-protoporphyrin-1-O-acyl-glucouronide.

### 3.4. Discussion

PPIX is an endogenous hepatotoxin, which causes cholestatic liver injury initiated from the PPIX-mediated blockage of the biliary system [90, 131]. ABCG2 facilitates in PPIX elimination from hepatocytes by excreting PPIX in the bile for fecal elimination. However, the presence of excessive PPIX in bile leads to its precipitation inside the bile duct and causes cholestasis. Prior to our study, little was known about how ABCG2 regulates PPIX-mediated hepatotoxicity. Using hPXR/Abcg2-null mice we showed that ABCG2 is essential in the hepatotoxicity induced by the co-treatment of RIF and INH. A previous study using different strains of genetic EPP mouse models also demonstrated that retention of PPIX in the liver can protect mice from PPIX-induced liver damage [193]. Thus, to further evaluate the role of ABCG2 on PPIX-induced hepatotoxicity, we treated Abcg2-null mice with well-established porphyrinogenic drugs DDC or GSF. Treatment with DDC or GSF in WT mice induced severe hepatic injury with portal inflammation and bile duct epithelial proliferation. In contrast, Abcg2-null mice were resistant to DDC or GSF induced hepatotoxicity with no change in liver injury markers of damage to the biliary system; thus, confirming ABCG2 is an important regulator in drug-induced hepatic porphyria.

As stated in the introduction, mouse models of drug-induced hepatic porphyria require hepatic metabolism of DDC or GSF and activation of ALAS1 to induce PPIX accumulation. Thus, we generated Fech-mut mice in the Abcg2-null background to eliminate the role of ABCG2-dysfunction on hepatic metabolism of porphyrinogen drugs. We found that PPIX-mediated liver injury was also abolished in Fech-mut/Abcg2-null mice. Also, liver injury markers in Fech-mut/Abcg2-null mice were in normal range and no damage to the biliary system was observed.

Together, results from genetic and drug-induced porphyria models confirmed that ABCG2 is a key modulator in PPIX-mediated cholestatic liver injury. PPIX is a highly hydrophobic molecule that precipitates in the bile when in excess [90]. Therefore, deficiency of ABCG2 decreases the amount of PPIX in the bile; consequently, preventing PPIX-mediated bile duct blockage and cholestatic liver injury.

In *Fech*-mut mice, *FECH* deficiency in the bone marrow is a major contributor for PPIX accumulation in the liver, and bone marrow transplantation in neonatal *Fech*-mut mice prevented liver damage [227]. ABCG2 is also highly expressed in erythroid progenitor cells [93]. Thus, the PPIX level in the serum of *Fech*-mut mice is significantly higher than WT mice [227, 228]. Excess PPIX in serum is collected by the liver for fecal excretion. ABCG2 deficiency prevents PPIX export from erythroid progenitor cells into the serum. A previous study showed that RBCs from *Abcg2*-null mice had around 10-fold higher levels of PPIX as compared to control [27]. Similarly, we also discovered that *Fech*-mut/*Abcg2*-null mice had 6-fold higher levels of PPIX in RBCs and a significantly lower PPIX level in serum as compared to *Fech*-mut mice, indicating an ABCG2 deficiency in the erythroid progenitor cells contained PPIX in the RBCs preventing its export into the serum. Old RBCs in the body are filtered in the body by the spleen for degradation. Thus, PPIX levels in the spleen of *Fech*-mut/*Abcg2*-null mice were increased as compared to *Fech*-mut mice. ABCG2 deficiency prevented the escape of PPIX from RBCs into serum, and part of the PPIX formed in the bone marrow of *Fech*-mut/*Abcg2*-null mice was redistributed in the spleen, decreasing available PPIX to be collected by the liver.

Due to the importance of ABCG2 in PPIX excretion, *Fech-mut/Abcg2*-null mice had the significantly higher amount of PPIX accumulation in the liver as compared to *Fech-mut* mice 2 h post D<sub>2</sub>-ALA treatment. As discussed in the introduction, PPIX accumulation in the drug-induced porphyria model is mainly caused by the dysregulated heme biosynthesis pathway in the liver. Also, redistribution of PPIX reduced the amount of PPIX collected by the hepatocytes of *Fech-mut/Abcg2*-null mice, but *Fech* mutation also dysregulates PPIX homeostasis in hepatocytes. The hepatocytes are the most important sites in animals for the metabolism of xenobiotics and endobiotics [229, 230]. We discovered a novel PPIX-glu metabolite of D<sub>16</sub>-PPIX using untargeted metabolomic analysis of liver samples obtained 2 h post D<sub>2</sub>-ALA treatment. In *Fech-mut/Abcg2*-null mice, metabolism of D<sub>16</sub>-PPIX to D<sub>16</sub>-PPIX-glu was dramatically induced. Also, D<sub>16</sub>-PPIX metabolism to D<sub>16</sub>-PPIX-glu was significantly increased in *Abcg2*-null mice further supporting the metabolism of PPIX in hepatocytes. Detoxification pathways for PPIX metabolism in the liver relieve hepatocytes from PPIX accumulation. We also discovered increased PPIX-glu/PPIX in drug-induced porphyria models supporting that PPIX metabolism protects hepatocytes from PPIX-induced toxicity in *Abcg2*-deficient mice.

In general, conjugated metabolites are considered as detoxified metabolites because they are more hydrophilic and easier to excrete from urine or bile than the parent compound [231, 232]. D<sub>16</sub>-PPIX-glu was excreted in bile independent of ABCG2 for fecal excretion in *Fech-mut/Abcg2*-null mice. Also, in *Abcg2*-null mice, the decrease in D<sub>16</sub>-PPIX-glu in the liver with time and the increase in D<sub>16</sub>-PPIX-glu gall bladder with time further confirmed excretion in the bile was independent of ABCG2. PPIX-glu is more hydrophilic than PPIX and does not form precipitates in the bile duct to block bile flow. Thus, *Abcg2* deficiency in hepatocytes

metabolizes accumulated PPIX to PPIX-glu conjugate which is eliminated through bile; whereas, in mice with functional ABCG2, unchanged PPIX is excreted into the bile duct where it precipitates and blocks the bile flow to cause cholestasis.

In summary, EPP-associated liver injury remains a major concern in the porphyria community [130, 233]. Although multiple pharmacological approaches have been attempted to manage the EPP-associated liver injury, none of them is effective in all cases and cannot be used to prevent final liver failure [90, 131]. Deficiency of ABCG2 increased the metabolism and detoxification of PPIX. Thus, ABCG2 could serve as a potential target for the management of PPIX-mediated liver injury. This project extended our knowledge of ABCG2 on PPIX distribution and metabolism.

## **4. Summary and perspectives**

### **4.1. Major Findings and Implications**

PPIX is the final intermediate in the biosynthesis of an important biological prosthetic group. Normally, PPIX is produced in a very low amount by most of the cells; but, to meet the excessive requirement of heme in hemoglobin and P450, PPIX is excessively produced by the bone marrow and the hepatocytes. The majority of PPIX produced in the liver and the bone marrow is very efficiently converted into the heme. Extra unconverted PPIX is collected by hepatocytes for fecal excretion. Disease conditions and some xenobiotics disrupt heme biosynthesis and PPIX homeostasis to cause PPIX accumulation which can lead to liver damage. During my graduate study, I worked on two projects with the aim to get greater insight into the mechanism of INH-induced PPIX accumulation and PPIX-mediated liver injury.

In the first part of my thesis work, we revealed porphyrinogenic properties of INH. Previously, INH was shown to potentiate porphyrinogenic properties of drugs like RIF and GSF. Moreover, INH was also contraindicated in EPP patients, but mechanisms by which INH potentiates liver toxicity in EPP patients was not clear. We showed for the first time that chronic INH treatment alone induces PPIX accumulation in the liver. INH-induced PPIX accumulation in the liver can disturb liver homeostasis which combined with other underlying problems or second hit to the

liver can result in the liver injury. INH is used as the first line of treatment to treat TB and could be potentially used by EPP patients suffering from TB. In EPP patients, INH can potentiate PPIX accumulation and liver injury. Furthermore, INH is commonly used with RIF for TB treatment. Our results, explained how INH could potentiate porphyrinogenic properties of RIF to cause liver injury. We also showed that INH causes PPIX accumulation in the liver but not in bone marrow cells. We further demonstrated that INH induces PPIX accumulation by inducing ALAS1 protein and downregulating FECH protein to potentiate PPIX accumulation (**Figure 24**). We showed that INH disturbs PPIX homeostasis only in the liver without disturbing bone marrow. Similar to previously reported INH-mediated CYP2E1 stabilization, we showed INH directly targets ALAS1 and FECH protein without affecting their mRNA level.

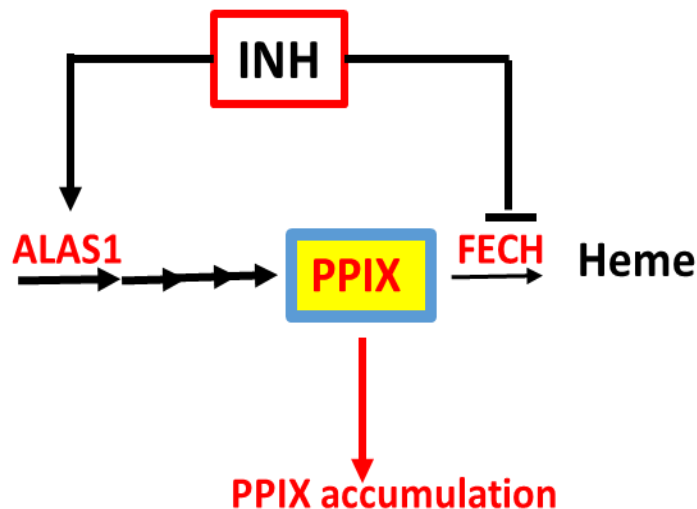


**Figure 24. A scheme showing mechanism of INH-induced PPIX accumulation.**

Isoniazid dysregulates heme biosynthesis pathway in the liver by stabilizing ALAS1 and downregulating FECH to cause PPIX accumulation.

In the second part of my thesis work, we revealed that ABCG2 plays a critical role in PPIX-mediated hepatotoxicity. The role of ABCG2 in excreting PPIX from the liver to bile for fecal elimination was already well established. Thus, it was believed that ABCG2 dysfunction would potentiate PPIX accumulation in hepatocytes and promote liver injury. However, for the first time we showed that ABCG2 is responsible for PPIX-mediated hepatotoxicity by pumping excessive PPIX in the bile duct, where PPIX precipitates to block bile flow to cause liver damage in PPIX-mediated liver injury. Using pharmacologic and genetic approaches we generated four different models with PPIX-mediated liver injury and showed that ABCG2 deficiency abolished PPIX-mediated hepatotoxicity. This work is important as it shows that ABCG2 is a key factor for PPIX-mediated liver injury. Thus, this work will greatly help in increasing the understanding of PPIX-mediated hepatotoxicity. This study will assist in developing a new treatment approach for the management of liver injury in EPP patients which will significantly improve their quality of life.

In EPP patients, excessive PPIX is produced from bone marrow during erythropoiesis, which is primarily responsible for PPIX-mediated hepatotoxicity. Bone marrow transplantation along with a liver transplant has shown to be effective in preventing recurrent PPIX-mediated liver injury, but this invasive treatment is limited by the availability of donors [100, 130, 136, 137]. The excessive PPIX produced by bone marrow during erythropoiesis in EPP patients is continuously pumped into the serum by ABCG2 and the liver collects PPIX from the serum to cause PPIX accumulation and liver injury. We showed that ABCG2 deficiency in erythroid progenitor cells redistributes PPIX in the RBCs to the spleen (**Figure 25**).

Furthermore, we showed that the deficiency of ABCG2 altered the excretion pathway of PPIX and increased PPIX metabolism and detoxification. We also showed that PPIX in the hepatocytes with ABCG2 deficiency was metabolized into detoxified PPIX-glu conjugate and excreted in bile for fecal elimination (**Figure 25**). Since conjugates are more hydrophilic as compared to the parent molecule, we believe PPIX-glu conjugate is easily excreted independently of ABCG2 from hepatocytes for fecal excretion without blocking the bile duct.

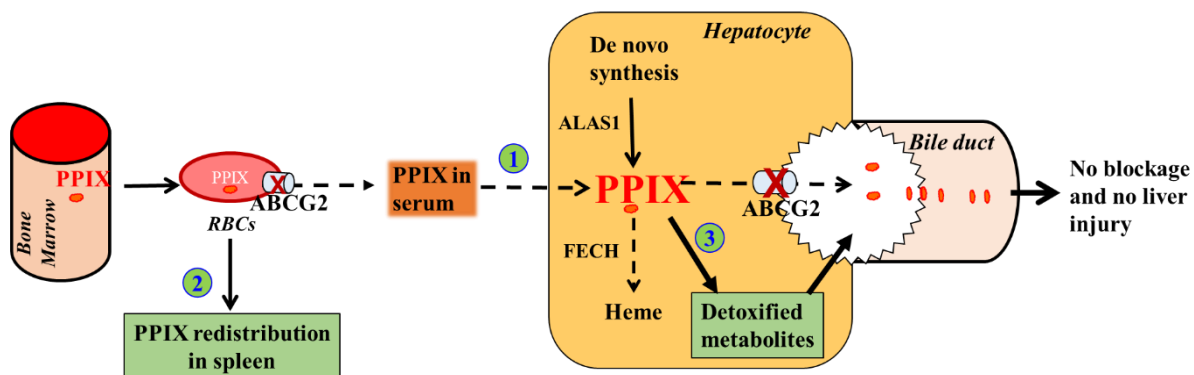


**Figure 25. A scheme showing mechanism by which Abcg2-deficiency prevents PPIX-mediated liver injury.**

ABCG2 deficiency prevents PPIX-mediated liver injury by (1) suppression of ABCG2 will decrease the transport of PPIX from RBCs to plasma, and sequentially reduce the delivery of PPIX to hepatocytes; (2) PPIX in RBCs will end up with RBC recycling in the spleen; (3) deficiency of ABCG2 in hepatocytes altered the excretion pathway of PPIX and increased its metabolism and detoxification.

Altogether, this thesis work has highlighted important aspects of mechanism and management of PPIX accumulation in the liver. We have developed two new *Abcg2*-deficient mouse models, namely hPXR/*Abcg2*-null mice and *Fech*-mut/*Abcg2*-null mice. The hPXR/*Abcg2*-null mouse model could be used to study the role of ABCG2 on hPXR ligands. The *Fech*-mut/*Abcg2*-null mouse model would aid in further studies on EPP-mediated toxicity. We also hope our results could aid in developing a new therapeutic approach for the management of PPIX-mediated hepatotoxicity.

#### **4.2. Limitations and future directions**

In the first part of my thesis we showed that INH causes PPIX accumulation but no liver injury was observed. Further studies are needed to correlate INH-induced PPIX accumulation to liver injury. Previous studies have also shown that INH can cause sideroblastic anemia [234]. Therefore, further studies are needed to evaluate the role of INH in disturbing heme homeostasis in bone marrow. The role of INH treatment on gene expression regulating heme biosynthesis in bone marrow also needs to be further evaluated. The present study does not explain the mechanism by which INH induces *ALAS1* and downregulates *FECH* only at the protein level. Therefore, future studies are needed to identify the mechanism by which INH selectively affects the protein levels of *ALAS1* and *FECH*. These studies could potentially unveil new pathways regulating heme biosynthesis and will provide a greater understanding of INH-induced hepatotoxicity. Since INH induced PPIX accumulation only occurs in the liver the role of INH hepatic metabolism and/or INH concentration in the liver needs to be further evaluated in upregulating *ALAS1* and downregulating *FECH*.

In the second part of my thesis research, all the experiments were conducted in mice with ABCG2-null background. Constitutive ABCG2-deficiency can result in upregulation of other compensatory mechanisms. Therefore, further studies using ABCG2 inhibitor are needed to confirm the therapeutic potential of this work. Another major limitation of this work is that only a mice model was used; therefore, clinical studies are also required to evaluate the therapeutic potential of this research.

We observed that ABCG2 deficiency in bone marrow causes PPIX redistribution to the spleen, but the role of PPIX redistribution in mitigating PPIX-induced liver injury needs to be further evaluated. We need to perform a splenectomy in *Fech-mut/Abcg2*-null mice to see whether PPIX-induced hepatotoxicity reappears. Moreover, to evaluate the role of *Abcg2* deficiency in bone marrow we could also transplant the bone marrow of *Fech-mut/Abcg2*-null mice in *Fech-mut* mice and vice versa, and assess liver injury in transplanted mice in order to confirm the role of *Abcg2*-deficiency in preventing PPIX-induced liver injury. In the present study, we did not explore elimination pathways of PPIX from the spleen. Further studies are needed to evaluate the role of PPIX degradation or elimination pathways in the spleen. Decreased PPIX in serum by *Abcg2*-deficiency could also help in attenuating PPIX-mediated photo-toxicity in EPP patients. PPIX-mediated photo-toxicity is caused by photoactivation of PPIX deposit from serum in the skin. Further studies are needed to evaluate the role of ABCG2 deficiency in bone marrow on PPIX-mediated photo-toxicity.

Present work did not elucidate transporters responsible for PPIX-glu excretion. Therefore, further studies are required to elucidate the mechanism of excretion of PPIX metabolites in hepatocytes. In the present study, the mechanism of PPIX metabolism was not explored. Further studies using liver microsomes or recombinant UDP-glucuronosyltransferase (UGT) enzymes need to be conducted to identify the mechanism of PPIX elimination. Furthermore, the present study did not elucidate the mechanism for elimination of PPIX-glu conjugate from the liver to bile. Further studies using mouse models with specific transporter knockout along with ABCG2 need to be conducted to evaluate the role of the transporters in eliminating PPIX-glu conjugates.

## APPENDIX A

### SEQUENCES OF REAL-TIME PCR PRIMERS

<b>Primer Name</b>	<b>Primer Sequence</b>
ALSA1-F	TCGCCGATGCCCATTCCTTATC
ALSA1-R	GGCCCAACTTCCATCATCT
FECH-F	CAGACAGATGAGGCTATCAAAGG
FECH-R	CACAGCTTGTTGGACTGGATG

## BIBLIOGRAPHY

1. Paoli, M., J. Marles-Wright, and A. Smith, *Structure-function relationships in heme-proteins*. DNA Cell Biol, 2002. **21**(4): p. 271-80.
2. Kirton, S.B., et al., *Prediction of binding modes for ligands in the cytochromes P450 and other heme-containing proteins*. Proteins, 2005. **58**(4): p. 836-44.
3. Smith, L.J., A. Kahraman, and J.M. Thornton, *Heme proteins--diversity in structural characteristics, function, and folding*. Proteins, 2010. **78**(10): p. 2349-68.
4. Chen, F.P., et al., *Ferrochelatase gene mutations in erythropoietic protoporphyria: focus on liver disease*. Cell Mol Biol (Noisy-le-grand), 2002. **48**(1): p. 83-9.
5. Cox, T.M., G.J. Alexander, and R.P. Sarkany, *Protoporphyria*. Semin Liver Dis, 1998. **18**(1): p. 85-93.
6. Magnus, I.A., et al., *Erythropoietic protoporphyria. A new porphyria syndrome with solar urticaria due to protoporphyrinaemia*. Lancet, 1961. **2**(7200): p. 448-51.

7. Dailey, H.A. and P.N. Meissner, *Erythroid heme biosynthesis and its disorders*. Cold Spring Harb Perspect Med, 2013. **3**(4): p. a011676.
8. Meerman, L., *Erythropoietic protoporphyria. An overview with emphasis on the liver*. Scand J Gastroenterol Suppl, 2000.(232): p. 79-85.
9. MacCormack, M.A., *Photodynamic therapy in dermatology: an update on applications and outcomes*. Semin Cutan Med Surg, 2008. **27**(1): p. 52-62.
10. Gold, M.H. and M.P. Goldman, *5-aminolevulinic acid photodynamic therapy: where we have been and where we are going*. Dermatol Surg, 2004. **30**(8): p. 1077-83; discussion 1083-4.
11. Ajioka, R.S., J.D. Phillips, and J.P. Kushner, *Biosynthesis of heme in mammals*. Biochim Biophys Acta, 2006. **1763**(7): p. 723-36.
12. Koningsberger, J.C., et al., *Exogenous protoporphyrin inhibits Hep G2 cell proliferation, increases the intracellular hydrogen peroxide concentration and causes ultrastructural alterations*. J Hepatol, 1995. **22**(1): p. 57-65.
13. Hunter, G.A. and G.C. Ferreira, *Molecular enzymology of 5-aminolevulinate synthase, the gatekeeper of heme biosynthesis*. Biochim Biophys Acta, 2011. **1814**(11): p. 1467-73.
14. Guernsey, D.L., et al., *Mutations in mitochondrial carrier family gene SLC25A38 cause nonsyndromic autosomal recessive congenital sideroblastic anemia*. Nat Genet, 2009. **41**(6): p. 651-3.
15. Bayeva, M., et al., *ATP-binding cassette B10 regulates early steps of heme synthesis*. Circ Res, 2013. **113**(3): p. 279-87.

16. Frydman, R.B. and G. Feinstein, *Studies on porphobilinogen deaminase and uroporphyrinogen 3 cosynthase from human erythrocytes*. *Biochim Biophys Acta*, 1974. **350**(2): p. 358-73.
17. Jordan, P.M. and D. Shemin, *Purification and properties of uroporphyrinogen I synthetase from Rhodopseudomonas spheroides*. *J Biol Chem*, 1973. **248**(3): p. 1019-24.
18. Charles A. Lewis, J.a.R.W., *Uroporphyrinogen decarboxylation as a benchmark for the catalytic proficiency of enzymes*. *Proc Natl Acad Sci U S A*, 2008. **105**(45): p. 17328-33.
19. Krishnamurthy, P.C., et al., *Identification of a mammalian mitochondrial porphyrin transporter*. *Nature*, 2006. **443**(7111): p. 586-9.
20. Krishnamurthy, P. and J.D. Schuetz, *The role of ABCG2 and ABCB6 in porphyrin metabolism and cell survival*. *Curr Pharm Biotechnol*, 2011. **12**(4): p. 647-55.
21. Proulx, K.L., S.I. Woodard, and H.A. Dailey, *In situ conversion of coproporphyrinogen to heme by murine mitochondria: terminal steps of the heme biosynthetic pathway*. *Protein Sci*, 1993. **2**(7): p. 1092-8.
22. Dailey, H.A., Jr., *Purification and characterization of the membrane-bound ferrochelatase from Spirillum itersonii*. *J Bacteriol*, 1977. **132**(1): p. 302-7.
23. Schwartz, S., et al., *Loss of hereditary uterine protoporphyria through chromosomal rearrangement in mutant Rhode Island red hens*. *Int J Biochem*, 1980. **12**(5-6): p. 935-40.
24. Shaw, G.C., et al., *Mitoferrin is essential for erythroid iron assimilation*. *Nature*, 2006. **440**(7080): p. 96-100.
25. Chen, W., et al., *Abcb10 physically interacts with mitoferrin-1 (Slc25a37) to enhance its stability and function in the erythroid mitochondria*. *Proc Natl Acad Sci U S A*, 2009. **106**(38): p. 16263-8.

26. Wendler, G., et al., *Protoporphyrin IX binding and transport by recombinant mouse PBR*. Biochem Biophys Res Commun, 2003. **311**(4): p. 847-52.
27. Jonker, J.W., et al., *The breast cancer resistance protein protects against a major chlorophyll-derived dietary phototoxin and protoporphyria*. Proc Natl Acad Sci U S A, 2002. **99**(24): p. 15649-54.
28. Solazzo, M., et al., *Mitochondrial expression and functional activity of breast cancer resistance protein in different multiple drug-resistant cell lines*. Cancer Res, 2009. **69**(18): p. 7235-42.
29. Kobuchi, H., et al., *Mitochondrial localization of ABC transporter ABCG2 and its function in 5-aminolevulinic acid-mediated protoporphyrin IX accumulation*. PLoS One, 2012. **7**(11): p. e50082.
30. Bishop, D.F., A.S. Henderson, and K.H. Astrin, *Human delta-aminolevulinate synthase: assignment of the housekeeping gene to 3p21 and the erythroid-specific gene to the X chromosome*. Genomics, 1990. **7**(2): p. 207-14.
31. Cox, T.C., et al., *Erythroid 5-aminolevulinate synthase is located on the X chromosome*. Am J Hum Genet, 1990. **46**(1): p. 107-11.
32. Cotter, P.D., et al., *Assignment of human erythroid delta-aminolevulinate synthase (ALAS2) to a distal subregion of band Xp11.21 by PCR analysis of somatic cell hybrids containing X; autosome translocations*. Genomics, 1992. **13**(1): p. 211-2.
33. Kolluri, S., et al., *Haem repression of the housekeeping 5-aminolaevulinic acid synthase gene in the hepatoma cell line LMH*. Biochem J, 2005. **392**(Pt 1): p. 173-80.
34. Zheng, J., et al., *Differential regulation of human ALAS1 mRNA and protein levels by heme and cobalt protoporphyrin*. Mol Cell Biochem, 2008. **319**(1-2): p. 153-61.

35. Sassa, S. and S. Granick, *Induction of  $\delta$ -aminolevulinic acid synthetase in chick embryo liver cells in culture*. Proc Natl Acad Sci U S A, 1970. **67**(2): p. 517-22.
36. Roberts, A.G. and G.H. Elder, *Alternative splicing and tissue-specific transcription of human and rodent ubiquitous 5-aminolevulinic acid synthase (ALAS1) genes*. Biochim Biophys Acta, 2001. **1518**(1-2): p. 95-105.
37. Cable, E.E., T.G. Miller, and H.C. Isom, *Regulation of heme metabolism in rat hepatocytes and hepatocyte cell lines: delta-aminolevulinic acid synthase and heme oxygenase are regulated by different heme-dependent mechanisms*. Arch Biochem Biophys, 2000. **384**(2): p. 280-95.
38. Tian, Q., et al., *Lon peptidase 1 (LONP1)-dependent breakdown of mitochondrial 5-aminolevulinic acid synthase protein by heme in human liver cells*. J Biol Chem, 2011. **286**(30): p. 26424-30.
39. Lathrop, J.T. and M.P. Timko, *Regulation by heme of mitochondrial protein transport through a conserved amino acid motif*. Science, 1993. **259**(5094): p. 522-5.
40. Dailey, T.A., J.H. Woodruff, and H.A. Dailey, *Examination of mitochondrial protein targeting of haem synthetic enzymes: in vivo identification of three functional haem-responsive motifs in 5-aminolevulinic acid synthase*. Biochem J, 2005. **386**(Pt 2): p. 381-6.
41. Munakata, H., et al., *Role of the heme regulatory motif in the heme-mediated inhibition of mitochondrial import of 5-aminolevulinic acid synthase*. J Biochem, 2004. **136**(2): p. 233-8.
42. Scassa, M.E., et al., *Insulin inhibits delta-aminolevulinic acid synthase gene expression in rat hepatocytes and human hepatoma cells*. Exp Cell Res, 1998. **244**(2): p. 460-9.

43. Varone, C.L., et al., *Transcriptional regulation of 5-aminolevulinic acid synthase by phenobarbital and cAMP-dependent protein kinase*. Arch Biochem Biophys, 1999. **372**(2): p. 261-70.
44. Giger, U. and U.A. Meyer, *Induction of delta-aminolevulinic acid synthase and cytochrome P-450 hemoproteins in hepatocyte culture. Effect of glucose and hormones*. J Biol Chem, 1981. **256**(21): p. 11182-90.
45. Wu, Z., et al., *Mechanisms controlling mitochondrial biogenesis and respiration through the thermogenic coactivator PGC-1*. Cell, 1999. **98**(1): p. 115-24.
46. Handschin, C., et al., *Nutritional regulation of hepatic heme biosynthesis and porphyria through PGC-1alpha*. Cell, 2005. **122**(4): p. 505-15.
47. Wu, N., et al., *Negative feedback maintenance of heme homeostasis by its receptor, Rev-erbalpha*. Genes Dev, 2009. **23**(18): p. 2201-9.
48. Gerhart-Hines, Z., et al., *The nuclear receptor Rev-erbalpha controls circadian thermogenic plasticity*. Nature, 2013. **503**(7476): p. 410-3.
49. Fraser, D.J., A. Zumsteg, and U.A. Meyer, *Nuclear receptors constitutive androstane receptor and pregnane X receptor activate a drug-responsive enhancer of the murine 5-aminolevulinic acid synthase gene*. J Biol Chem, 2003. **278**(41): p. 39392-401.
50. Podvynec, M., et al., *Identification of the xenosensors regulating human 5-aminolevulinic acid synthase*. Proc Natl Acad Sci U S A, 2004. **101**(24): p. 9127-32.
51. Fraser, D.J., et al., *Drugs mediate the transcriptional activation of the 5-aminolevulinic acid synthase (ALAS1) gene via the chicken xenobiotic-sensing nuclear receptor (CXR)*. J Biol Chem, 2002. **277**(38): p. 34717-26.

52. Li, F., et al., *Human PXR modulates hepatotoxicity associated with rifampicin and isoniazid co-therapy*. Nat Med, 2013. **19**(4): p. 418-20.
53. Bhasker, C.R., et al., *The putative iron-responsive element in the human erythroid 5-aminolevulinate synthase mRNA mediates translational control*. J Biol Chem, 1993. **268**(17): p. 12699-705.
54. Melefors, O., et al., *Translational control of 5-aminolevulinate synthase mRNA by iron-responsive elements in erythroid cells*. J Biol Chem, 1993. **268**(8): p. 5974-8.
55. Wingert, R.A., et al., *Deficiency of glutaredoxin 5 reveals Fe-S clusters are required for vertebrate haem synthesis*. Nature, 2005. **436**(7053): p. 1035-39.
56. Napier, I., P. Ponka, and D.R. Richardson, *Iron trafficking in the mitochondrion: novel pathways revealed by disease*. Blood, 2005. **105**(5): p. 1867-74.
57. Rouault, T.A. and W.H. Tong, *Iron-sulphur cluster biogenesis and mitochondrial iron homeostasis*. Nat Rev Mol Cell Biol, 2005. **6**(4): p. 345-51.
58. Sadlon, T.J., et al., *Regulation of erythroid 5-aminolevulinate synthase expression during erythropoiesis*. Int J Biochem Cell Biol, 1999. **31**(10): p. 1153-67.
59. Smith, S.J. and T.M. Cox, *Translational control of erythroid delta-aminolevulinate synthase in immature human erythroid cells by heme*. Cell Mol Biol (Noisy-le-grand), 1997. **43**(1): p. 103-14.
60. Kennedy, J.C., R.H. Pottier, and D.C. Pross, *Photodynamic therapy with endogenous protoporphyrin IX: basic principles and present clinical experience*. J Photochem Photobiol B, 1990. **6**(1-2): p. 143-8.
61. Shimizu, Y., et al., *Excretion of porphyrins in urine and bile after the administration of delta-aminolevulinic acid*. J Lab Clin Med, 1978. **92**(5): p. 795-802.

62. Whatley, S.D., et al., *C-terminal deletions in the ALAS2 gene lead to gain of function and cause X-linked dominant protoporphyria without anemia or iron overload*. Am J Hum Genet, 2008. **83**(3): p. 408-14.
63. Holme, S.A., et al., *Seasonal palmar keratoderma in erythropoietic protoporphyria indicates autosomal recessive inheritance*. J Invest Dermatol, 2009. **129**(3): p. 599-605.
64. Lindblad, B., S. Lindstedt, and G. Steen, *On the enzymic defects in hereditary tyrosinemia*. Proc Natl Acad Sci U S A, 1977. **74**(10): p. 4641-5.
65. Fujita, H., et al., *Decreased erythrocyte delta-aminolevulinate dehydratase activity after styrene exposure*. Biochem Pharmacol, 1987. **36**(5): p. 711-6.
66. Stephen O. Duke, J.M.B., T. D. Sherman, John Lydon, Hiroshi Matsumoto, *The role of protoporphyrin IX in the mechanism of action of diphenyl ether herbicides*. Pest Management Science, 1990. **30**(4): p. 367-378.
67. Sinclair, P.R., et al., *Protoporphyrinogen accumulation in cultured hepatocytes treated with the diphenyl ether herbicide, acifluorfen*. Cell Mol Biol (Noisy-le-grand), 1994. **40**(7): p. 891-7.
68. Bonkovsky, H.L., et al., *Heme synthetase deficiency in human protoporphyria. Demonstration of the defect in liver and cultured skin fibroblasts*. J Clin Invest, 1975. **56**(5): p. 1139-48.
69. Thapar, M. and H.L. Bonkovsky, *The diagnosis and management of erythropoietic protoporphyria*. Gastroenterol Hepatol (N Y), 2008. **4**(8): p. 561-6.
70. Whitcombe, D.M., et al., *Assignment of the human ferrochelatase gene (FECH) and a locus for protoporphyria to chromosome 18q22*. Genomics, 1991. **11**(4): p. 1152-4.

71. Gouya, L., et al., *Inheritance in erythropoietic protoporphyria: a common wild-type ferrochelatase allelic variant with low expression accounts for clinical manifestation.* Blood, 1999. **93**(6): p. 2105-10.
72. Nelson, J.C., et al., *The ratio of erythrocyte zinc-protoporphyrin to protoporphyrin IX in disease and its significance in the mechanism of lead toxicity on haem synthesis.* Ann Clin Biochem, 1998. **35** ( Pt 3): p. 422-6.
73. Labbe, R.F., H.J. Vreman, and D.K. Stevenson, *Zinc protoporphyrin: a metabolite with a mission.* Clin Chem, 1999. **45**(12): p. 2060-72.
74. Gupta, V., et al., *Salicylic acid induces mitochondrial injury by inhibiting ferrochelatase heme biosynthesis activity.* Mol Pharmacol, 2013. **84**(6): p. 824-33.
75. Cole, S.P., D.T. Zelt, and G.S. Marks, *Comparison of the effects of griseofulvin and 3,5-diethoxycarbonyl-1,4-dihydro-2,4,6-trimethylpyridine on ferrochelatase activity in chick embryo liver.* Mol Pharmacol, 1981. **19**(3): p. 477-80.
76. Cole, S.P. and G.S. Marks, *Ferrochelatase and N-alkylated porphyrins.* Mol Cell Biochem, 1984. **64**(2): p. 127-37.
77. Felsher, B.F. and A.G. Redeker, *Acute intermittent porphyria: effect of diet and griseofulvin.* Medicine (Baltimore), 1967. **46**(2): p. 217-23.
78. Troadec, M.B., et al., *Targeted deletion of the mouse Mitoferrin1 gene: from anemia to protoporphyria.* Blood, 2011. **117**(20): p. 5494-502.
79. Yamamoto, M., et al., *Abcb10 role in heme biosynthesis in vivo: Abcb10 knockout in mice causes anemia with protoporphyrin IX and iron accumulation.* Mol Cell Biol, 2014. **34**(6): p. 1077-84.
80. Braun, J., *Erythrocyte zinc protoporphyrin.* Kidney Int Suppl, 1999. **69**: p. S57-60.

81. Takashi Amo, N.K., Masataka Uchida, Hirofumi Fujita, Eri Oyanagi, Toshihiko Utsumi, Tetsuya Ogino, Keiji Inoue, Taro Shuin, Kozo Utsumi, Junzo Sasaki, *Mechanism of cell death by 5-aminolevulinic acid-based photodynamic action and its enhancement by Mn<sup>2+</sup>, deferoxamine, and NOC-18 in human histiocytic lymphoma cell line U937*. Cell Biochem Funct, 2009. **27**: p. 503-515.
82. Juzeniene, A., V. Iani, and J. Moan, *Clearance mechanism of protoporphyrin IX from mouse skin after application of 5-aminolevulinic acid*. Photodiagnosis Photodyn Ther, 2013. **10**(4): p. 538-45.
83. Blake, E. and A. Curnow, *The hydroxypyridinone iron chelator CP94 can enhance PpIX-induced PDT of cultured human glioma cells*. Photochem Photobiol, 2010. **86**(5): p. 1154-60.
84. Anderson, K.E., U. Freddara, and A. Kappas, *Induction of hepatic cytochrome P-450 by natural steroids: relationship to the induction of delta-aminolevulinic acid synthase and porphyrin accumulation in the avian embryo*. Arch Biochem Biophys, 1982. **217**(2): p. 597-608.
85. Schauder, A., A. Avital, and Z. Malik, *Regulation and gene expression of heme synthesis under heavy metal exposure--review*. J Environ Pathol Toxicol Oncol, 2010. **29**(2): p. 137-58.
86. Anderson, K.E., et al., *Increased erythrocyte uroporphyrinogen-l-synthetase, delta-aminolevulinic acid dehydratase and protoporphyrin in hemolytic anemias*. Am J Med, 1977. **63**(3): p. 359-64.

87. Taketani, S., et al., *Induction of peripheral-type benzodiazepine receptors during differentiation of mouse erythroleukemia cells. A possible involvement of these receptors in heme biosynthesis.* J Biol Chem, 1994. **269**(10): p. 7527-31.
88. Pastorino, J.G., et al., *Protoporphyrin IX, an endogenous ligand of the peripheral benzodiazepine receptor, potentiates induction of the mitochondrial permeability transition and the killing of cultured hepatocytes by rotenone.* J Biol Chem, 1994. **269**(49): p. 31041-6.
89. Jonker, J.W., et al., *Breast cancer resistance protein (Bcrp1/Abcg2) is expressed in the harderian gland and mediates transport of conjugated protoporphyrin IX.* Am J Physiol Cell Physiol, 2007. **292**(6): p. C2204-12.
90. Anstey, A.V. and R.J. Hift, *Liver disease in erythropoietic protoporphyria: insights and implications for management.* Postgrad Med J, 2007. **83**(986): p. 739-48.
91. Bloomer, J.R., *The liver in protoporphyria.* Hepatology, 1988. **8**(2): p. 402-7.
92. Smith, K.M., *Protoporphyrin IX: some recent research.* Acc. Chem. Res, 1979. **12**(10): p. 374-381.
93. Zhou, S., et al., *Increased expression of the Abcg2 transporter during erythroid maturation plays a role in decreasing cellular protoporphyrin IX levels.* Blood, 2005. **105**(6): p. 2571-6.
94. Brancalion, L., et al., *Characterization of the photoproducts of protoporphyrin IX bound to human serum albumin and immunoglobulin G.* Biophys Chem, 2004. **109**(3): p. 351-60.
95. Desuzinges-Mandon, E., et al., *ABCG2 transports and transfers heme to albumin through its large extracellular loop.* J Biol Chem, 2010. **285**(43): p. 33123-33.

96. Lim, H.W., *Mechanisms of phototoxicity in porphyria cutanea tarda and erythropoietic protoporphyria*. Immunol Ser, 1989. **46**: p. 671-85.
97. Baart de la Faille, H., et al., *Erythropoietic protoporphyria: clinical aspects with emphasis on the skin*. Curr Probl Dermatol, 1991. **20**: p. 123-34.
98. Dubrey, S.W., et al., *Extreme photosensitivity in a patient with erythropoietic protoporphyria*. Br J Hosp Med (Lond), 2015. **76**(1): p. 52-3.
99. Horner, M.E., et al., *Cutaneous porphyrias part I: epidemiology, pathogenesis, presentation, diagnosis, and histopathology*. Int J Dermatol, 2013. **52**(12): p. 1464-80.
100. Wahlin, S., et al., *Erythropoietic protoporphyria in Sweden: demographic, clinical, biochemical and genetic characteristics*. J Intern Med, 2011. **269**(3): p. 278-88.
101. Holme, S.A., et al., *Symptomatic response of erythropoietic protoporphyria to iron supplementation*. J Am Acad Dermatol, 2007. **56**(6): p. 1070-2.
102. Bossi, K., et al., *Homeostasis of iron and hepcidin in erythropoietic protoporphyria*. Eur J Clin Invest, 2015. **45**(10): p. 1032-41.
103. Tintle, S., et al., *Cutaneous porphyrias part II: treatment strategies*. Int J Dermatol, 2014. **53**(1): p. 3-24.
104. Krook, G. and B. Haeger-Aronsen, *beta-Carotene in the treatment of erythropoietic protoporphyria. A short review*. Acta Derm Venereol Suppl (Stockh), 1982. **100**: p. 125-9.
105. Warren, L.J. and S. George, *Erythropoietic protoporphyria treated with narrow-band (TL-01) UVB phototherapy*. Australas J Dermatol, 1998. **39**(3): p. 179-82.
106. Collins, P. and J. Ferguson, *Narrow-band UVB (TL-01) phototherapy: an effective preventative treatment for the photodermatoses*. Br J Dermatol, 1995. **132**(6): p. 956-63.

107. Mathews-Roth, M.M., et al., *A double-blind study of cysteine photoprotection in erythropoietic protoporphyria*. *Photodermatol Photoimmunol Photomed*, 1994. **10**(6): p. 244-8.
108. Sawyer, T.K., et al., *4-Norleucine, 7-D-phenylalanine-alpha-melanocyte-stimulating hormone: a highly potent alpha-melanotropin with ultralong biological activity*. *Proc Natl Acad Sci U S A*, 1980. **77**(10): p. 5754-8.
109. Fabrikant, J., K. Touloei, and S.M. Brown, *A review and update on melanocyte stimulating hormone therapy: afamelanotide*. *J Drugs Dermatol*, 2013. **12**(7): p. 775-9.
110. Langendonk, J.G., et al., *Afamelanotide for erythropoietic protoporphyria*. *N Engl J Med*, 2015. **373**(1): p. 48-59.
111. Biolcati, G., et al., *Long-term observational study of afamelanotide in 115 patients with erythropoietic protoporphyria*. *Br J Dermatol*, 2015. **172**(6): p. 1601-12.
112. Minder, E.I. and X. Schneider-Yin, *Afamelanotide (CUV1647) in dermal phototoxicity of erythropoietic protoporphyria*. *Expert Rev Clin Pharmacol*, 2015. **8**(1): p. 43-53.
113. Lengweiler, S., et al., *Evaluation of the immunogenicity of the synthetic alpha-melanocyte-stimulating hormone (alpha-MSH) analogue afamelanotide ([Nle4-D-Phe7]-alpha-MSH, Scenesse(R)) in erythropoietic protoporphyria patients by ELISA detecting both anti-afamelanotide and anti-alpha-MSH antibodies*. *Skin Pharmacol Physiol*, 2015. **28**(2): p. 103-13.
114. Minder, E.I., et al., *A systematic review of treatment options for dermal photosensitivity in erythropoietic protoporphyria*. *Cell Mol Biol (Noisy-le-grand)*, 2009. **55**(1): p. 84-97.
115. Harms, J., et al., *An alpha-melanocyte-stimulating hormone analogue in erythropoietic protoporphyria*. *N Engl J Med*, 2009. **360**(3): p. 306-7.

116. Bloomer, J.R. and R. Enriquez, *Evidence that hepatic crystalline deposits in a patient with protoporphyria are composed of protoporphyrin*. Gastroenterology, 1982. **82**(3): p. 569-73.
117. Todd, D.J., *Gallstones in children*. Am J Dis Child, 1991. **145**(9): p. 971-2.
118. Doss, M.O. and M. Frank, *Hepatobiliary implications and complications in protoporphyria, a 20-year study*. Clin Biochem, 1989. **22**(3): p. 223-9.
119. Lee, R.G., D.L. Avner, and M.M. Berenson, *Structure-function relationships of protoporphyrin-induced liver injury*. Arch Pathol Lab Med, 1984. **108**(9): p. 744-6.
120. Szechcinski, J., A. Skoczynska, and Z. Andreasik, *[Liver cirrhosis in congenital erythropoietic protoporphyria]*. Pol Tyg Lek, 1986. **41**(28): p. 899-901.
121. Meerman, L., et al., *Biliary fibrosis associated with altered bile composition in a mouse model of erythropoietic protoporphyria*. Gastroenterology, 1999. **117**(3): p. 696-705.
122. Ma, J., et al., *A novel splicing mutation and haplotype analysis of the FECH gene in a Chinese family with erythropoietic protoporphyria*. J Eur Acad Dermatol Venereol, 2010. **24**(6): p. 726-9.
123. Bruguera, M. and C. Herrero, *[Liver disease in erythropoietic protoporphyria]*. Gastroenterol Hepatol, 2005. **28**(10): p. 632-6.
124. Gordeuk, V.R., et al., *Iron therapy for hepatic dysfunction in erythropoietic protoporphyria*. Ann Intern Med, 1986. **105**(1): p. 27-31.
125. Bloomer, J.R. and C.A. Pierach, *Effect of hematin administration to patients with protoporphyria and liver disease*. Hepatology, 1982. **2**(6): p. 817-21.
126. Gorchein, A. and G.R. Foster, *Liver failure in protoporphyria: long-term treatment with oral charcoal*. Hepatology, 1999. **29**(3): p. 995-6.

127. Van Hattum, J., et al., *Chenodeoxycholic acid therapy in erythrohepatic protoporphyria*. J Hepatol, 1986. **3**(3): p. 407-12.
128. Gross, U., M. Frank, and M.O. Doss, *Hepatic complications of erythropoietic protoporphyria*. Photodermatol Photoimmunol Photomed, 1998. **14**(2): p. 52-7.
129. Komatsu, K., et al., *Erythropoietic protoporphyria with severe liver dysfunction and acute pancreatitis*. J Gastroenterol, 2000. **35**(5): p. 391-5.
130. Singal, A.K., et al., *Liver transplantation in the management of porphyria*. Hepatology, 2014. **60**(3): p. 1082-9.
131. Casanova-Gonzalez, M.J., et al., *Liver disease and erythropoietic protoporphyria: a concise review*. World J Gastroenterol, 2010. **16**(36): p. 4526-31.
132. McGuire, B.M., et al., *Liver transplantation for erythropoietic protoporphyria liver disease*. Liver Transpl, 2005. **11**(12): p. 1590-6.
133. Samuel, D., et al., *Liver transplantation for protoporphyria. Evidence for the predominant role of the erythropoietic tissue in protoporphyrin overproduction*. Gastroenterology, 1988. **95**(3): p. 816-9.
134. Dellon, E.S., et al., *Treatment of recurrent allograft dysfunction with intravenous hematin after liver transplantation for erythropoietic protoporphyria*. Transplantation, 2002. **73**(6): p. 911-5.
135. de Torres, I., A.J. Demetris, and P.S. Randhawa, *Recurrent hepatic allograft injury in erythropoietic protoporphyria*. Transplantation, 1996. **61**(9): p. 1412-3.
136. Dowman, J.K., et al., *UK experience of liver transplantation for erythropoietic protoporphyria*. J Inherit Metab Dis, 2011. **34**(2): p. 539-45.

137. Rand, E.B., et al., *Sequential liver and bone marrow transplantation for treatment of erythropoietic protoporphyria*. Pediatrics, 2006. **118**(6): p. e1896-9.
138. Rank, J.M., R. Carithers, and J. Bloomer, *Evidence for neurological dysfunction in end-stage protoporphyric liver disease*. Hepatology, 1993. **18**(6): p. 1404-9.
139. Oustric, V., et al., *Antisense oligonucleotide-based therapy in human erythropoietic protoporphyria*. Am J Hum Genet, 2014. **94**(4): p. 611-7.
140. Poh-Fitzpatrick, M.B., et al., *Erythropoietic protoporphyria: altered phenotype after bone marrow transplantation for myelogenous leukemia in a patient heteroallelic for ferrochelatase gene mutations*. J Am Acad Dermatol, 2002. **46**(6): p. 861-6.
141. Meyer-Betz, F., *Untersuchungen über die biologische (photodynamische) Wirkung des Hämatoporphyrins und anderer Derivate des Blut- und Gallenfarbstoffs*. Dtsch. Arch. Klin. Med., 1913. **122**: p. 476–503.
142. Kosenow, W. and A. Treibs, *[Light hypersensitivity and porphyrinemia]*. Z Kinderheilkd, 1953. **73**(1): p. 82-92.
143. Kosenow, W., *Erythrozyten-Primärfluoreszenz bei Porphyrin-Dermatosen*. Med. Klin., 1954. **49**: p. 1099–1103.
144. Anderson, K.E., et al., *Porphyrogenic effects and induction of heme oxygenase in vivo by delta-aminolevulinic acid*. Biochim Biophys Acta, 1981. **676**(3): p. 289-99.
145. Karu, T. and V. Letokhov, *Possible benefits of two-quantum excitation in ALA-PDT? J Photochem Photobiol B*, 1994. **23**(2-3): p. 261-2.
146. Mordon, S., *A commentary on the role of skin temperature on the effectiveness of ALA-PDT in Dermatology*. Photodiagnosis Photodyn Ther, 2014. **11**(3): p. 416-9.

147. Rollakanti, K.R., et al., *Techniques for fluorescence detection of protoporphyrin IX in skin cancers associated with photodynamic therapy*. *Photonics Lasers Med*, 2013. **2**(4): p. 287-303.
148. Ishizuka, M., et al., *Novel development of 5-aminolevulinic acid (ALA) in cancer diagnoses and therapy*. *Int Immunopharmacol*, 2011. **11**(3): p. 358-65.
149. Henderson, B.W. and T.J. Dougherty, *How does photodynamic therapy work?* *Photochem Photobiol*, 1992. **55**(1): p. 145-57.
150. Dougherty, T.J., *An update on photodynamic therapy applications*. *J Clin Laser Med Surg*, 2002. **20**(1): p. 3-7.
151. Oleinick, N.L. and H.H. Evans, *The photobiology of photodynamic therapy: cellular targets and mechanisms*. *Radiat Res*, 1998. **150**(5 Suppl): p. S146-56.
152. Pass, H.I., *Photodynamic therapy in oncology: mechanisms and clinical use*. *J Natl Cancer Inst*, 1993. **85**(6): p. 443-56.
153. Fukuda, H., S. Paredes, and A.M. Batlle, *Tumor-localizing properties of porphyrins. In vitro studies using the porphyrin precursor, aminolevulinic acid, in free and liposome encapsulated forms*. *Drug Des Deliv*, 1989. **5**(2): p. 133-9.
154. Mfouo-Tynga, I. and H. Abrahamse, *Cell death pathways and phthalocyanine as an efficient agent for photodynamic cancer therapy*. *Int J Mol Sci*, 2015. **16**(5): p. 10228-10241.
155. Mroz, P., et al., *Cell death pathways in photodynamic therapy of cancer*. *Cancers (Basel)*, 2011. **3**(2): p. 2516-39.
156. Dougherty, T.J., et al., *Photodynamic therapy*. *J Natl Cancer Inst*, 1998. **90**(12): p. 889-905.

157. Garg, A.D., et al, *Photodynamic therapy: illuminating the road from cell death towards anti-tumour immunity*. Apoptosis, 2010. **15**(9): p. 1050-71.
158. Castano, A.P., P. Mroz, and M.R. Hamblin, *Photodynamic therapy and anti-tumour immunity*. Nat Rev Cancer, 2006. **6**(7): p. 535-45.
159. Mroz, P., et al, *Stimulation of anti-tumor immunity by photodynamic therapy*. Expert Rev Clin Immunol, 2011. **7**(1): p. 75-91.
160. Mroz, P., et al, *Photodynamic therapy of tumors can lead to development of systemic antigen-specific immune response*. PLoS One, 2010. **5**(12): p. e15194.
161. Nestor, M.S., et al, *The use of photodynamic therapy in dermatology: results of a consensus conference*. J Drugs Dermatol, 2006. **5**(2): p. 140-54.
162. Goldman MP, A.D., Kincad S., *PDT/ALA in the treatment of actinic damage: real world experience*. J Lasers Surg Med. , 2002. **14**(S).
163. EN, D., *Photodynamic inactivation of bacteria*. Curr Bioact Compd., 2006. **2**: p. 127-142.
164. Goslinski T, K.K., Piskorz J, Kryjewski M, Wierzehowski M, Sobiak S., *Prospects for photodynamic antimicrobial chemotherapy—PACT*. Postepy Mikrobiologii., 2008. **47**: p. 447–456.
165. Donnelly, R.F., P.A. McCarron, and M.M. Tunney, *Antifungal photodynamic therapy*. Microbiol Res, 2008. **163**(1): p. 1-12.
166. Akilov, O.E., et al, *The role of photosensitizer molecular charge and structure on the efficacy of photodynamic therapy against Leishmania parasites*. Chem Biol, 2006. **13**(8): p. 839-47.
167. O'Riordan, K., O.E. Akilov, and T. Hasan, *The potential for photodynamic therapy in the treatment of localized infections*. Photodiagnosis Photodyn Ther, 2005. **2**(4): p. 247-62.

168. Hamblin, M.R. and T. Hasan, *Photodynamic therapy: a new antimicrobial approach to infectious disease?* Photochem Photobiol Sci, 2004. **3**(5): p. 436-50.
169. Singla, A., et al., *Lamin aggregation is an early sensor of porphyria-induced liver injury.* J Cell Sci, 2013. **126**(Pt 14): p. 3105-12.
170. Mitchell, J.R., et al., *Isoniazid liver injury: clinical spectrum, pathology, and probable pathogenesis.* Ann Intern Med, 1976. **84**(2): p. 181-92.
171. Maddrey, W.C. and J.K. Boitnott, *Isoniazid hepatitis.* Ann Intern Med, 1973. **79**(1): p. 1-12.
172. Black, M., et al., *Isoniazid-associated hepatitis in 114 patients.* Gastroenterology, 1975. **69**(2): p. 289-302.
173. Chalasani, N., et al., *Features and outcomes of 899 patients with drug-induced liver injury: the DILIN prospective study.* Gastroenterology, 2015. **148**(7): p. 1340-52 e7.
174. Pessayre, D., et al., *Isoniazid-rifampin fulminant hepatitis. A possible consequence of the enhancement of isoniazid hepatotoxicity by enzyme induction.* Gastroenterology, 1977. **72**(2): p. 284-9.
175. Pilheu, J.A., M.C. De Salvo, and J.A. Barcat, *[Effect of isoniazid and rifampicin regimens on the liver of tuberculosis patients].* Medicina (B Aires), 1979. **39**(3): p. 298-304.
176. Pilheu, J.A., et al., *[Light and electron microscopy studies of the liver in tuberculosis patients receiving rifampin and isoniazid].* Medicina (B Aires), 1981. **41**(4): p. 439-45.
177. Watanabe, M., *The synergistic effect of isonicotinic acid hydrazide (INH) and griseofulvin (GF) on porphyrin metabolism.* J Dermatol, 1991. **18**(1): p. 39-42.

178. Liu, K., et al., *A metabolomic perspective of griseofulvin-induced liver injury in mice*. *Biochem Pharmacol*, 2015. **98**(3): p. 493-501.
179. Taketani, S., *Measurement of ferrochelatase activity*. *Curr Protoc Toxicol*, 2001. **Chapter 8**: p. Unit 8 7.
180. Rossi, E., K.A. Costin, and P. Garcia-Webb, *Ferrochelatase activity in human lymphocytes, as quantified by a new high-performance liquid-chromatographic method*. *Clin Chem*, 1988. **34**(12): p. 2481-5.
181. Li, F.M., C.K. Lim, and T.J. Peters, *An HPLC assay for rat liver ferrochelatase activity*. *Biomed Chromatogr*, 1987. **2**(4): p. 164-8.
182. Sinclair, P.R., N. Gorman, and N.W. Cornell, *Measurement of ALA synthase activity*. *Curr Protoc Toxicol*, 2001. **Chapter 8**: p. Unit 8 2.
183. Alsarra, I.A., et al., *Direct UPLC-MS-MS validated method for the quantification of 5-aminolevulinic acid: application to in-vitro assessment of colonic-targeted oral tablets*. *J Chromatogr Sci*, 2011. **49**(6): p. 428-33.
184. Sachar, M., K.E. Anderson, and X. Ma, *Protoporphyrin IX: the good, the bad, and the ugly*. *J Pharmacol Exp Ther*, 2016. **356**(2): p. 267-75.
185. Brady, A.M. and E.A. Lock, *Inhibition of ferrochelatase and accumulation of porphyrins in mouse hepatocyte cultures exposed to porphyrinogenic chemicals*. *Arch Toxicol*, 1992. **66**(3): p. 175-81.
186. Teng, L., et al., *Silencing of ferrochelatase enhances 5-aminolevulinic acid-based fluorescence and photodynamic therapy efficacy*. *Br J Cancer*, 2011. **104**(5): p. 798-807.
187. Kemmner, W., et al., *Silencing of human ferrochelatase causes abundant protoporphyrin-IX accumulation in colon cancer*. *FASEB J*, 2008. **22**(2): p. 500-9.

188. Poloyac, S.M., et al., *The effect of isoniazid on CYP2E1- and CYP4A-mediated hydroxylation of arachidonic acid in the rat liver and kidney*. Drug Metab Dispos, 2004. **32**(7): p. 727-33.
189. Yue, J., et al., *CYP2E1 mediated isoniazid-induced hepatotoxicity in rats*. Acta Pharmacol Sin, 2004. **25**(5): p. 699-704.
190. Chien, J.Y., K.E. Thummel, and J.T. Slattery, *Pharmacokinetic consequences of induction of CYP2E1 by ligand stabilization*. Drug Metab Dispos, 1997. **25**(10): p. 1165-75.
191. Singla, A., et al., *Oxidative stress, Nrf2 and keratin up-regulation associate with Mallory-Denk body formation in mouse erythropoietic protoporphyria*. Hepatology, 2012. **56**(1): p. 322-31.
192. Williams, M., J. Van der Zee, and J. Van Steveninck, *Toxic dark effects of protoporphyrin on the cytochrome P-450 system in rat liver microsomes*. Biochem J, 1992. **288** ( Pt 1): p. 155-9.
193. Lyoumi, S., et al., *Protoporphyrin retention in hepatocytes and Kupffer cells prevents sclerosing cholangitis in erythropoietic protoporphyria mouse model*. Gastroenterology, 2011. **141**(4): p. 1509-19, 1519 e1-3.
194. Thomas, B.H., W. Zeitz, and L.W. Whitehouse, *Effect of rifampin, phenobarbital pretreatment, and acetylator phenotype on acetylisoniazid metabolism in the rabbit*. Can J Physiol Pharmacol, 1987. **65**(3): p. 419-23.
195. Linton, K.J. and C.F. Higgins, *Structure and function of ABC transporters: the ATP switch provides flexible control*. Pflugers Arch, 2007. **453**(5): p. 555-67.

196. Moitra, K., et al, *Moving out: from sterol transport to drug resistance - the ABCG subfamily of efflux pumps*. Drug Metabol Drug Interact, 2011. **26**(3): p. 105-11.
197. Mo, W. and J.T. Zhang, *Human ABCG2: structure, function, and its role in multidrug resistance*. Int J Biochem Mol Biol, 2012. **3**(1): p. 1-27.
198. Sarkadi, B., et al, *Human multidrug resistance ABCB and ABCG transporters: participation in a chemoimmunity defense system*. Physiol Rev, 2006. **86**(4): p. 1179-236.
199. Gutmann, H., et al, *Distribution of breast cancer resistance protein (BCRP/ABCG2) mRNA expression along the human GI tract*. Biochem Pharmacol, 2005. **70**(5): p. 695-9.
200. Zhang, W., et al, *The expression and functional characterization of ABCG2 in brain endothelial cells and vessels*. FASEB J, 2003. **17**(14): p. 2085-7.
201. Mao, Q., *BCRP/ABCG2 in the placenta: expression, function and regulation*. Pharm Res, 2008. **25**(6): p. 1244-55.
202. Fetsch, P.A., et al, *Localization of the ABCG2 mitoxantrone resistance-associated protein in normal tissues*. Cancer Lett, 2006. **235**(1): p. 84-92.
203. Enokizono, J., et al, *Quantitative investigation of the role of breast cancer resistance protein (Bcrp/Abcg2) in limiting brain and testis penetration of xenobiotic compounds*. Drug Metab Dispos, 2008. **36**(6): p. 995-1002.
204. van Herwaarden, A.E., et al, *Multidrug transporter ABCG2/breast cancer resistance protein secretes riboflavin (vitamin B2) into milk*. Mol Cell Biol, 2007. **27**(4): p. 1247-53.
205. Olsen, H.G., et al, *Genetic support for a quantitative trait nucleotide in the ABCG2 gene affecting milk composition of dairy cattle*. BMC Genet, 2007. **8**: p. 32.
206. Ron, M., et al, *Short communication: a polymorphism in ABCG2 in Bos indicus and Bos taurus cattle breeds*. J Dairy Sci, 2006. **89**(12): p. 4921-3.

207. Maliepaard, M., et al., *Subcellular localization and distribution of the breast cancer resistance protein transporter in normal human tissues*. *Cancer Res*, 2001. **61**(8): p. 3458-64.
208. Mao, Q. and J.D. Unadkat, *Role of the breast cancer resistance protein (ABCG2) in drug transport*. *AAPS J*, 2005. **7**(1): p. E118-33.
209. Stacy, A.E., P.J. Jansson, and D.R. Richardson, *Molecular pharmacology of ABCG2 and its role in chemoresistance*. *Mol Pharmacol*, 2013. **84**(5): p. 655-69.
210. Imai, Y., et al., *Breast cancer resistance protein exports sulfated estrogens but not free estrogens*. *Mol Pharmacol*, 2003. **64**(3): p. 610-8.
211. Janvilisri, T., et al., *Sterol transport by the human breast cancer resistance protein (ABCG2) expressed in Lactococcus lactis*. *J Biol Chem*, 2003. **278**(23): p. 20645-51.
212. Saison, C., et al., *Null alleles of ABCG2 encoding the breast cancer resistance protein define the new blood group system Junior*. *Nat Genet*, 2012. **44**(2): p. 174-7.
213. Sachar, M., et al., *Chronic treatment with isoniazid causes protoporphyrin IX accumulation in mouse liver*. *Chem Res Toxicol*, 2016.
214. Fickert, P., et al., *A new xenobiotic-induced mouse model of sclerosing cholangitis and biliary fibrosis*. *Am J Pathol*, 2007. **171**(2): p. 525-36.
215. De Matteis, F., et al., *Labelling in vivo and chirality of griseofulvin-derived N-alkylated protoporphyrins*. *Biochem J*, 1991. **280** ( Pt 3): p. 813-6.
216. De Matteis, F., *The effects of drugs on the activities of 5-aminolaevulinate synthetase and other enzymes in the pathway of haem biosynthesis*. *Biochem J*, 1972. **130**(2): p. 52P-53P.

217. De Matteis, F. and A.H. Gibbs, *Drug-induced conversion of liver haem into modified porphyrins. Evidence for two classes of products.* Biochem J, 1980. **187**(1): p. 285-8.
218. Davies, R., et al., *Hepatic gene expression in protoporphyric Fech mice is associated with cholestatic injury but not a marked depletion of the heme regulatory pool.* Am J Pathol, 2005. **166**(4): p. 1041-53.
219. Tutois, S., et al., *Erythropoietic protoporphyria in the house mouse. A recessive inherited ferrochelatase deficiency with anemia, photosensitivity, and liver disease.* J Clin Invest, 1991. **88**(5): p. 1730-6.
220. Boulechfar, S., et al., *Ferrochelatase structural mutant (Fechm1Pas) in the house mouse.* Genomics, 1993. **16**(3): p. 645-8.
221. Fontanellas, A., et al., *Successful therapeutic effect in a mouse model of erythropoietic protoporphyria by partial genetic correction and fluorescence-based selection of hematopoietic cells.* Gene Ther, 2001. **8**(8): p. 618-26.
222. Richard, E., et al., *Hematopoietic stem cell gene therapy of murine protoporphyria by methylguanine-DNA-methyltransferase-mediated in vivo drug selection.* Gene Ther, 2004. **11**(22): p. 1638-47.
223. Pawliuk, R., et al., *Long-term cure of the photosensitivity of murine erythropoietic protoporphyria by preselective gene therapy.* Nat Med, 1999. **5**(7): p. 768-73.
224. Richard, E., et al., *Gene therapy of a mouse model of protoporphyria with a self-inactivating erythroid-specific lentiviral vector without preselection.* Mol Ther, 2001. **4**(4): p. 331-8.

225. Fontanellas, A., et al., *Reversion of hepatobiliary alterations by bone marrow transplantation in a murine model of erythropoietic protoporphyria*. *Hepatology*, 2000. **32**(1): p. 73-81.
226. Latli, B., et al., *Synthesis of deleobuvir, a potent hepatitis C virus polymerase inhibitor, and its major metabolites labeled with carbon-13 and carbon-14*. *J Labelled Comp Radiopharm*, 2015. **58**(6): p. 250-60.
227. Duchartre, Y., et al., *Neonatal bone marrow transplantation prevents liver disease in a murine model of erythropoietic protoporphyria*. *J Hepatol*, 2011. **55**(1): p. 162-70.
228. Lyoumi, S., et al., *Increased plasma transferrin, altered body iron distribution, and microcytic hypochromic anemia in ferrochelatase-deficient mice*. *Blood*, 2007. **109**(2): p. 811-8.
229. Niwa, T., N. Murayama, and H. Yamazaki, *Oxidation of endobiotics mediated by xenobiotic-metabolizing forms of human cytochrome*. *Curr Drug Metab*, 2009. **10**(7): p. 700-12.
230. Bock, K.W., *Homeostatic control of xeno- and endobiotics in the drug-metabolizing enzyme system*. *Biochem Pharmacol*, 2014. **90**(1): p. 1-6.
231. Xu, C., C.Y. Li, and A.N. Kong, *Induction of phase I, II and III drug metabolism/transport by xenobiotics*. *Arch Pharm Res*, 2005. **28**(3): p. 249-68.
232. Shimada, T., *Xenobiotic-metabolizing enzymes involved in activation and detoxification of carcinogenic polycyclic aromatic hydrocarbons*. *Drug Metab Pharmacokinet*, 2006. **21**(4): p. 257-76.
233. Seth, A.K., et al., *Liver transplantation for porphyria: who, when, and how?* *Liver Transpl*, 2007. **13**(9): p. 1219-27.

234. Piso, R.J., K. Kriz, and M.C. Desax, *Severe isoniazid related sideroblastic anemia*.  
Hematol Rep, 2011. **3**(1): p. e2.

Please check these references: